ORNL/TM-2023/2974

Operation of the Fast Neutron Coincidence Collar (FNCL) with a DD-Neutron Generator

Robert D. McElroy Jr.
Sean O'Brien
Alex Laminack

August 2023

OAK RIDGE National Laboratory

ORNL IS MANAGED BY UT-BATTELLE LLC FOR THE US DEPARTMENT OF ENERGY

ORNL/TM-2023/2974

Nuclear Nonproliferation Division

OPERATION OF THE FAST NEUTRON COINCIDENCE COLLAR (FNCL) WITH THE DD-NEUTRON GENERATOR

Robert D. McElroy Jr.
Sean O'Brien
Alex Laminack

August 2023

Prepared by
OAK RIDGE NATIONAL LABORATORY
Oak Ridge, TN 37831
managed by
UT-BATTELLE LLC
for the
US DEPARTMENT OF ENERGY
under contract DE-AC05-00OR22725

CONTENTS

LIST OF FIGURES iv
LIST OF TABLES vii
ABBREVIATIONS viii
ACKNOWLEDGMENTS ix
ABSTRACT 1
1. INTRODUCTION 1
1.1 THE FAST NEUTRON COLLAR 1
2. NEUTRON GENERATORS 2
2.1 MP320 DD NEUTRON GENERATOR 3
2.2 NGEN-350 NEUTRON GENERATOR 4
3. BENCHMARK MEASUREMENTS 6
3.1 PASSIVE ISOTOPICS SOURCE MEASUREMENTS 6
3.1.1 Estimated Detection Efficiency 6
3.1.2 Initial Passive Measurements 7
3.2 AM(LI) ISOTOPICS SOURCE MEASUREMENTS 9
3.3 MP320 NEUTRON GENERATOR MEASUREMENTS 10
3.4 NGEN-350 NEUTRON GENERATOR MEASUREMENTS 11
4. SIMULATED ASSEMBLIES FOR THE MCNP PERFORMANCE STUDY 14
4.1 DESCRIPTION OF THE SIMULATED CALBRATION ASSEMBLIES 14
4.2 DESCRIPTION OF THE ASSORTED INTACT FUEL ASSEMBLIES 15
4.3 DESCRIPTION OF THE ASSEMBLIES CONTAINING BURNABLE POISON RODS POISON RODS 16
4.4 DESCRIPTION OF THE ASSEMBLIES FOR PARTIAL DEFECT ANALYSIS 17
5. EXPECTED PERFORMANCE FOR FUEL ASSEMBLIES 18
5.1 OPTIMIZATION OF THE FNCL/NGEN-350 RESPONSE 20
5.1.1 Empty Chamber Response 21
5.1.2 Optimization for Fuel Assembly Measurement 24
6. FNCL/NGEN-350 ADAPTER MODULE 29
6.1 EXPECTED PERFORMANCE OF THE OPTIMIZED NGEN-350/FNCL 31
6.2 SIMULATED CALIBRATION OF THE NGEN-350/FNCL 32
6.3 NGEN-350/FNCL SIMULATED PERFORMANCE FOR VARIOUS INTACT ASSEMBLIES 32
6.4 NGEN-350/FNCL SIMULATED PERFORMANCE FOR BURNABLE POISONS 34
6.5 NGEN-350/FNCL SIMULATED PARTIAL DEFECT ANALYSIS 37
7. DISCUSSION 39
8. CONCLUSION 39
9. REFERENCES 40
APPENDIX A. FNCL SIMULATION AND ANALYSIS SOFTWARE A-1

LIST OF FIGURES

Figure 1. Photograph of the CAEN FNCL detector assembly (left), the acquisition electronics (center), and an isometric view showing the arrangement of the 12 EJ309 neutron detectors [10] (right). 2
Figure 2. Photograph of the MP320 controller (left) and the detached MP320 DD neutron generator tube (right). 3
Figure 3. Photograph of the nGen-350 neutron generator at ORNL. 4
Figure 4. Photograph of the nGen-310 neutron generator tube (shown without the required control electronics module) from the Starfire data sheet [21]. 4
Figure 5. Photograph of the assembled nGen350 steady-state DD neutron generator (left) and disassembled (right). 4
Figure 6. Comparison of the estimated pulse height threshold setting relative to the Am(Li) and ^{240}Pu fission neutron energy distributions. 6
Figure 7. Illustration of the measurement arrangement of the uranium oxide containers in the FNCL using Am(Li) isotopic interrogation sources with the FNCL in the pressurized water reactor (left) and boiling water reactor (right) configurations. 8
Figure 8. FNCL Am(Li) induced net doubles rate as a function of ^{235}U mass. 9
Figure 9. Screenshot of the MCNP input file for the MP320/FNCL test configuration for small containers (left) and a photograph of the assembled FNCL with the MP320. 9
Figure 10. FNCL MP320 induced net doubles rate as a function of ^{235}U mass for the highly enriched uranium containers (points represent a single 5 minute active measurement). 10
Figure 11. Screenshot of the MCNP input file for the nGen-350/FNCL test configuration for small containers (left) and a photograph of the assembled FNCL with the nGen-350 during initial testing. 11
Figure 12. FNCL nGen-350 induced net doubles rate as a function of ^{235}U mass for the highly enriched uranium containers. 12
Figure 13. Cross sections of the mock calibration fuel assemblies generated from the MCNP input files. 13
Figure 14. Cross sections of the mock intact fuel assemblies generated from the MCNP input files. 14
Figure 15. Distribution of the poison rods (red circles) within the simulated 17 ×17 fuel assemblies. 16
Figure 16. Distribution of the DU pins (red) within the simulated 17 × 17 assembly. 16
Figure 17. Illustration of the three active interrogation configurations considered for this preliminary analysis using Am(Li) isotopic sources (left), the MP320 DD generator (middle), and the nGen350 DD generator (right). 17
Figure 18. Comparison of the total induced fission rates as a function of pin position within a 17 × 17 fuel assembly from an Am(Li) isotopic (left), MP320 DD neutron generator (middle), and the nGen350 DD neutron generator (right). 17
Figure 19. Comparison of the MP320/FNCL simulated response as a function of ^{235}U content (neutron yield 1.4E6 n/s) with the measured response of the traditional fast mode Am(Li) UNCL system. 18
Figure 20. Fission maps for a 17 × 17 fuel assembly for the different neutron interrogation sources considered for the FNCL. 19
Figure 21. Induced fission cross sections for ^{235}U and ^{238}U [24]. 20
Figure 22. Illustration of the moderator/insert simulation geometry. 21
Figure 23. Neutron fluence as a function of energy in the center of the empty FNCL cavity for various thicknesses of HDPE (with a cadmium layer) between the generator and FNCL. 21

Figure 24. Neutron fluence as a function of energy in the center of the empty FNCL cavity for two of the thicker HDPE slabs (with a cadmium layer) located between the generator and FNCL. 22
Figure 25. Average neutron energy in the center of the empty FNCL cavity as a function of thickness for various slab materials. 22
Figure 26. Expected neutron singles rates for empty FNCL cavity as a function of thickness for various slab materials. 23
Figure 27. Expected neutron singles rates for a 17 × 17 un-poisoned fuel assembly (left) and a poisoned 17 × 17 fuel assembly (right) loaded into the FNCL cavity as a function of thickness for various slab materials. 23
Figure 28. Average neutron energy in the center of a 17 × 17 un-poisoned fuel assembly (left) and a poisoned 17 × 17 fuel assembly (right) loaded into the FNCL cavity as a function of thickness for various slab materials. 24
Figure 29. Expected neutron singles rates for a 17 × 17 un-poisoned fuel assembly (left) and a poisoned 17 × 17 fuel assembly (right) loaded into the FNCL cavity as a function of thickness for various slab materials (yield:1.4E6 n/s). 24
Figure 30. Ratio of the $^{238}U/^{235}U$ induced fission rates for a 17 × 17 un-poisoned fuel assembly (left) and a poisoned 17 × 17 fuel assembly (right) loaded into the FNCL cavity as a function of thickness for various slab materials. 24
Figure 31. Expected neutron coincidence rates for a 17 × 17 un-poisoned fuel assembly (left) and a poisoned 17 × 17 fuel assembly (right) loaded into the FNCL cavity as a function of thickness for various slab materials (yield: 1.4×10^6 n/s). 25
Figure 32. Relative ^{235}U induced fission rate maps for a 17 × 17 un-poisoned fuel assembly. 26
Figure 33. Relative ^{238}U induced fission rate maps for a 17 × 17 un-poisoned fuel assembly with a 7 cm flux-tailoring slab with and without cadmium. 26
Figure 34. Detection efficiency as a function of pin position with the 17 × 17 un-poisoned fuel assembly. 27
Figure 35. Relative doubles rate contribution as a function of pin position for a 17 × 17 un-poisoned fuel assembly. 27
Figure 36. Estimated doubles rate precision (300 s interrogation, generator yield:1E6 n/s) for the Cal-6 assembly. 28
Figure 37. Simple mounting approach. 29
Figure 38. Selected generator mounting approach, the nGen-350 is mounted with the generator tube oriented vertically (left) and the moderating “shoe” generator mounting bracket (right). 30
Figure 39. MCNP VISED screenshots of the modified FNCL detector arrangement about a fuel assembly (left) and a vertical cross section through the neutron generator holder. 30
Figure 40. nGen-350/FNCL simulated calibration curve overlain with the measured UNCL-II calibration results [25]. 31
Figure 41. Results of the MCNP simulations for the nGen-350/FNCL for the assorted intact fuel assemblies in the thermal mode. 32
Figure 42. Simulated assay results for the various burnable poison loadings with and without the heavy metal and poison rod correction. 34
Figure 43. Simulated assay results for the partial defect loadings with and without application of the heavy metal correction. 37
Figure A-1. Multiplicity analysis and simulation GUI. A-3
Figure A-2. The pulse filter window is where all pulse processing is set and applied before analysis. A-4
Figure A-3. Pulse amplitude plotter in ADC mode, note the large number of overflow pulses on the far right of the histogram. A-5
Figure A-4. Energy calibration tool. A-6

Figure A-5. The Pulse stream viewer can reveal major changes in average count rates. A-6
Figure A-6. Pulse shape discrimination editor. A-7
Figure A-7. PSD waveform viewer shows particle determination given PSD editor settings. A-8
Figure A-8. Pile-up rejector showing a piled-up and non–piled-up pulse given the rejector settings. A-8
Figure A-9. Example of a pulse waveform rejected for flat top. A-9
Figure A-10. Batch save of FNCL waveform pulses to flat files. A-9
Figure A-11. Multiplicity counting rates window. A-10
Figure A-12. Particle die-away time fit with a single exponential function on the interval distribution. A-10
Figure A-13. FNCL model generation for Am(Li) source holder models. A-11
Figure A-14. Tool that combines multiple particle history files into a single pulse stream. A-12
Figure A-15. NBL can on side inside FNCL-cavity with MP320 neutron generator with side shielding. A-12
Figure A-16. Fuel assembly specification with option to launch an editor to modify the fuel assembly. A-13
Figure A-17. The fuel assembly editor can vary number of pins, materials, and locations of cooling channels. A-13
Figure A-18. Am(Li) source holder are specified by a the Am(Li) Block Type drop-down. A-14
Figure A-19. MP320 neutron generator specification GUI, where additional neutron moderator and lead photon shielding can be added. A-14
Figure A-20. nGen350 neutron generator with 16 × 16 fuel assembly, two perspectives. A-15
Figure A-21. Impact of raising ADC low level discrimination threshold on multiplet rates. A-16
Figure A-22. Position of NBL cans to maximize interrogation neutron interactions given the small volume of material for all reported measurements. A-17
Figure A-23. Singles and doubles rates reported by the FNCL DAQ for the PWR Am(Li) interrogations sources and for the Mp320, with and without extra PE. A-18
Figure A-24.Singles and doubles rates for passive measurements reported by the FNCL DAQ for the PWR Am(Li) source holder and for the Mp320, with and without extra PE. A-19
Figure A-25. Californium-252 and cesium-137 sources with cadmium sheet shielding. A-20
Figure A-26. A 17 × 17 fuel assembly with 20 gadolinium poison rod positions marked in green, and the cooling channels are checked. A-21
Figure A-27. Simulated rates across fuel enrichments for the several interrogation sources. The Mp320 without extra PE has the highest rates. A-21
Figure A-28. Relative difference between the simulated singles, doubles, and triples rates between fuel assemblies with gadolinium poison rods and a fuel assembly without gadolinium poison rods that preserves the total mass of ^{235}U using the PWR Am(Li) source holder. A-22
Figure A-29. Relative difference between the simulated singles, doubles, and triples rates between fuel assemblies with gadolinium poison rods and a fuel assembly without gadolinium poison rods that preserves the total mass of ^{235}U using the MP320 neutron generator. A-23
Figure A-30. Relative difference between the simulated singles, doubles, and triples rates between fuel assemblies with gadolinium poison rods and a fuel assembly without gadolinium poison rods that preserves the total mass of ^{235}U using the MP320 neutron generator with extra PE. A-24
Figure A-31. Resulting count rates, reported by the FNCL-DAQ, over a range of "auto" neutron yield settings. A-25
Figure A-32. Rates reported by the FNCL-DAQ for several U-standards. A-26

LIST OF TABLES

Table 1. DD neutron generator vendor stated characteristics. 6
Table 2. FNCL passive measurement results (count time = 300 s). 8
Table 3. FNCL active measurement results for the Am(Li) interrogating neutron sources [2]. 9
Table 4. FNCL active measurement results for the MP320 neutron generator (300 s active measurement) [2]. 11
Table 5. FNCL active measurement results for the nGen-350 neutron generator (300 s active measurement). 12
Table 6. FNCL average of the active measurement results for the nGen-350 neutron generator (300 s active measurement). 13
Table 7. Input parameters for the 17 × 17 calibration assemblies. 15
Table 8. Input parameters for the various intact fuel assemblies. 16
Table 9. Input parameters for the burnable poison fuel assemblies. 16
Table 10. ^{235}U linear density for the poison rod configurations. 17
Table 11. Input parameters for the fuel assemblies for partial defect analysis. 17
Table 12. Uranium-238 fraction of total fission event rate. 19
Table 13. Simulated nGen-350/FNCL calibration measurement results for the calibration assemblies‡. 32
Table 14. Simulated nGen-350/FNCL measurement results for the unpoisoned, intact fuel assemblies‡. 34
Table 15. Simulated nGen-350/FNCL uncorrected measurement results for the poisoned, intact fuel assemblies‡. 36
Table 16. Simulated defect analysis results for the poisoned, intact fuel assemblies using the compact neutron generator operating at 200,000. 37
Table 17. Simulated measurement results for the partial defect assembly configurations.‡ 38
Table 18. Simulated defect analysis results for the partial defect assembly configurations†. 38

ABBREVIATIONS

ADC	alternating direct current
BWR	boiling water reactor
DAQ	data acquisition
DU	depleted uranium
FNCL	Fast Neutron Coincidence Collar
HDPE	high-density polyethylene
IAEA	International Atomic Energy Agency
ORNL	Oak Ridge National Laboratory
PE	polyethylene
PSD	pulse shape discrimination
PWR	pressurized water reactor
UNCL	Uranium Neutron Coincidence Collar

ACKNOWLEDGMENTS

This material is based upon work supported by the NA-241's Next Generation Safeguards Initiative within the Office of Nonproliferation and Arms Control, National Nuclear Security Administration, US Department of Energy.

ABSTRACT

For more than 30 years, the quantitative assay of the ^{235}U content of light water reactor fresh fuel assemblies relied on measuring coincidence neutrons from fissions induced by an Am(Li) neutron source using ^{3}He based detectors. The Fast Neutron Collar (FNCL) [1] developed by the International Atomic Energy Agency (IAEA), replaces traditional ^{3}He proportional counters with an array of liquid scintillator detectors arranged about the fuel assembly to provide improved measurement precision and reduced sensitivity to gadolinium poison rods. The FNCL relies on Am(Li) neutron sources that are no longer commercially available. This work examines the replacement of Am(Li) sources with a commercial off-the-shelf deuterium–deuterium (DD) neutron generator. In addition to mitigating supply concerns, the neutron generator offers advantages in measurement precision and potential automation of sequential passive/active neutron measurements.

This report presents the initial performance results for both the integrated DD/FNCL [2] and Am(Li)/FNCL assays of compact depleted uranium, low-enriched uranium, and highly enriched uranium standards along with an estimate of the expected performance for fresh fuel assemblies. A discussion of the design and operation of the "FNCL Analysis and Simulation Software" [3] is also provided.

1. INTRODUCTION

The Uranium Neutron Coincidence Collar (UNCL) [4], [5], [6], [7], [8], [9] is an active neutron interrogation system used to provide the ^{235}U linear density of fresh fuel assemblies during routine inspection activities in support of international safeguards [10]. The UNCL is rectangular in configuration, three sides of which are arrays of ^{3}He proportional counters embedded in high-density polyethylene (HDPE). The fourth (active) side contains the Am(Li) neutron source, which is also embedded in HDPE. During use, the collar is placed around the fuel assembly, bringing the Am(Li) neutron source into close proximity with the fuel assembly while encompassing three of the four sides with the neutron detector array. Neutrons emitted from the Am(Li) source induce fission within the fuel assembly, resulting in the emission of additional neutrons. Neutron coincidence counting is employed to distinguish the induced fission from the interrogating source events. The ^{235}U linear density (i.e., mass ^{235}U per unit length of fuel assembly) is inferred from the observed neutron coincidence rate, and the result is compared with the declared value for the fuel assembly.

The UNCL is based on ^{3}He thermal neutron detectors and provides a modest neutron detection efficiency of about 12% for ^{252}Cf spontaneous fission neutrons. Because it is based on thermal neutron detection, its characteristic die-away time of 50 μs requires a comparatively long coincidence gate width, typically 64 μs. The high count rate from the Am(Li) interrogating neutron source coupled with the long coincidence gate leads to high accidentals coincidence rates, which ultimately limit the measurement precision achievable with the UNCL. The UNCL has been used in the field for safeguards for 40 years, and during that time the design and components have changed little. However, sensitivity to poison rods and long assay times required for fast mode measurements have resulted in numerous research efforts to develop an improved system. The Am(Li) neutron sources required by the UNCL system have become difficult to obtain commercially such that alternative neutron interrogation sources are also being developed for the UNCL measurement. Ongoing UNCL developments fall into three categories: improved ^{3}He designs, alternative detector technologies, and alternative interrogation methodologies [11], [12], [13], [14], [15].

1.1 THE FAST NEUTRON COLLAR

The Fast Neutron coincidence Collar (FNCL) [1], [16], [2] (Figure 1) has been introduced as an alternative for the UNCL measurement of low-enriched uranium fuel assemblies. The FNCL, available from CAEN Industries, replaces the ^{3}He detector assembly with 12 EJ-309 liquid scintillation neutron detectors. Unlike the UNCL, the FNCL is based on fast neutron detection, allowing much shorter coincidence gating, resulting in improved measurement precision by reducing the accidental coincidence rate. Like the UNCL, the FNCL relies on Am(Li) to supply the interrogating neutron flux. However, because the neutrons emitted by the Am(Li) source have an average energy of only a few hundred keV, most of these neutrons fall below the detection energy threshold of the scintillation detectors. That is, the detector is insensitive to the interrogating neutron source, further reducing the accidental coincidence rate and improving the measurement precision. Measurements by Beaumont et al. indicate that the FNCL provides significant improvement in measurement precision, reducing the required measurement times by a factor of 12 relative to the standard UNCL measurement. Their measurements using the FNCL suggest that measurement biases due to the presence of gadolinium poison rods are also reduced by factor of 3, from 9% to 3%.

Figure 1. Photograph of the CAEN FNCL detector assembly (left), the acquisition electronics (center), and an isometric view showing the arrangement of the 12 EJ309 neutron detectors [10] (right).

The accidentals coincidence rate associated with the interrogating neutron source and the long coincidence gate width used with ^{3}He based neutron counting systems limits the measurement precision achievable with the UNCL. Increases in the interrogating neutron source strength beyond 10^{5} n/s offer little to no improvement in measurement precision. The coincidence gate typically applied with the scintillation-based neutron detectors used with the FNCL (60 ns) is roughly 1/1,000th the width of that used with the ^{3}He systems (64 μs), which in principle allows the use of much larger interrogation sources and further improvement in the achievable measurement precision. However, the required Am(Li) sources are no longer commercially available, and sources for new systems are typically salvaged from existing measurement systems. Increasing the interrogating source strength using larger or multiple Am(Li) sources is somewhat problematic, and obtaining the additional improvement in FNCL measurement precision will require an alternative neutron source. Coupling the FNCL with a DD neutron generator will address the source supply limitation as well as provide a significantly higher interrogating neutron flux. Commercial off-the-shelf DD neutron generators are available with typical neutron yields up to 2×10^{6} n/s, 40 times greater than available from a single Am(Li) source.

2. NEUTRON GENERATORS

Due to delays in the production and delivery of the nGen-350, initial testing of the FNCL coupled with a neutron generator was carried out using an alternate generator that was already available at Oak Ridge National Laboratory (ORNL). The two DD neutron generators evaluated during this project were the ThermoFisher MP320 [17] and the Starfire nGen-350 [18].

2.1 MP320 DD NEUTRON GENERATOR

The ThermoFisher Scientific model MP320 [17] used for this evaluation was also used in previous evaluations of the potential use of the DD generator as a potential alternative to Am(Li) sources. The generator properties are summarized in

Table 1. DD neutron generator vendor stated characteristics.

. The generator (Figure 2) may be operated in steady-state (non-pulsed) mode with a maximum yield of ~2×10^6 n/s and an average neutron energy of 2.48 MeV. Although not a small neutron generator tube by today's standards, the 12.1 cm diameter tube can be fit within the Large Volume - Active Well Coincidence Counter (LV-AWCC) [19] or standard AWCC end-plugs for active interrogation of small containers of ^{235}U materials. The principal drawbacks of the tube are its overall length (~56 cm) and location of the target line (i.e., point of neutron generation), which is ~14.4 cm from the end of the tube. This results in a greater source-to-sample separation, additional shielding, and larger system footprint.

Figure 2. Photograph of the MP320 controller (left) and the detached MP320 DD neutron generator tube (right).

2.2 NGEN-350 NEUTRON GENERATOR

A detailed evaluation of the performance of the Starfire nGen-350 neutron generator can be found in Reference [20]. A summary of the findings is presented here. Only limited testing of the FNCL with the nGen-350 was performed during the period of performance of this project due to pandemic-related delays of the delivery of the generator.

The nGen-350 neutron generator (Figure 3) was modified from the Starfire nGen-310-DD steady-state DD neutron generator. The nGen-310 [21] is a light-weight, sealed fusion neutron generator with a compact form factor with maximum yield of 10^7 n/s. Most other neutron generator tubes of similar yield place the neutron generation point (the accelerator target-line) several centimeters from the end of the tube. The Starfire design places the neutron generation point within 0.5 cm of the tube end, providing additional flexibility in integrating the tube into the measurement system. A photograph of the nGen-310 is shown in Figure 4. The nGen-310 generator tube is used as the core of the nGen-350 and is mounted within the nGen-350 cooling duct/generator housing. The generator properties are summarized in

Table 1. DD neutron generator vendor stated characteristics.

.

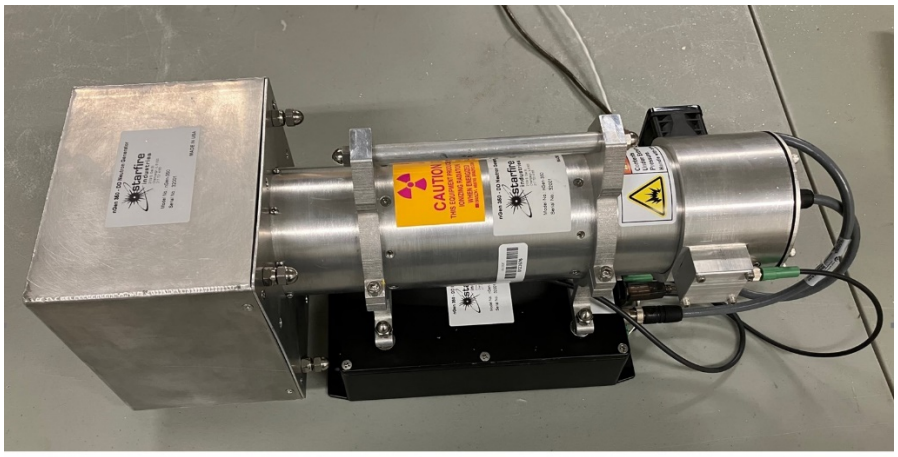

Figure 3. Photograph of the nGen-350 neutron generator at ORNL.

Figure 4. Photograph of the nGen-310 neutron generator tube (shown without the required control electronics module) from the Starfire data sheet [21].

An important and distinguishing capability of the nGen-350 is the neutron yield stabilization provided by the continuous feedback monitor installed in the unit. The stabilization mechanism consists of six RDT Domino® Solid-State Tile Detectors [22] arranged in an approximate "C" configuration about the generator tube and embedded in a 13 × 16 × 16 cm block of HDPE, which is in turn is surrounded by a layer of flex boron. The neutron detectors use a micro-structured semiconductor neutron detector (MSND®) technology with ^{6}Li Converter."

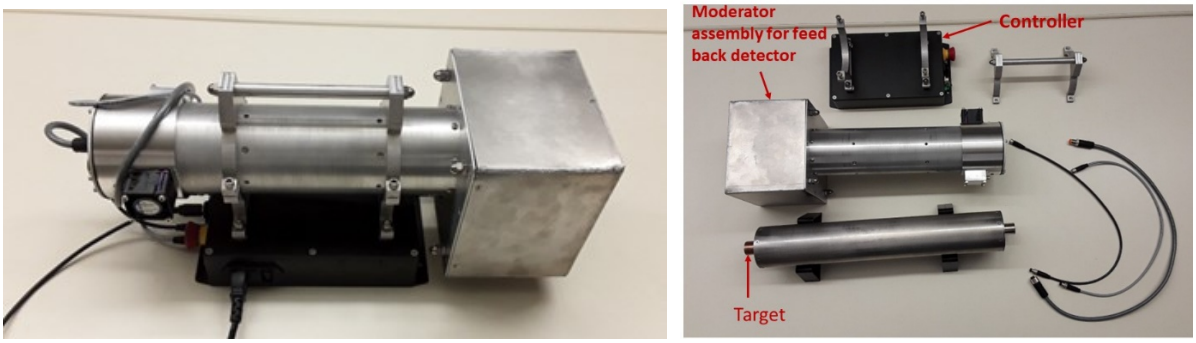

Figure 5. Photograph of the assembled nGen350 steady-state DD neutron generator (left) and disassembled (right).

Table 1. DD neutron generator vendor stated characteristics.

Generator Make/Model	ThermoFisher Scientific MP320 [14]	Starfire nGen350 [15]
Type of generator:	DD	DD
Maximum emission rate:	2×10^6 n/s	~1×10^6 n/s
Neutron energy:	2.48 MeV	2.48 MeV
Output stabilizer	NA	Active feedback (with external detector)
Stability		< 0.1% variation after warmup
Steady state/pulsed:	Both	Steady state only
Pulsed mode		
Frequency range:	250 Hz to 20 kHz	N/A
Duty cycle:	5%–100%, 5 µs minimum pulse width	N/A
Generator tube dimensions		
Diameter:	12.06 cm	9.0 cm
Length:	55.88 cm	50.0 cm
Target line:	13.97 cm	~1.5 cm
Weight	11.3 kg	11.45 kg

3. BENCHMARK MEASUREMENTS

No representative or surrogate fuel assemblies were available for performance testing at this stage of the project. Instead, benchmark measurements for the FNCL coupled with the Am(Li) source, the MP320, and the nGen-350 generators were performed using a series of low-enriched uranium and highly enriched uranium items to validate MCNP6 Version 1.0 [23] simulations for the fuel assemblies.

3.1 PASSIVE ISOTOPICS SOURCE MEASUREMENTS

3.1.1 Estimated Detection Efficiency

The detection efficiency is the product of the geometric efficiency, detector efficiency, and electronic cross-talk filter.

Geometric efficiency (solid angle): Each of the three FNCL detector panels includes four liquid scintillation detectors, each measuring 10 × 10 × 10 cm. The face of each panel is 12 cm from the center of the assay cavity. Each panel then provides a solid angle of 1.71 steradians or a geometric efficiency of 13.6% and for the collection of three panels, 40.8%.

Detector efficiency: In principle, a neutron of any energy can introduce a pulse in the detector electronics chain. However, a pulse height threshold and a Pulse Shape Discriminator (PSD) are both applied to the detector signal to reject electronic noise and gamma-ray events. In this case, the detector efficiency is primarily limited by the pulse height threshold. The typical electronic settings place the pulse height threshold sufficiently high that only a small fraction of the (α, n) neutrons emitted by Am(Li) are detected. Using the Geiger and Van der Zwaan representation of the Am(Li) neutron energy distribution, the pulse height threshold is set to the equivalent neutron energy of 1.1 MeV. With such a high energy threshold, only 70% of the spontaneous fission neutrons will be passed by the filter (Figure 6). The combination of solid angle and application of the pulse height threshold reduce the maximum expected detection efficiency for spontaneous fission neutrons to 28.5%.

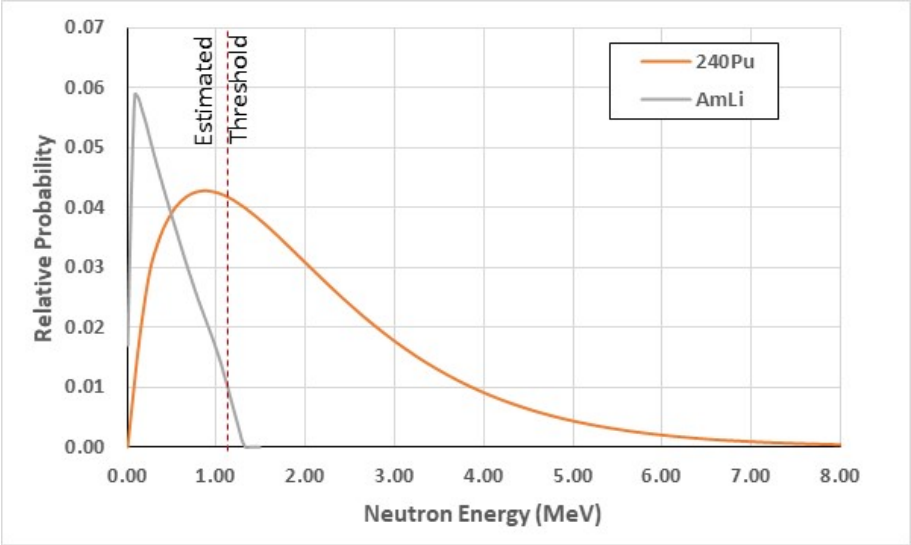

Figure 6. Comparison of the estimated pulse height threshold setting relative to the Am(Li) and ^{240}Pu fission neutron energy distributions.

An estimate of the neutron detection efficiency for ^{252}Cf and ^{240}Pu can be made using the Am(Li) measurement to estimate the neutron energy detection threshold, the Watt energy and the neutron multiplicity distributions. The surface area subtended by the four scintillator blocks comprising one side of the collar is 13.6%, so that the maximum theoretical detection efficiency of the detector arrangement is 41%. The observed neutron detection efficiency for the Am(Li) sources was 0.4%; corrected for the solid angle, the intrinsic Am(Li) detection efficiency is ~1%. Assuming the Geiger and Van der Zwaan energy distribution, the neutron energy threshold is approximately 1 MeV. Using the Watt neutron energy distribution for ^{252}Cf, we then estimate the intrinsic detection efficiency for ^{252}Cf spontaneous fission neutrons to be 70%. Combining this with the solid angle, we arrive at a ^{252}Cf detection efficiency of 28.5%. Because some fraction of the ^{252}Cf neutrons have sufficient neutron energy to be detected more than once by scattering from one detector into the next, the cross-talk filter must be applied.

Cross-talk filter: Following detection of a neutron within any detector within a panel (group of four detectors) the default implementation of the anti–cross talk filter in the FNCL rejects any subsequent neutron detected within the same panel during the anticoincidence time window (60 ns). Such that the anti-cross-talk filters allow a maximum of 1 neutron per fission event to be detected per detector panel or a maximum of 3 neutrons per fission event. This leads to an effective reduction in neutron detection efficiency with increasing nu-bar or highly multiplying events.

To illustrate this effect, consider a fission event emitting three neutrons. The detection efficiency for the first neutron is $3 \times 0.136 \times 0.7 = 0.285$, while for the 2nd neutron, the detection efficiency is reduced by one panel to $2 \times 0.136 \times 0.7 = 0.190$, and for the 3rd neutron, the detection efficiency is reduced by $1 \times 0.136 \times 0.7 = 0.095$. The probability of detecting the three neutron event is $0.285 \times 0.190 \times 0.095 = 0.005$. (If it were possible to operate without the cross-talk filter, the detection efficiency for the three neutron event would be $0.285^3 \times 11/12 \times 10/12 = 0.016$ or three times greater.) The impact of the filter on the ^{240}Pu and ^{252}Cf spontaneous fission multiplicity distributions results in the expected neutron detection efficiency for ^{240}Pu of 0.20 and for ^{252}Cf of 0.15.

3.1.2 Initial Passive Measurements

Initial measurements included examination of the passive response of the FNCL to ^{252}Cf, ^{240}Pu, and Am(Li). Table 2 provides the measurement results from several isotopic sources positioned in the center

of the assay volume. These measurements were repeated but with the source placed inside a lead pig (wall thickness ~1 cm) to examine the gamma-ray sensitivity of the FNCL. Comparison of the measured apparent detection efficiency based on the singles rates with the expected efficiency results shows a significant discrepancy in the ^{252}Cf efficiency.

Table 2. FNCL passive measurement results (count time = 300 s).

	Source Yield (n/s)	Singles Rate (cps)	Doubles (1/s)	Simple Efficiency (%)	Certificate Free Efficiency (%)
Empty Cavity	0	17.2 ± 0.8	4.9 ± 0.4	—	—
Cf-6081	111,191 ± 1112	32,348.4 ± 36.0	5,769.6 ± 15.6	29.1 ± 0.3	11.79 ± 0.03
Cf-5442	65,221 ± 653	19,662.0 ± 27.6	3,376.8 ± 11.6	30.1 ± 0.6	11.36 ± 0.04
Cf-7007	10,516 ± 106	3,126.6 ± 11.2	558.8 ± 4.7	29.7 ± 0.6	11.82 ± 0.11
^{240}Pu (14.9 g)	17,566 ± 176	3,692.4 ± 12.0	580.8 ± 4.8	21.0 ± 0.2	20.9 ± 0.19
Am(Li)	48,600 ± 1,458	201.7 ± 2.9	11.4 ± 6.7	0.4 ± 0.0	—
Repeat measurements with source placed inside a lead pig					
Empty Cavity	0	17.2 ± 0.8	4.9 ± 0.4	—	—
Cf-6081	111,191 ± 1,112	27,333.6 ± 33.6	5,320.8 ± 14.4	24.6 ± 0.2	12.87 ± 0.04
Cf-5442	65,221 ± 653	18,141.6 ± 26.4	3,473.3 ± 11.8	27.8 ± 0.6	12.66 ± 0.05
Cf-7007	10,516 ± 106	2,712.0 ± 10.4	539.3 ± 4.7	25.8 ± 0.5	13.15 ± 0.13
^{240}Pu (14.9 g)	17,566 ± 176	3,011 ± 109	521.2 ± 4.6	17.1 ± 0.6	23.00 ± 0.86
Am-5468	48,600 ± 1,458	138.8 ± 2.4	9.4 ± 0.6	0.3 ± 0.0	—

Note: An oddity of the FNCL analysis software is that count rates are reported as an average over the 12 detector modules rather than as the sum. The values presented in each of the tables in this work represent the summed rates.

Normally, the detection efficiency would be determined simply by dividing the measured singles rates by the item's neutron emission rate. However, the ^{252}Cf results differed significantly from the expected values. For low multiplication items, the multiplicity point model equation can be solved to allow for an efficiency determination without knowing the fissile mass of the item:

$$\varepsilon = \frac{2}{f_d}\frac{\overline{\nu_{s1}}}{\overline{\nu_{s2}}}\cdot\frac{D}{S}\cdot(1+\alpha)$$

For the ^{252}Cf sources, the value of $\alpha = 0$, the value of α for the ^{240}Pu source has been previously determined to be 0.11.

The detection efficiency for both the simple and certificate-free efficiencies are provided in Table 2. The ^{240}Pu measurements provide self-consistent efficiencies and agree with the expected values. The ^{252}Cf results indicate that the measured value for the singles rates are higher than expected. It is apparent that the pulse shape discrimination is not adequately rejecting the gamma-ray contribution as currently configured. However, based on the ^{240}Pu result, the expected detection efficiency for induced fission neutrons from ^{235}U will be 19.2%. It is also noted that the detection efficiency for Am(Li) neutrons is less than 1% such that the interrogation source introduces only a minimal interference to the coincidence assay.

3.2 AM(LI) ISOTOPICS SOURCE MEASUREMENTS

An example of the testing arrangement of the FNCL using Am(Li) interrogation sources is illustrated in Figure 7. The uranium oxide standards were placed on a low mass stand at the vertical center of the assay cavity.

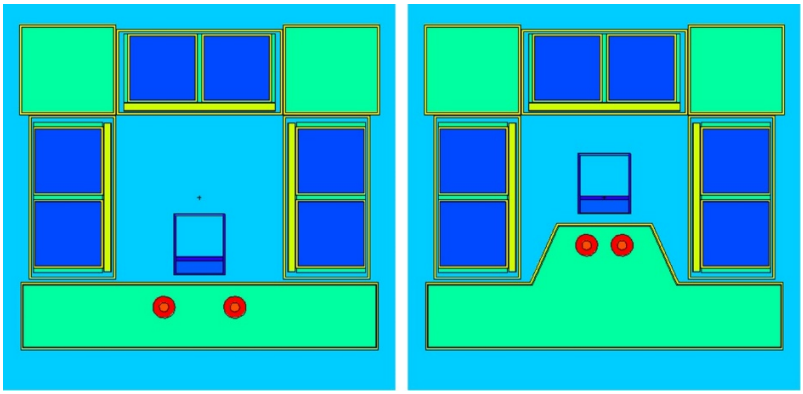

Figure 7. Illustration of the measurement arrangement of the uranium oxide containers in the FNCL using Am(Li) isotopic interrogation sources with the FNCL in the pressurized water reactor (left) and boiling water reactor (right) configurations.

The performance of the FNCL in active mode was first examined using two Am(Li) neutron sources with a combined yield of approximately 98,000 n/s. The assays consist of a passive measurement followed by the active measurement, and each has a duration of 300 s. Table 3 provides a comparison of the measurement and predicted coincidence rates for the New Brunswick Laboratory (NBL) container measurements using Am(Li) sources with the flat active panel shown in Figure 7. Similar measurements using a standard UNCL have been previously performed [5]. Comparison with the earlier measurements confirms the improvement in measurement precision gained by use of the scintillation detectors. For these simple container measurements, equivalent measurement precision was achieved by the FNCL in 1/12th the time required by the UNCL measurement. A plot of the net doubles rates as a function of ^{235}U mass is shown in Figure 8.

Table 3. FNCL active measurement results for the Am(Li) interrogating neutron sources [2].

	Approx. Yield (n/s)	Mass ^{235}U (g)	Measured Rates						Simulated	
			Singles (cps)		Doubles (1/s)		Net Doubles (1/s)		Doubles (1/s)	
Empty	10^5	0.0	161.3	± 2.7	5.3	± 0.7	—	—	—	—
Blank Can	10^5	0.0	159.2	± 2.8	4.5	± 0.8	−0.8	± 1.0	—	—
Can1	10^5	39.2	184.0	± 3.0	9.3	± 0.9	4.0	± 1.1	4.8	± 0.1
Can2	10^5	102.1	223.7	± 3.2	17.6	± 1.0	12.3	± 1.2	10.4	± 0.1
Can3	10^5	183.7	256.9	± 3.5	22.0	± 1.1	16.7	± 1.3	16.1	± 0.1

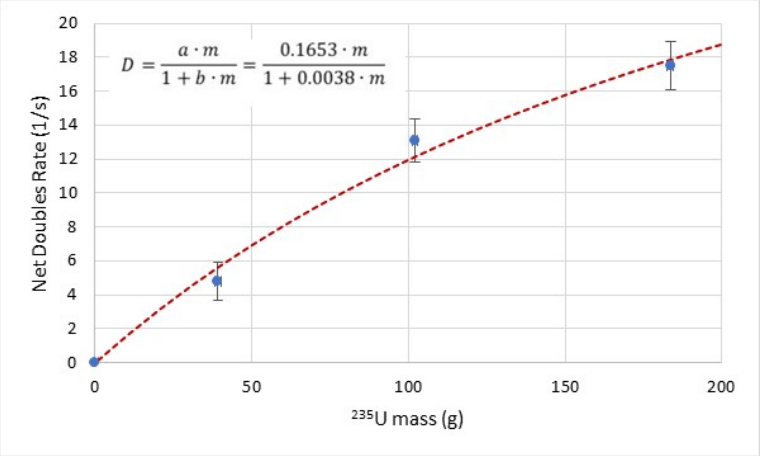

Figure 8. FNCL Am(Li) induced net doubles rate as a function of ^{235}U mass.

3.3 MP320 NEUTRON GENERATOR MEASUREMENTS

The testing arrangement of the MP320/FNCL combination is illustrated in Figure 9. The MP320 has been mounted in an HDPE adapter assembly to position the neutron production target line at the vertical midpoint of the FNCL. The module also affords a degree of personnel shielding and houses a ^{3}He flux monitor tube. The ^{3}He flux monitor is positioned behind the generator to minimize detection of neutrons emitted or scattered from the assay cavity.

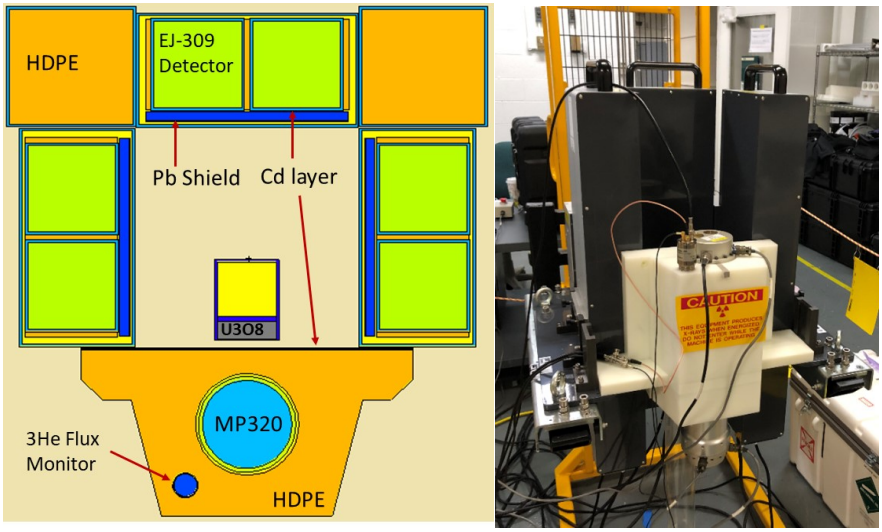

Figure 9. Screenshot of the MCNP input file for the MP320/FNCL test configuration for small containers (left) and a photograph of the assembled FNCL with the MP320. The cylindrical U_3O_8 items have been laid on their sides.

The same measurements performed to characterize the Am(Li)/FNCL system were also performed for the MP320/FNCL combination. The same standards, geometries, and count times were used to simplify the comparison. Examples of the initial active measurement using the MP320 generator are presented in Table 4. A plot of the net doubles rates as a function of ^{235}U mass is shown in Figure 10. The ^{3}He flux monitor was used to normalize the measured FNCL singles and doubles rates.

Table 4. FNCL active measurement results for the MP320 neutron generator (300 s active measurement) [2].

	Approx. Yield (n/s)	Mass ^{235}U (g)	Normalized Rates						Simulated Rates	
			Singles (cps)		Doubles (1/s)		Net Doubles (1/s)		Singles (1/s)	Doubles (1/s)
Blank	1.4×10^6	0.0	30,673	± 35	3957.0	± 12.0	—		31,216	0.0
Can1	1.4×10^6	39.2	31,085	± 35	3979.6	± 12.0	22.6	± 12.0	31,986	28.5
Can2	1.4×10^6	102.1	32,102	± 36	4001.3	± 12.0	44.3	± 12.0	32,086	53.3
Can3	1.4×10^6	183.7	32,240	± 35	4016.6	± 12.0	59.6	± 12.0	32,196	79.3
Can4	1.4×10^6	3.9	25,980	± 32	3501.7	± 10.4	−455.3	± 10.4	31,915	8.6
Can5	1.4×10^6	5.9	30,814	± 36	3912.8	± 10.4	−44.1	± 10.4	31,917	9.7

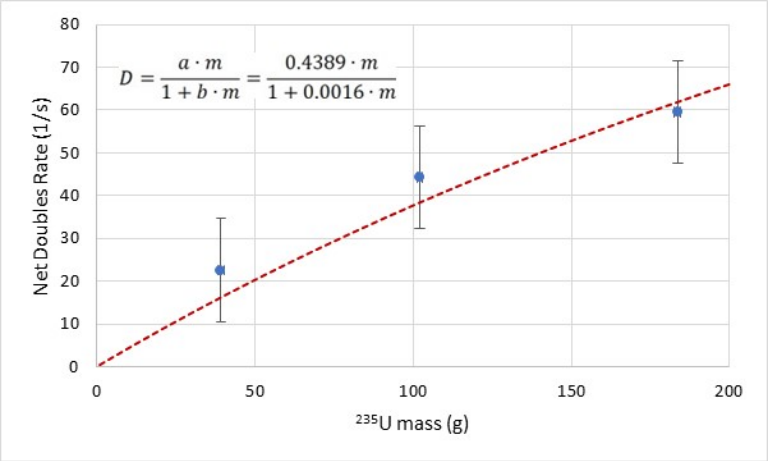

Figure 10. FNCL MP320 induced net doubles rate as a function of ^{235}U mass for the highly enriched uranium containers (points represent a single 5 minute active measurement).

Calculation of the net doubles rate for the development of a calibration curve was complicated by the magnitude and variability of the coincidence background. Assay of a measurement blank was required to provide a proper measurement reference for subtraction of the large active background doubles rates. In addition, it was necessary to normalize the measured rates to account for drifting of the MP320 neutron output and separately subtract the accidental coincidence contribution as it varies from run to run. This analysis is not currently implemented within the FNCL operating software and is performed offline.

With the MP320 generator producing ~1.4×10^6 n/s, a coincidence background of 300 cps/detector was observed. From the observed singles rates, the 60 ns coincidence gate would produce an accidental coincidence contribution to the background doubles rate of 10–20 cps/detector. Most of the background coincidence rate is believed to be caused by multiple detections of a given neutron. We are presently evaluating the effectiveness of the FNCL cross-talk filter and methods to reduce the large coincidence background. During this evaluation, we also noted some data acquisition issues with the system; for instance, 1 or more of the 12 detectors may occasionally drop out, leading to unpredictable count rates. An example of such an occurrence is included in Table 5 to illustrate the impact on the measurement.

3.4 NGEN-350 NEUTRON GENERATOR MEASUREMENTS

The FNCL measurement performance for the uranium oxide containers was examined using a variety of moderating (HDPE) and reflective (e.g., lead, steel) materials placed between the FNCL and the neutron generator. Initially, the intent of these measurements was simply to provide benchmark measurements for

the MCNP modeling campaign; however, these measurements later became more focused on reduction of gamma-ray and cross-talk interferences. The measurement configuration is illustrated in Figure 11.

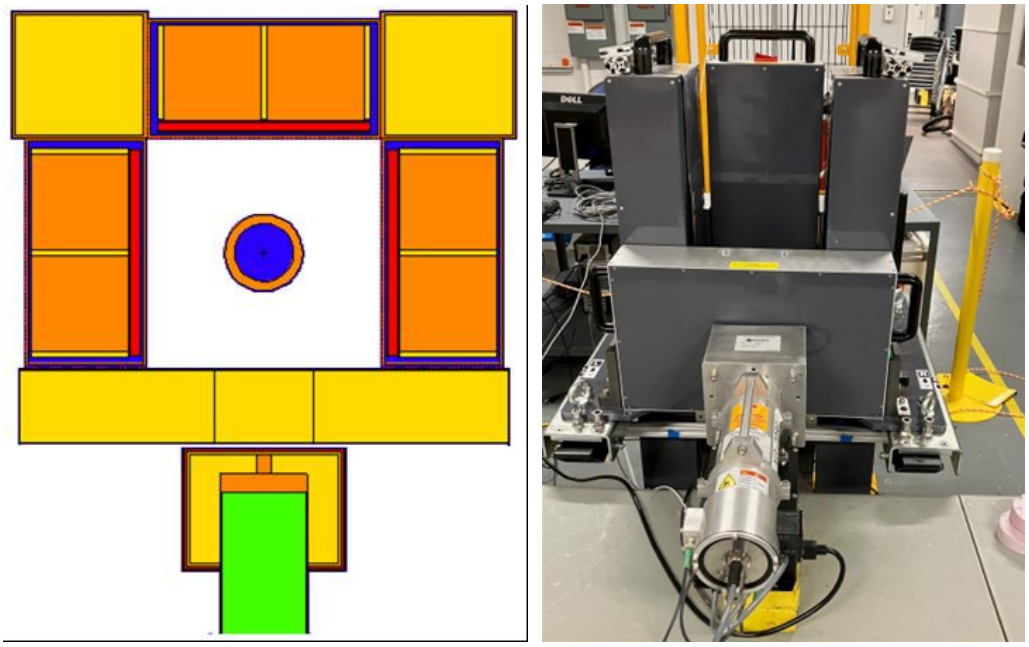

Figure 11. Screenshot of the MCNP input file for the nGen-350/FNCL test configuration for small containers (left) and a photograph of the assembled FNCL with the nGen-350 during initial testing. The cylindrical U_3O_8 items have been mounted vertically within the assay cavity center.

Measurements were performed for various thicknesses (from 1.27 to 10 cm) of HDPE placed between the generator and assay cavity. Figure 11 shows an example where the 10 cm (4 in.) thick HDPE source holder slab was used to moderate the interrogating neutron flux in an attempt to reduce the cross-talk doubles rate and to shield the FNCL detector slabs from any X-rays produced by the generator.

Table 5. FNCL active measurement results for the nGen-350 neutron generator (300 s active measurement).

	Empty		Can 1		Can 2		Can 3	
Day	Singles	Doubles	Singles	Doubles	Singles	Doubles	Singles	Doubles
1	17,849 ± 8	39.7 ± 3	17,692 ± 8	49.9 ± 3	17,909 ± 8	56.1 ± 3	18,208 ± 8	61.7 ± 3
2	18,328 ± 8	40.4 ± 3	17,897 ± 8	48.2 ± 3			18,238 ± 8	57 ± 3
3	18,266 ± 8	40 ± 3	17,845 ± 8	48 ± 3			18,242 ± 8	58.5 ± 3
4	18,296 ± 8	40.1 ± 3	17,975 ± 8	48.3 ± 3			†17,079 ± 8	45.7 ± 3
5	18,377 ± 8	40.1 ± 3	17,998 ± 8	48.5 ± 3			18,266 ± 8	58.2 ± 3
6	18,399 ± 8	41.3 ± 3	17,929 ± 8	47.9 ± 3			18,367 ± 8	58.7 ± 3
7	18,430 ± 8	40.6 ± 3	17,956 ± 8	48.2 ± 3			18,261 ± 8	58.5 ± 3

† Impact of detector drop out.

Table 5. FNCL active measurement results for the nGen-350 neutron generator (300 s active measurement) (continued).

Day	Empty		Can 1		Can 2		Can 3	
	Singles	Doubles	Singles	Doubles	Singles	Doubles	Singles	Doubles
8	18,414 ± 8	40.8 ± 3	17,968 ± 8	47.8 ± 3			18,277 ± 8	57.6 ± 3
9	18,443 ± 8	40.7 ± 3	17,957 ± 8	48.1 ± 3			18,327 ± 8	57.6 ± 3
10	18,440 ± 8	40.9 ± 3	18,053 ± 8	48.2 ± 3			18,435 ± 8	58.3 ± 3
11	18,429 ± 8	40.8 ± 3	17,982 ± 8	48 ± 3			18,349 ± 8	57.6 ± 3
12	18,530 ± 8	41.2 ± 3	18,077 ± 8	48.7 ± 3	15,275 ± 8	34.7 ± 3	18,405 ± 8	58.7 ± 3
13	18,462 ± 8	41.3 ± 3	17,994 ± 8	48.6 ± 3	18,193 ± 8	54.1 ± 3		
14	18,411 ± 8	40.8 ± 3	18,039 ± 8	48.7 ± 3	18,240 ± 8	54.9 ± 3	18,440 ± 8	58.1 ± 3
15	18,321 ± 8	40.3 ± 3			18,048 ± 8	54.1 ± 3		
16	18,253 ± 8	40 ± 3			17,936 ± 8	53.1 ± 3		

Table 6. FNCL average of the active measurement results for the nGen-350 neutron generator (300 s active measurement).

	Approx. Yield (n/s)	Mass ^{235}U (g)	Normalized Rates						Simulated Rates	
			Singles (cps)		Doubles (1/s)		Net Doubles (1/s)		Singles (1/s)	Doubles (1/s)
Blank	1.0×10^6	0.0	18,353	± 39	40.56	± 0.12			17,875	0
Can1	1.0×10^6	39.2	17,954	± 26	48.36	± 0.14	7.80	± 0.19	18,352	11.5
Can2	1.0×10^6	102.1	18,065	± 66	54.46	± 0.50	13.90	± 0.51	18,396	15.8
Can3	1.0×10^6	183.7	18,318	± 23	58.37	± 0.34	17.81	± 0.36	18,261	18.2

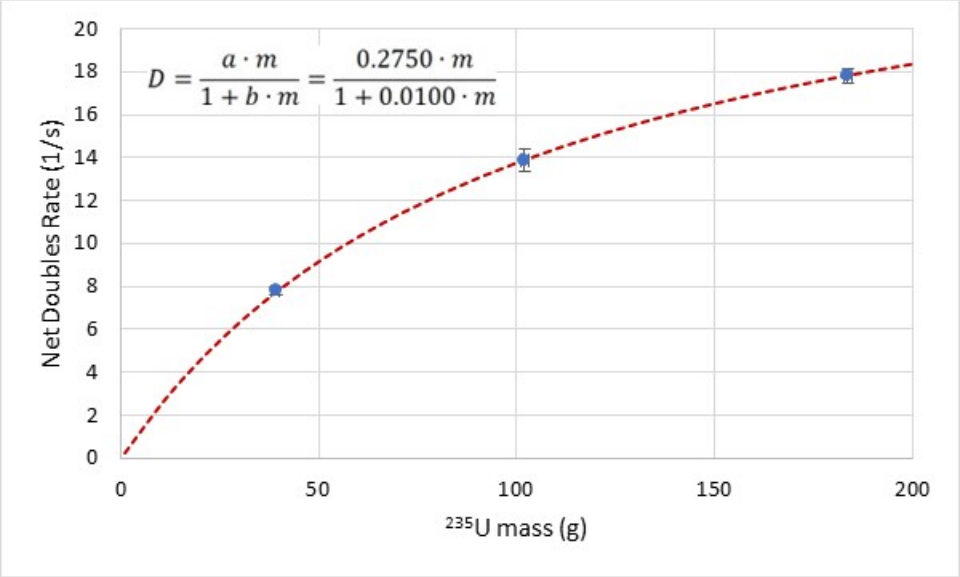

Figure 12. FNCL nGen-350 induced net doubles rate as a function of ^{235}U mass for the highly enriched uranium containers.

4. SIMULATED ASSEMBLIES FOR THE MCNP PERFORMANCE STUDY

To provide a performance comparison between the standard UNCL and the FNCL with a DD generator, both configurations were modeled using MCNP6 Version 1.0 [23]. The performance of these systems was examined using the same series of simulated fuel assemblies as detailed for use in a recent comparison of alternative neutron detector techniques [11].[1] These assembly definitions are somewhat crude (lacking structural elements, and some material densities differ from true assemblies) but are sufficient to demonstrate relative performance of the DD/UNCL compared to the standard unit. The fuel assembly test cases include:

- Eight calibration assemblies, each a 17 × 17 array with 264 fuel pins and 25 cooling channels. The ^{235}U enrichment was varied to provide linear mass densities 15–65 g ^{235}U/cm.
- Twelve assorted fuel configurations consisting of 14 × 14, 15 ×15, 16 × 16, and 17 × 17 intact arrays.
- Three sets of six assemblies, each a 17 × 17 array, containing differing numbers of burnable poison rods of varying composition.
- Six "partial defect" assemblies, each a 17 ×17 array, substituting depleted uranium (DU) rods for an increasing number of fuel pins.

The simulated fuel assemblies used in this study are described in the following sections.

4.1 DESCRIPTION OF THE SIMULATED CALBRATION ASSEMBLIES

The comparison between the Am(Li) and DD generator performance included simulations of 8 17 × 17 fuel assemblies consisting of 264 fuel pins and 25 empty fuel guide tubes (Figure 13). For each assembly, the ^{235}U enrichment varied while all other parameters remained unchanged (Table 7). Each assembly was 300 cm in length.

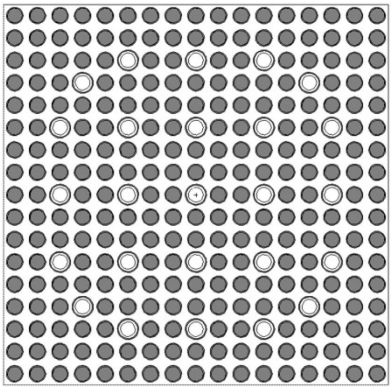

Figure 13. Cross sections of the mock calibration fuel assemblies generated from the MCNP input files. The 17 × 17 assemblies consist of 264 fuel pins and 25 empty guide tubes.

[1] This description of the simulated fuel assemblies was taken from a prior DD neutron collar evaluation [13].

Table 7. Input parameters for the 17 × 17 calibration assemblies.

Assembly	Cal 1	Cal 2	Cal 3	Cal 4	Cal 5	Cal 6	Cal 7	Cal 8
Grid	17 × 17	17 × 17	17 × 17	17 × 17	17 × 17	17 × 17	17 × 17	17 × 17
Fuel pins	264	264	264	264	264	264	264	264
Array size (cm)	21.4	21.4	21.4	21.4	21.4	21.4	21.4	21.4
Pellet density (g/cm^3)	10.41	10.41	10.41	10.41	10.41	10.41	10.41	10.41
Pellet OD (cm)	0.8255	0.8255	0.8255	0.8255	0.8255	0.8255	0.8255	0.8255
Cladding OD (cm)	0.95	0.95	0.95	0.95	0.95	0.95	0.95	0.95
Cladding thickness (cm)	0.057	0.057	0.057	0.057	0.057	0.057	0.057	0.057
Enrichment (%)	1.16	1.54	1.93	2.70	3.47	4.24	4.63	5.01
Linear density (g ^{235}U/cm)	15.05	19.97	25.02	35.01	44.99	54.98	60.02	64.95

4.2 DESCRIPTION OF THE ASSORTED INTACT FUEL ASSEMBLIES

The UNCL is generally calibrated using a single set of assemblies, and this calibration is applied to other assemblies by application of appropriate correction factors [13]. This collection of 12 assemblies consists of various configurations, which serve to evaluate the effectiveness of the heavy metal correction factor (Figure 14). The 12 assemblies include 14 × 14, 15 × 15, 16 × 16, and 17 × 17 arrays with various arrangements of empty channels. The parameters for these assemblies are provided in Table 8.

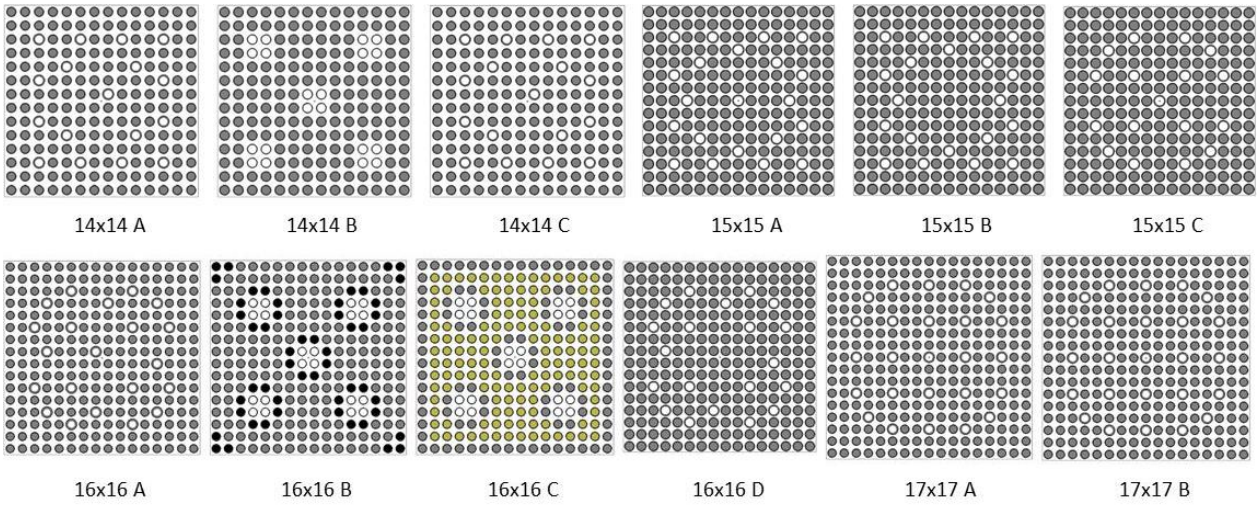

Figure 14. Cross sections of the mock intact fuel assemblies generated from the MCNP input files.

Table 8. Input parameters for the various intact fuel assemblies.

Assembly	14×14 A	14×14 B	14×14 C	15×15 A	15×15 B	15×15 C	16×16 A	16×16 B	16×16 C	16×16 D	17×17 A	17×17 B
Grid:	14 × 14	14 × 14	14 × 14	15 × 15	15 × 15	15 × 15	16 × 16	16 × 16	16 × 16	16 × 16	17 × 17	17 × 17
Array size (cm)	19.7	20.6	19.7	21.4	21.5	21.7	19.7	20.7	20.7	22.96	21.4	21.4
Pellet density (g/cm^3)	10.42	10.44	10.42	10.64	10.45	10.52	10.42	10.42	10.42	10.5	10.52	10.52
Pellet OD (cm)	0.875	0.968	0.875	0.929	0.911	0.940	0.784	0.819	0.819	0.911	0.819	0.819
Cladding OD (cm)	1.016	1.118	1.016	1.072	1.075	1.09	0.914	0.95	0.95	1.075	0.95	0.95
Cladding (cm)	0.062	0.066	0.062	0.062	0.073	0.064	0.057	0.057	0.057	0.073	0.057	0.057
Fuel pins 1	179	176	179	204	205	208	235	184	136	236	264	264
Enrichment type	3.80	3.13	2.00	4.50	5.00	4.55	4.50	4.50	2.92	4.50	3.22	4.20
Fuel pins 2								52	100			
Enrichment								4.00	2.42			
Linear density (g U/cm)	989	1,192	989	1,297	1,231	1,339	1,042	1,115	1,060	1,424	1,282	1,305
Linear density (g ^{235}U/cm)	37.57	37.31	19.77	58.37	61.54	60.91	46.89	50.13	30.93	64.08	41.54	54.19

4.3 DESCRIPTION OF THE ASSEMBLIES CONTAINING BURNABLE POISON RODS POISON RODS

To examine the impact of burnable poison rods on the performance of the UNCL, 18 different loadings of gadolinium were simulated. The 18 configurations included 6 different configurations of increasing numbers of poison rods, each at 3 different gadolinium loadings. The details of the assemblies are listed in Table 9. The different configurations are designated by the number of poison rods and the gadolinium weight percentage. For example, BF6_4 indicates an assembly containing four burnable poison rods, each containing 6 w% gadolinium. The ^{235}U linear density for each of the burnable poison cases is shown in Table 10.

Table 9. Input parameters for the burnable poison fuel assemblies. The designation designator, n, in each assembly name represents the gadolinium content in wt% for each of the three gadolinium loadings (e.g., BP6-4 indicates 6 gadolinium wt% with four poison rods).

Assembly	BPn_4	BPn_8	BPn_12	BPn_16	BPn_20	BPn_24
Grid	17 × 17	17 × 17	17 × 17	17 × 17	17 × 17	17 × 17
Array size (cm)	21.4	21.4	21.4	21.4	21.4	21.4
Pellet density (g/cm^3)	10.41	10.41	10.41	10.41	10.41	10.41
Poison density (g/cm^3)	10.21	10.21	10.21	10.21	10.21	10.21
Pellet OD (cm)	0.8255	0.8255	0.8255	0.8255	0.8255	0.8255
Cladding OD (cm)	0.95	0.95	0.95	0.95	0.95	0.95
Cladding thickness (cm)	0.057	0.057	0.057	0.057	0.057	0.057
Fuel pin enrichment (%)	4.00	4.00	4.00	4.00	4.00	4.00
Poison rod enrichment (%)	2.60	2.60	2.60	2.60	2.60	2.60
Fuel pins	260	256	252	248	244	240
Poison rods	4	8	12	16	20	24
Linear density (g ^{235}U/cm)	51.54	51.22	50.90	50.58	50.26	49.94

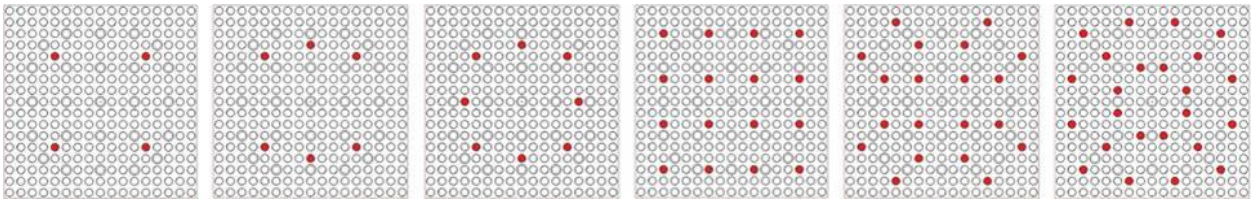

Figure 15. Distribution of the poison rods (red circles) within the simulated 17 ×17 fuel assemblies. *From left to right*, the assemblies contain 4, 8, 12, 16, 20, and 24 burnable poison rods.

Table 10. ^{235}U linear density for the poison rod configurations.

Gd content (wt%)	BPn-4	BPn-8	BPn-12	BPn-16	BPn-20	BPn-24
6	51.54	51.22	50.90	50.58	50.26	49.94
8	51.53	51.20	50.87	50.54	50.20	49.87
10	51.52	51.17	50.83	50.49	50.15	49.80

4.4 DESCRIPTION OF THE ASSEMBLIES FOR PARTIAL DEFECT ANALYSIS

To examine the response of the collar for partial defect analysis, a series of six simulated fuel assemblies were configured with an increasing number of DU rods substituted for fuel rods (Figure 16). The reference assembly has the same configuration as the calibration simulation CAL-6. The simulations will determine whether the DD/UNCL is more or less sensitive to substitution than the traditional collar. The assembly parameters are summarized in Table 11.

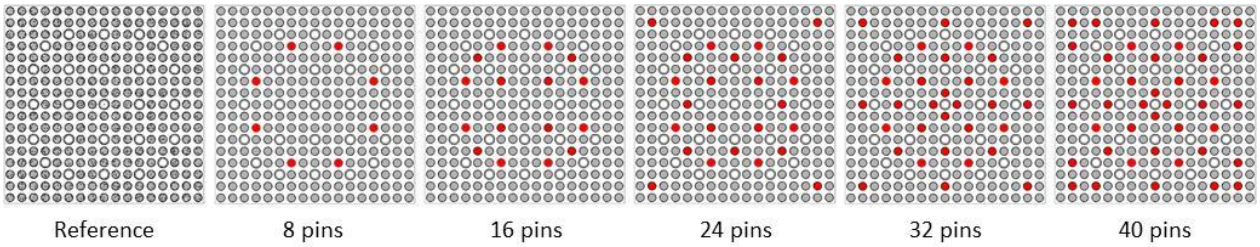

Figure 16. Distribution of the DU pins (red) within the simulated 17 × 17 assembly.

Table 11. Input parameters for the fuel assemblies for partial defect analysis.

Assembly	PD-0	PD-8	PD-16	PD-24	PD-32	PD-40
Grid:	17 × 17	17 × 17	17 × 17	17 × 17	17 × 17	17 × 17
Array size (cm)	21.4	21.4	21.4	21.4	21.4	21.4
Pellet density (g/cm^3)	10.41	10.41	10.41	10.41	10.41	10.41
Pellet OD (cm)	0.8255	0.8255	0.8255	0.8255	0.8255	0.8255
Cladding OD (cm)	0.95	0.95	0.95	0.95	0.95	0.95
Cladding thickness (cm)	0.057	0.057	0.057	0.057	0.057	0.057
Fuel pin enrichment (%)	4.24	4.24	4.24	4.24	4.24	4.24
DU rod enrichment (%)	0.20	0.20	0.20	0.20	0.20	0.20
Fuel pins	264	256	248	240	232	224
DU rods	0	8	16	24	32	40
Linear density (g ^{235}U/cm)	54.97	53.38	51.80	50.21	48.62	47.03

5. EXPECTED PERFORMANCE FOR FUEL ASSEMBLIES

Despite the challenges of the benchmarking measurements and the conclusion that modifications to the neutron generator interface modules will be required, it is still instructive to examine the potential performance of the DD/FNCL for the measurement of fresh fuel assemblies. The simulated assay using the FNCL of a collection of 15 × 15 and 17 × 17 light water fuel assemblies was modeled using MCNP [23]. The differences in the neutron interrogation configurations are shown in Figure 17. The Am(Li) source holder and MP320 interface module represent the existing instrumentation, although the nGen350 module is notional and configured to provide minimal moderation to the interrogating flux. The nGen350 interface module will be significantly altered from this simplistic model.

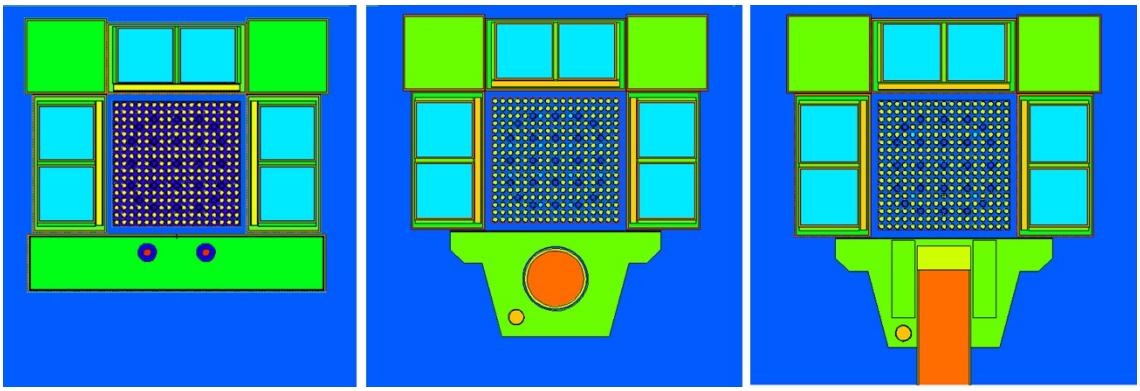

Figure 17. Illustration of the three active interrogation configurations considered for this preliminary analysis using Am(Li) isotopic sources (left), the MP320 DD generator (middle), and the nGen350 DD generator (right).

It is important not only to understand the expected detection efficiencies and count rates from the assay system, but also to understand the response uniformity and how penetrating the measurement is. Figure 18 presents the fission maps (the fission rate from each fuel pin was determined and plotted as a function of position within the assembly) for a 17 × 17 pin fuel assembly with ^{235}U linear density of 65 g/cm. This figure illustrates that placement of the neutron emission point in close proximity to the assembly as with the nonoptimized nGen350 model results in a very localized interrogation of the assembly and that a standoff distance of several centimeters will be necessary.

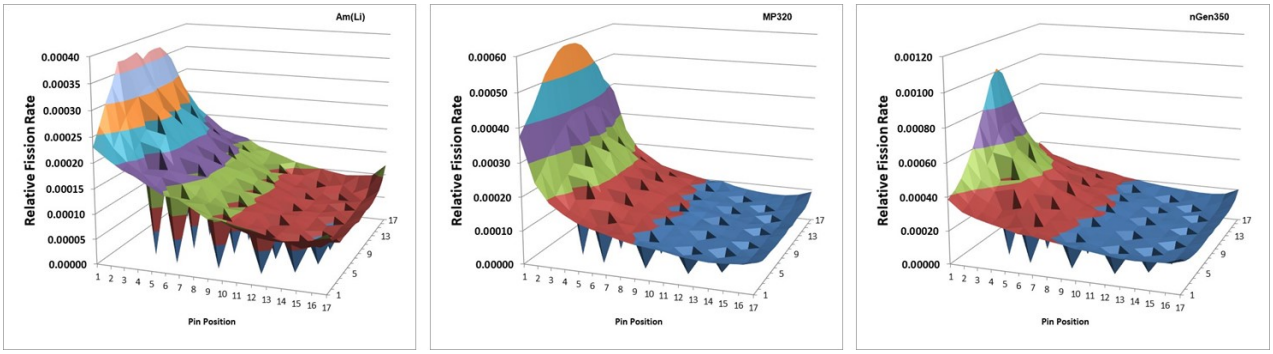

Figure 18. Comparison of the total induced fission rates as a function of pin position within a 17 × 17 fuel assembly from an Am(Li) isotopic (left), MP320 DD neutron generator (middle), and the nGen350 DD neutron generator (right).

From these simulations, basic response functions relating the coincidence rate and the linear density of the fuel assemblies can be constructed. As an example, Figure 19 provides a comparison of the simulated

response function for the MP320/FNCL system with a measured UNCL fast mode calibration. The slope of the MP320/FNCL response is not as steep as the UNCL response because of the increased sensitivity to ^{238}U when using the DD generator. Based on the response curve and simulations for a variety of other poisoned and non-poisoned assemblies, the MP320/FNCL can be expected to perform as well as the Am(Li)-based measurement system in terms of measurement precision. The measurement interferences discussed above will have to be addressed to exceed that performance.

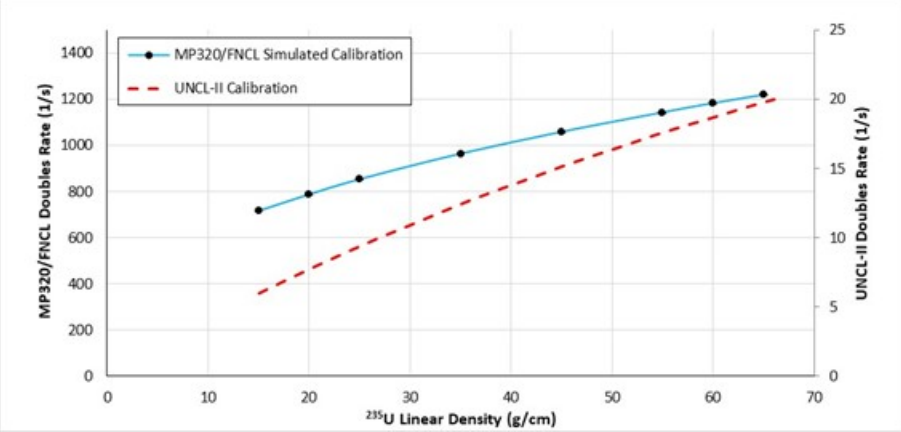

Figure 19. Comparison of the MP320/FNCL simulated response as a function of ^{235}U content (neutron yield 1.4E6 n/s) with the measured response of the traditional fast mode Am(Li) UNCL system.

Because the DD generator emits 2.48 MeV neutrons, we expect a greater sensitivity to the ^{238}U component of the items than when using Am(Li). On a per gram basis, even with the 2.48 MeV interrogating neutrons, the ^{235}U fission signal is 14 times greater than that of ^{238}U. However, for the low-enriched fuel assemblies of interest, the ^{238}U mass is 20 times greater than that of the ^{235}U, and the contribution to the observed doubles rates will be comparable. Various moderator/absorber combinations are under investigation to attempt to tailor the interrogating neutron energy distribution to reduce the sensitivity to ^{238}U. Table 12 compares the estimated relative fission rates for a variety of items and enrichments for the FNCL and UNCL, illustrating the need to lower the interrogating neutron energy.

Table 12. Uranium-238 fraction of total fission event rate.

Item	Enrichment (%)	Interrogating Source/System		
		Am(Li)/FNCL	MP320/FNCL	Am(Li)/UNCL
Can4	2	0.022	0.745	
Can1	20	0.011	0.227	
Can2	52	0.004	0.067	
Can3	93	0.000	0.006	
17 × 17 array, 20 g ^{235}U/cm	1.54	0.089	0.537	0.118
17 × 17 array, 60 g ^{235}U/cm	4.63	0.082	0.373	0.089

The distributions of fission events as a function of pin position within a fuel assembly are shown in Figure 20. The Am(Li) interrogation induces relatively few ^{238}U fission events and a relatively uniform interrogation of the fuel assembly. Because there is insufficient moderation of the interrogating neutron flux, the two DD generator configurations produce significantly more ^{238}U fission events than the Am(Li) sources. This figure also illustrates that direct interrogation of the fuel assembly with the nGen-350 without any flux tailoring or standoffs results in a very non-uniform interrogation of the assembly. To

minimize the ^{238}U sensitivity relative to the ^{235}U sensitivity of the nGen-350/FNCL combination a series of MCNP simulations were performed where varying amounts of moderating/reflecting materials were placed between the generator and the FNCL.

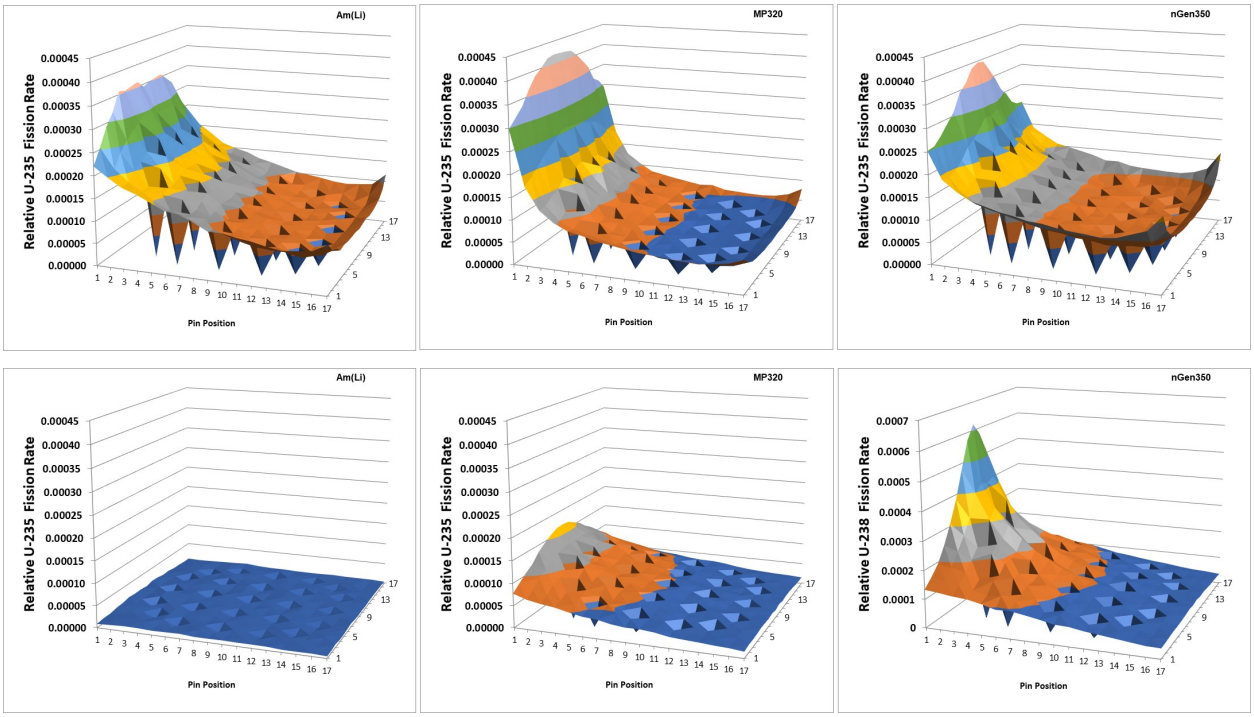

Figure 20. Fission maps for a 17 × 17 fuel assembly for the different neutron interrogation sources considered for the FNCL. The top row shows the maps for fission in induced in ^{235}U, and the bottom row shows the maps for fission induced in ^{238}U. Note, the change in scale for the unoptimized nGen350 simulations.

5.1 OPTIMIZATION OF THE FNCL/NGEN-350 RESPONSE

The objective of the optimization is to reduce the relative fission rate of ^{238}U without increasing the sensitivity to gadolinium poison rods. Ideally, it would be desirable to reduce the interrogating 2.5 MeV neutron energy to less than the ^{238}U fission threshold energy of approximately 1 MeV (Figure 21).

Efforts to optimize the interrogation of the fuel assemblies examined various thicknesses and combinations of HDPE, HDPE with a cadmium outer layer, borated plastic, Teflon, graphite, nickel, steel, and lead. For practicality, the maximum thickness of the flux-tailoring module was limited to 10 cm. Beyond this thickness, the module becomes excessively heavy (>20 kg) and unwieldy. In the optimization process we examined the following:

- **Singles rates:** Minimize the singles rate to minimize accidentals coincidence rate. The FNCL detectors operate with a 60 ns coincidence gate width; at count rates above 13,000 cps the accidentals coincidence rate begins to exceed 1/s.

- **^{238}U Sensitivity:** Minimize the relative ^{238}U/^{235}U induced fission rate and minimize the average fast neutron energy within the assay volume.

- **Spatial uniformity:** Minimize spatial dependence of the active neutron response (the product of the detection efficiency and induced fission rate as a function of pin position).

- Minimize sensitivity to poison rods.

- **Doubles rate precision:** Equal or exceed the measurement precision provided by the FNCL/Am(Li) source measurement.

Unfortunately, for the FNCL application, there is no practical, effective flux-tailoring method that does not also result in significant production of thermal and epithermal neutrons that will increase the sensitivity to poisons.

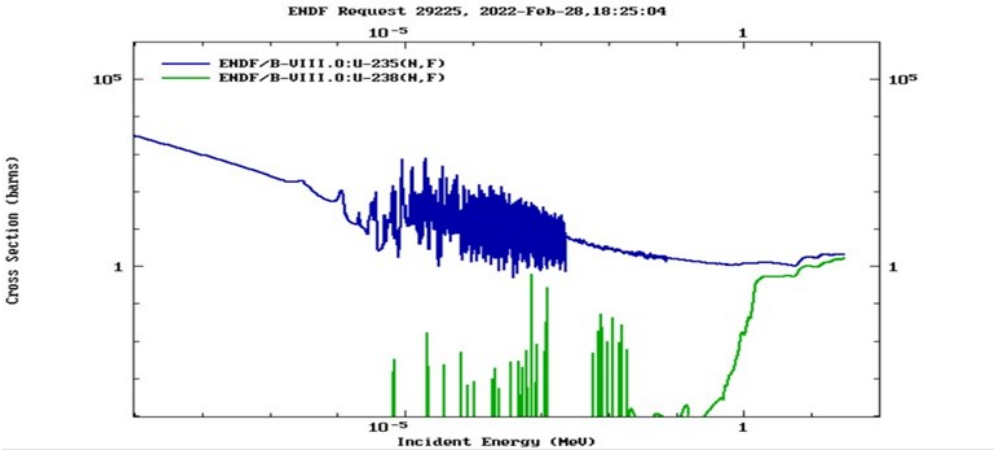

Figure 21. Induced fission cross sections for ^{235}U and ^{238}U [24].

5.1.1 Empty Chamber Response

The influence of various moderating and reflecting materials on the average neutron energy distribution was examined by simulation of various combinations of moderating and reflective materials. Various thicknesses from 1 to 10 cm were examined. The moderating materials included HDPE, Teflon, graphite, flex boron, and borated polyethylene while the insert materials included Cd, Ni, Pb, Cu, and stainless steel. The reflective materials were introduced as an insert into the moderating materials rather than as a full slab. This was to allow the moderator to shield the side detector panels from direct irradiation by the 2.5 MeV DD neutrons to minimize cross talk and reduce the singles rates. Figure 22 shows the simulated measurement geometry for an HDPE moderator with a nickel insert. Ultimately, the inserts proved to be ineffective, and the simulations focused on monolithic moderating slabs. With the exception of the bare HDPE slab geometry, all moderator/insert geometries included 1 mm thick cadmium layer between the slab and the detector assembly.

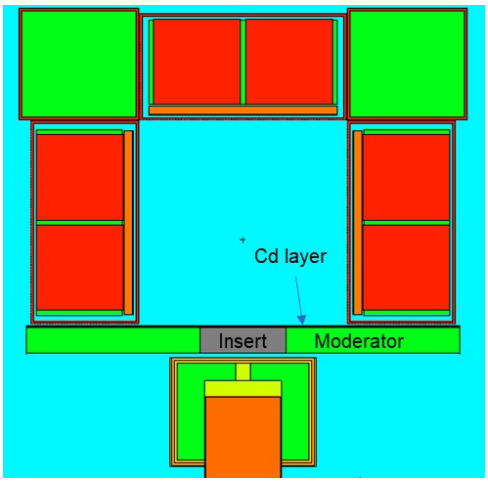

Figure 22. Illustration of the moderator/insert simulation geometry.

5.1.1.1 Empty Chamber Response —Neutron Energy Distribution

The emitted DD neutrons are essentially monoenergetic. The 2.5 MeV energy is sufficiently high to induce fission in the ^{238}U within the fuel assembly. Neutrons scattering in moderating/reflective material between the generator and the fuel assembly will lose energy, increasing the relative probability of inducing ^{235}U instead of ^{238}U. The plots in Figure 23 are an overlay of the neutron energy distributions for various thickness of HDPE with a cadmium liner. Figure 25 show a subset of those plots for two of the thicker HDPE slabs. Unfortunately, no matter how thick the slab, a significant fraction of the DD neutrons reach the assay volume without appreciable loss of energy. This was true of all permutations of moderator and reflector, including supplemental models where additional HDPE was installed behind the generator.

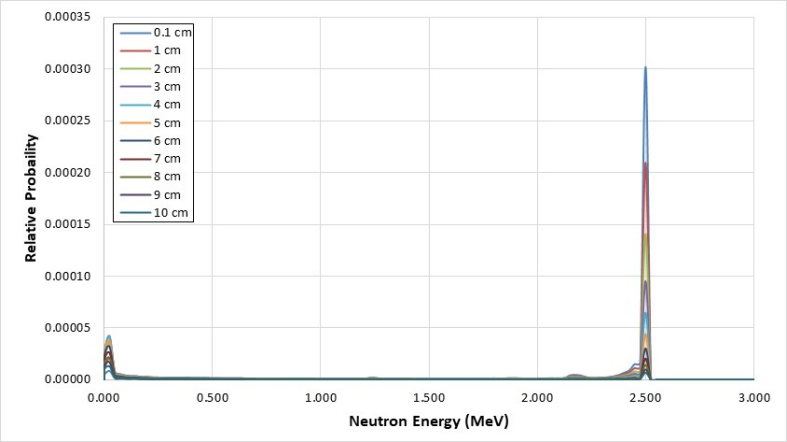

Figure 23. Neutron fluence as a function of energy in the center of the empty FNCL cavity for various thicknesses of HDPE (with a cadmium layer) between the generator and FNCL.

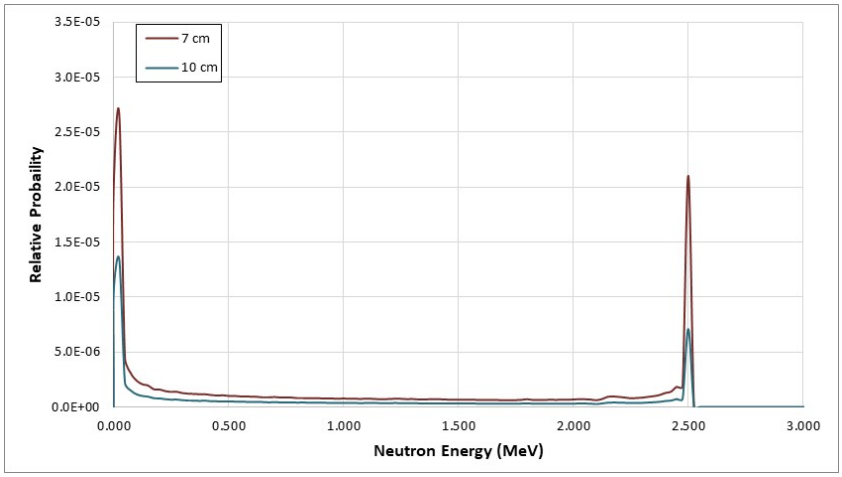

Figure 24. Neutron fluence as a function of energy in the center of the empty FNCL cavity for two of the thicker HDPE slabs (with a cadmium layer) located between the generator and FNCL.

Figure 25 shows the average energy of the center cavity neutron flux for a selection of the materials examined (there was no significant difference between Ni, Cu, stainless steel, or Pb reflective inserts). Slab thicknesses up to 10 cm were considered because greater thicknesses were considered to be impractical for the FNCL application. The HDPE slab without the cadmium layer was effective in bringing down the average interrogating energy; however, this would be the equivalent of operating the FNCL in thermal mode with increased sensitivity to poison rods. With the inclusion of the cadmium layer, the models suggest that a minimum of 6 cm of HDPE would be required to reduce the average interrogating energy below the ^{238}U threshold.

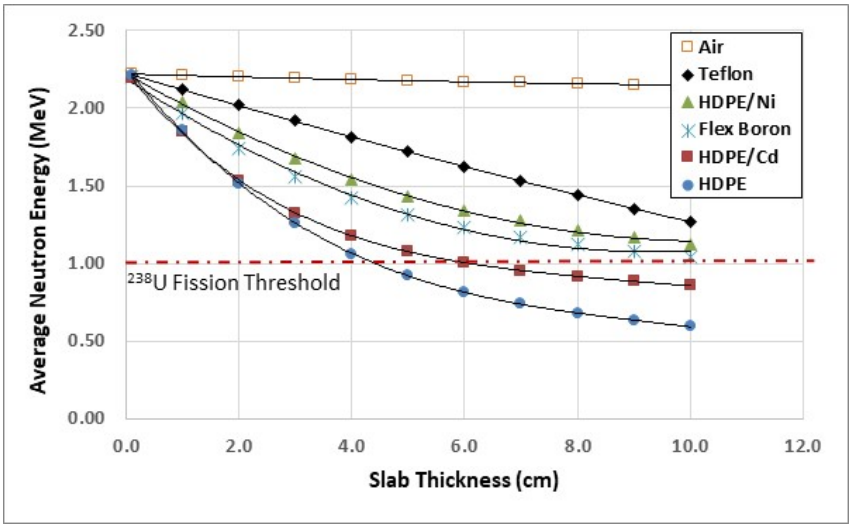

Figure 25. Average neutron energy in the center of the empty FNCL cavity as a function of thickness for various slab materials.

5.1.1.2 Empty Chamber Response—Expected Singles Rates

The addition of the moderating/reflective slabs impacts the magnitude of the interrogating flux and the neutron detection rate. The magnitude of the flux will be discussed in the context of fuel assay in a following section. The empty chamber singles rate as a function of material and thickness is shown in Figure 26. The curve labeled "air" shows the impact of increased distance from the FNCL detectors. The

figures also shows that detection rate is unaffected by the addition of the cadmium layer because these low energy neutrons are below the detection threshold of the FNCL detectors.

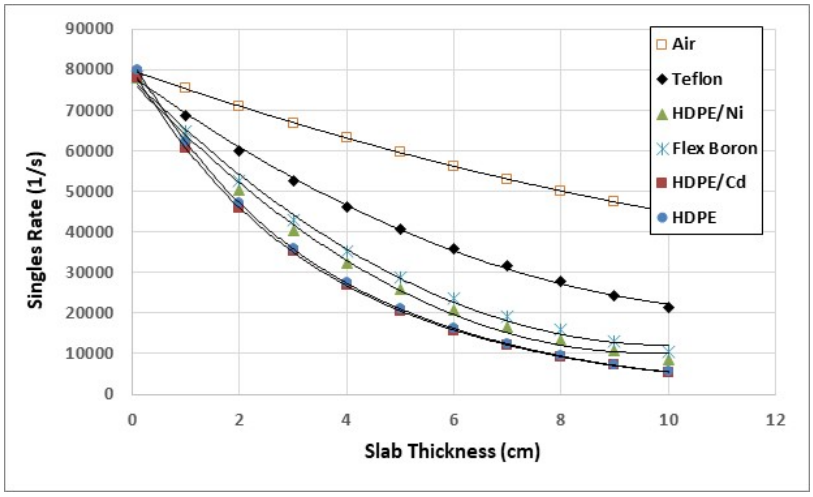

Figure 26. Expected neutron singles rates for empty FNCL cavity as a function of thickness for various slab materials.

5.1.2 Optimization for Fuel Assembly Measurement

To examine the impact of the various moderator/reflective materials on the assay of a fuel assembly, simulated assays were performed for each of the 44 fuel assemblies described in Section 4 (Figure 27). The results for two of those assemblies (calibration assembly Cal-6 and poisoned assembly BP-24) are discussed here.

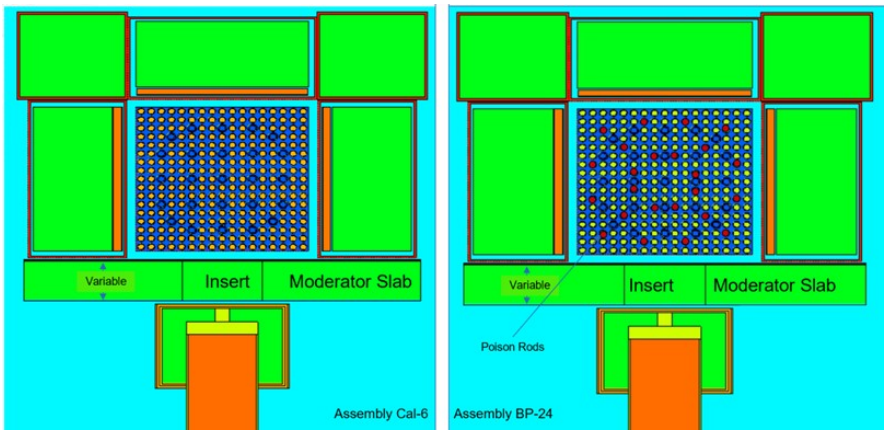

Figure 27. Expected neutron singles rates for a 17 × 17 un-poisoned fuel assembly (left) and a poisoned 17 × 17 fuel assembly (right) loaded into the FNCL cavity as a function of thickness for various slab materials.

The average neutron energy at the center of the two assemblies and the expected singles count rates are provided in Figure 28 and Figure 29. Perhaps surprisingly, there is minimal difference in the response for the poisoned and non-poisoned fuel assemblies. However, the plots in Figure 28 illustrate the cadmium-lined HDPE slab provides superior interrogation of the center of the assay cavity relative to the other materials.

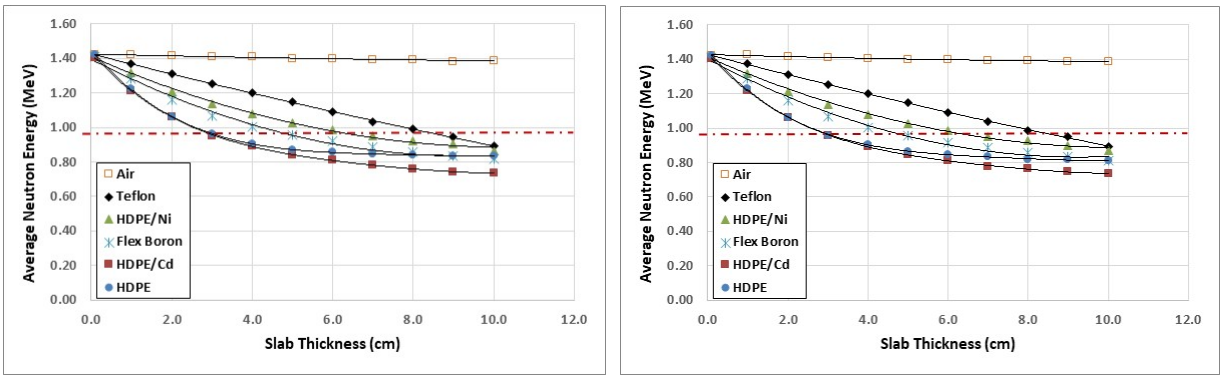

Figure 28. Average neutron energy in the center of a 17 × 17 un-poisoned fuel assembly (left) and a poisoned 17 × 17 fuel assembly (right) loaded into the FNCL cavity as a function of thickness for various slab materials.

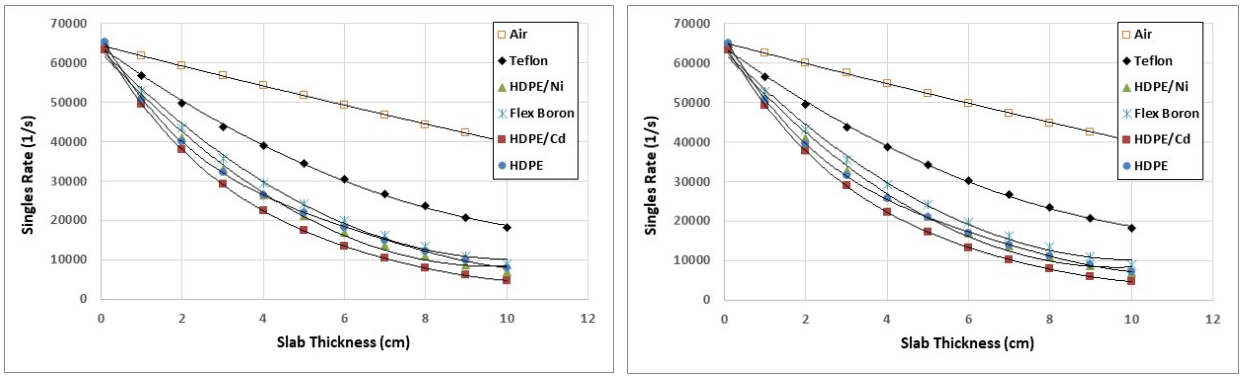

Figure 29. Expected neutron singles rates for a 17 × 17 un-poisoned fuel assembly (left) and a poisoned 17 × 17 fuel assembly (right) loaded into the FNCL cavity as a function of thickness for various slab materials (yield:1.4E6 n/s).

Figure 30 shows the ratio of induced fission rates for ^{238}U and ^{235}U for the various flux-tailoring materials. The lower the ratio the more sensitive the measurement is to the ^{235}U content of the fuel assembly. From these plots it is obvious that the poison rods have no significant impact on the ratio. The HDPE and HDPE with cadmium liner provide the most favorable ratios.

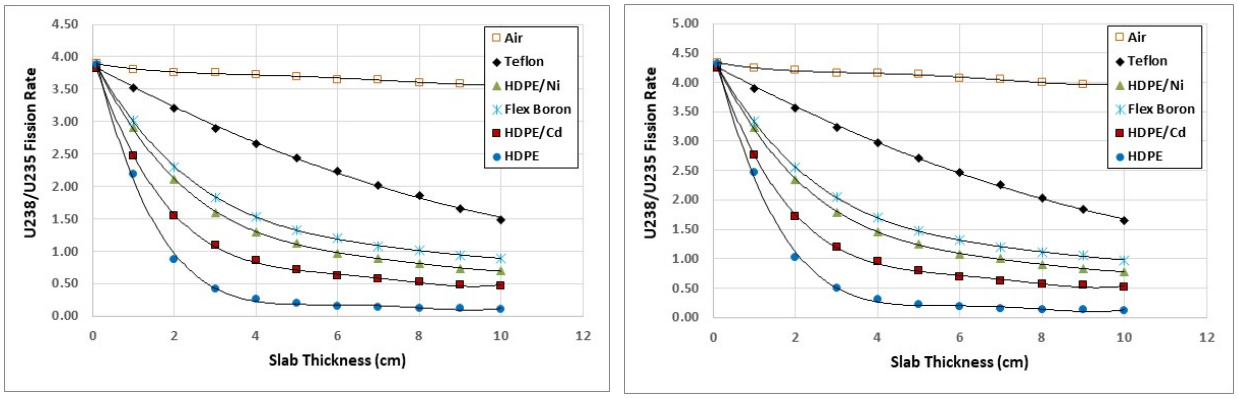

Figure 30. Ratio of the $^{238}U/^{235}U$ induced fission rates for a 17 × 17 un-poisoned fuel assembly (left) and a poisoned 17 × 17 fuel assembly (right) loaded into the FNCL cavity as a function of thickness for various slab materials.

Finally, the expected coincidence rates as a function of the thickness of flux-tailoring material is provided in Figure 31. Except for the bare HDPE slab, the presence of the gadolinium poison rods has minimal impact on the expected coincidence rates. The poison rods prevent the thermal neutron flux from reaching the interior of the fuel assembly, reducing the ^{235}U induced fission rate. Because of this sensitivity to the poison rods and the reduced sensitivity to the center of the assembly, the bare HDPE slab is not suitable for the flux-tailoring slab. For the bare HDPE slab, the poison rods have a disproportionate impact on the fission rates and the measured doubles rate.

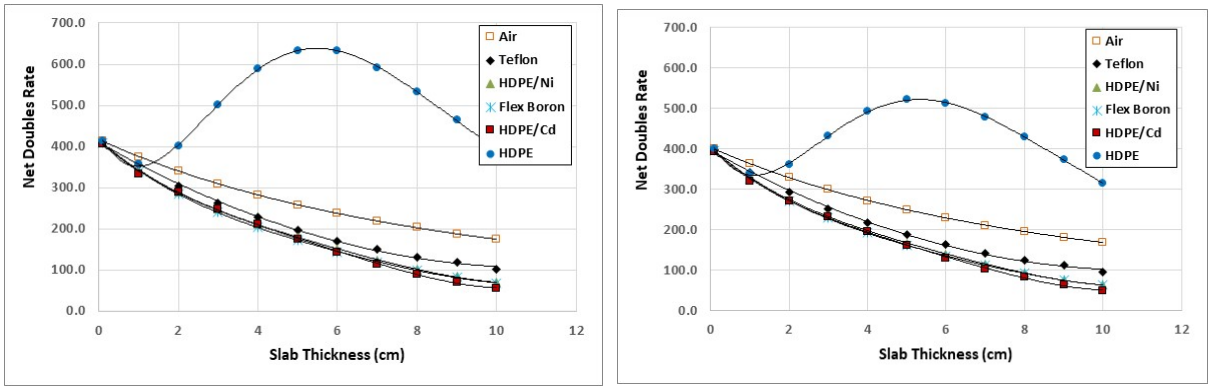

Figure 31. Expected neutron coincidence rates for a 17 × 17 un-poisoned fuel assembly (left) and a poisoned 17 × 17 fuel assembly (right) loaded into the FNCL cavity as a function of thickness for various slab materials (yield: 1.4×10^6 n/s).

To further examine the performance of the nGen-350/FNCL system for fuel assemblies, fission maps showing the relative induced fission rate for each pin in the assembly were generated from the simulations. Figure 32 provides a comparison of the induced ^{235}U fission rate distribution in the Cal-6 fuel assembly with a 7 cm thick HDPE slab with and without a 1 mm thick cadmium liner. Without the cadmium liner, the fission rates are seven times greater, but most of that increase is generated within the four rows of tubes nearest the generator. Without the cadmium liner, the measurement would be insensitive to partial defect in half the assembly.

The simulated induced ^{238}U fission rate for the Cal-6 assembly is shown in Figure 33 with the 7 cm thick HDPE slab with and without the cadmium liner. The removal of the cadmium liner results in a small increase in the ^{238}U fission rate caused primarily by the ^{235}U fission neutrons.

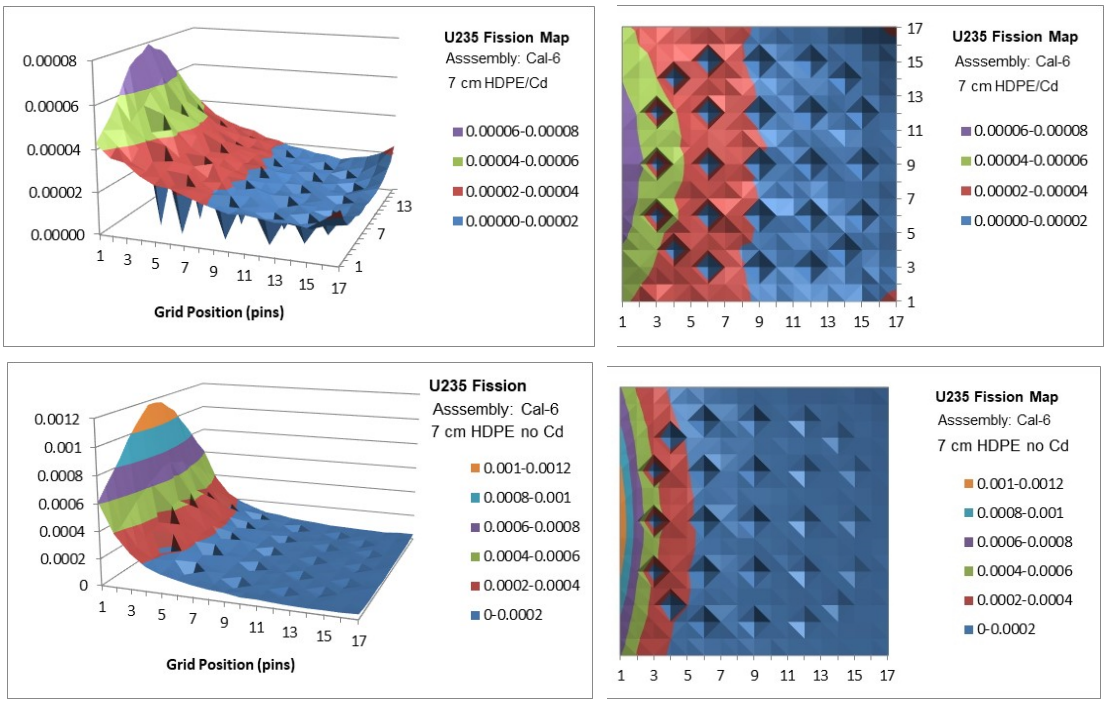

Figure 32. Relative ^{235}U induced fission rate maps for a 17 × 17 un-poisoned fuel assembly. The upper plots show the rates for the 7 cm HDPE with cadmium layer, and the lower plots show the rates without the cadmium layer. The plot shows the induced fission rate for each pin. The grid positions showing a fission rate of 0 correspond to cooling channels. The maximum fission rates are adjacent to the generator head.

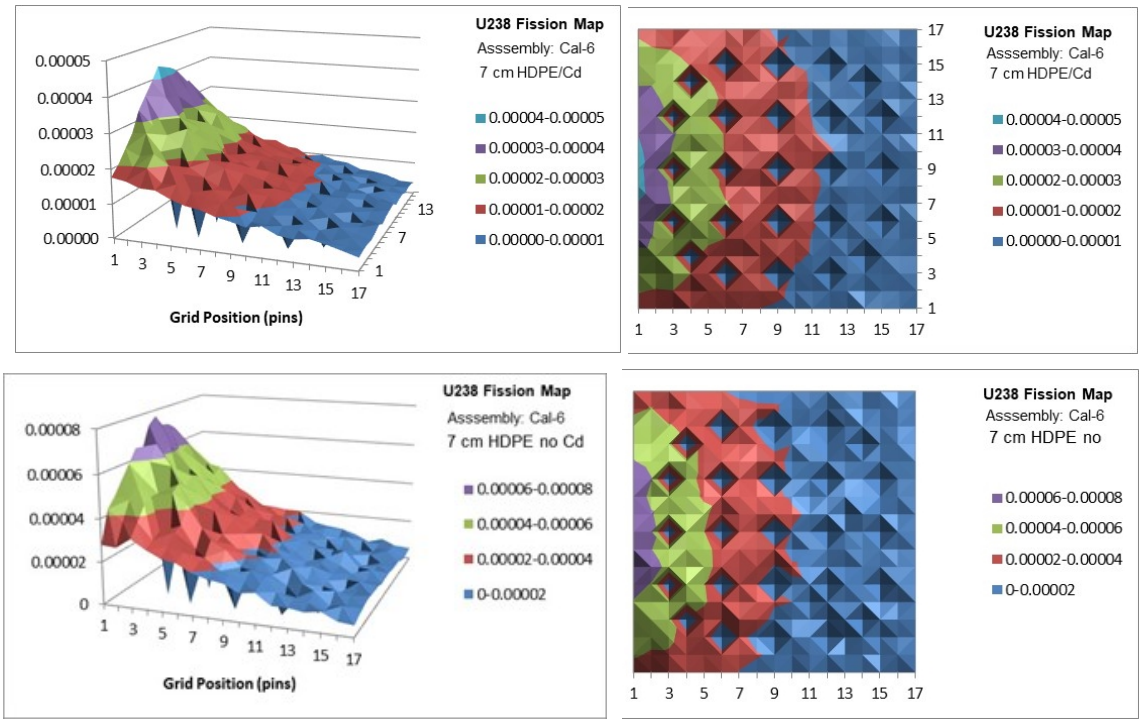

Figure 33. Relative ^{238}U induced fission rate maps for a 17 × 17 un-poisoned fuel assembly with a 7 cm flux-tailoring slab with and without cadmium. The plot shows the induced fission rate for each pin. The grid positions showing a fission rate of 0 correspond to cooling channels. The maximum fission rates are adjacent to the generator head.

Although the induced fission distribution is asymmetric because of the single sided interrogation, the detection efficiency is also asymmetric because of the U-shaped detector arrangement. The large mass of the fuel assembly and the uranium in the surrounding fuel rods impacts the probability that a neutron will be detected. Figure 34 shows the neutron detection efficiency as a function of pin position within the 17 × 17 Cal-6 fuel assembly.

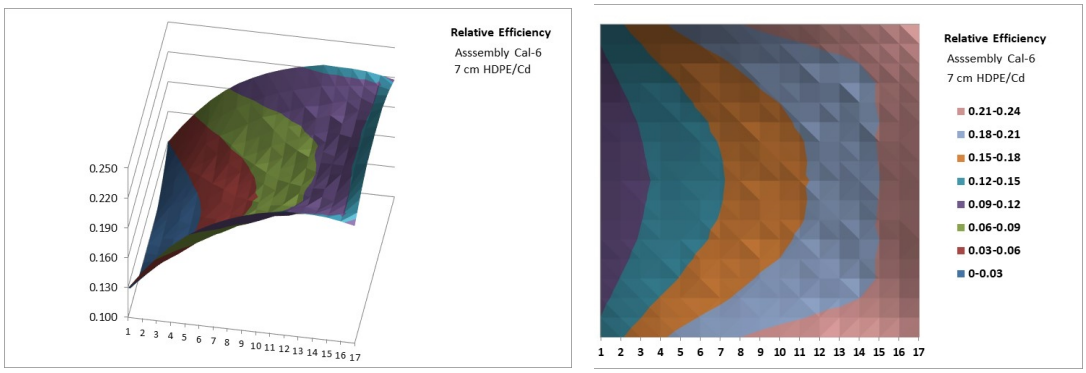

Figure 34. Detection efficiency as a function of pin position with the 17 × 17 un-poisoned fuel assembly. The minimum detection efficiency is adjacent to the generator head.

The decrease in detection efficiency near the neutron generator more than compensates for the increase in induced fission rate for pins near the generator. A map of the simulated neutron coincidence rate for each pin in the Cal-6 assembly is shown in Figure 35. Because the extremes of the efficiency and fission rate offset each other, the minimum response is 0.7 times the average, and the maximum response is 1.6 times the average.

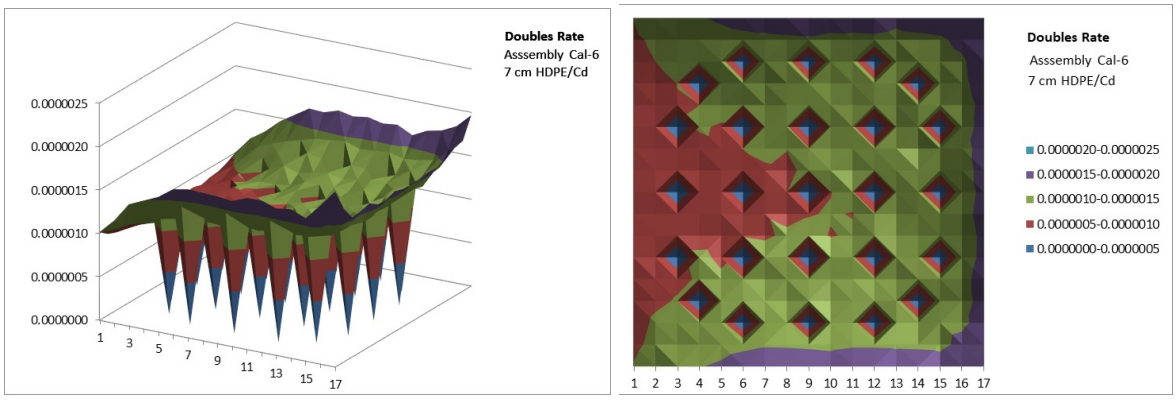

Figure 35. Relative doubles rate contribution as a function of pin position for a 17 × 17 un-poisoned fuel assembly. The plot shows the doubles rate contribution for each pin. The grid positions showing doubles rate of 0 correspond to cooling channels. The minimum rates are adjacent to the generator head.

5.1.2.1 Selection of the Flux-Tailoring Material

Based on the evaluation of the performance for the 44 notional fuel assemblies described in Section 4, the optimal material for the measurement is the cadmium-lined HDPE. Except for the HDPE without cadmium liner, which is rejected for extreme sensitivity to poisons and extremely non-uniform spatial response, the HDPE/Cd combination provide the lowest singles rate, highest precision, and least sensitivity to ^{238}U of the materials evaluated.

From Figure 30, the $^{238}U/^{235}U$ induced fission rate ratio declines rapidly until the HDPE thickness (for the HDPE/Cd slab) reaches ~6 cm, while increasing the thickness beyond 6 cm accrues only minimal additional gains. Estimating the measurement precision for the Cal-6 assembly (Figure 36) suggests that the optimal thickness is approximately 3 cm. However, the cross-talk filters implemented for the FNCL system have provided minimal success in rejecting double detections of a single DD neutron. This results in an apparent doubles background that degrades the measurement precision. Increasing the thickness of the slab reduces the number of 2.5 MeV neutrons reaching the detector panels, lowering the cross-talk event rate. From the benchmark measurement performed with the nGen-350 and the FNCL, a thickness of ~7.6 cm was found to provide the optimal measurement precision.

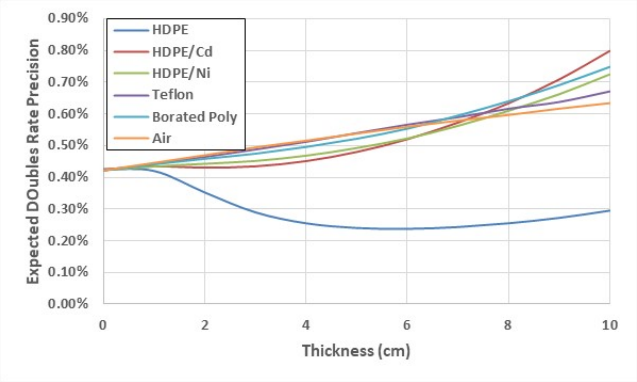

Figure 36. Estimated doubles rate precision (300 s interrogation, generator yield:1E6 n/s) for the Cal-6 assembly.

6. FNCL/NGEN-350 ADAPTER MODULE

To facilitate loading/unloading of fuel assemblies into the collar and to minimize the need to attach and remove the generator tube multiple times during the course of an inspection, the IAEA has requested that mounting FNCL bracket be modified so that the active slab (generator assembly) is relocated to one of the other sides of the collar. This would allow loading/unloading of the fuel assemblies without the need to repeatedly mount/dismount the generator.

Conceptually the simplest approach to the integration of the nGen-350 would be to mount the generator tube/detector module horizontally with the face abutting a flux-tailoring slab as shown in Figure 37. The generator would be mounted behind a 7.62 cm thick moderator slab to reduce the multiple scatter neutron detection rate from the generator. However, the generator tube would protrude 30 cm beyond the edge of the FNCL mounting bracket. To avoid interference with the Genie lift, it would be necessary to orient the tube to extend out from the side of the Genie lift forks, resulting in an inherent asymmetry in the configuration. Additionally, such an arrangement would position the generator in an exposed manner more vulnerable to inadvertent damage.

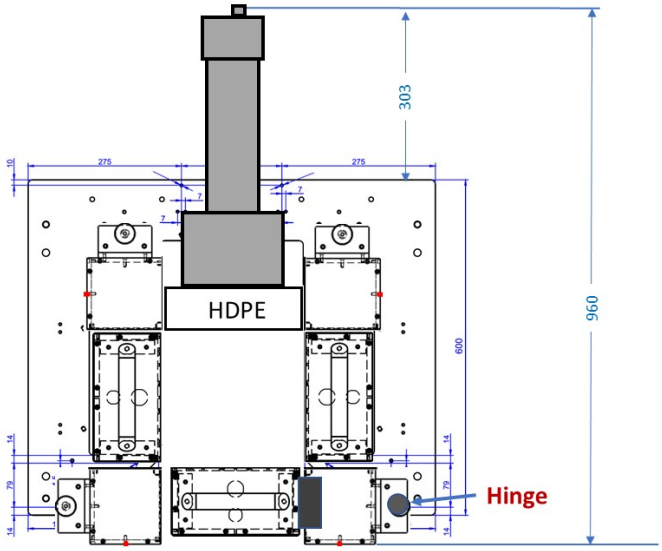

Figure 37. Simple mounting approach.

Instead, the generator tube will be placed in vertical orientation at the back of the Genie lift fork. The requirement for the moderating shielding will be partially accommodated by the nGen-350 detector module (Figure 38). The neuron generator will be mounted within a moderating "shoe" to provide the required thickness of HDPE. The two side detector panels will remain in their current orientation, the 3rd detector panel will be attached to a hinged moderating panel and mounted at the open end of the FNCL detector mounting plate.

1. The generator will be mounted into a U-shaped HDPE clamshell (shoe) to provide an equivalent of a 3 in. block of poly between the generator and the assembly. The clamshell is attached to a 4 in. thick block of HDPE. The external surfaces of the HDPE will be covered with a layer of cadmium and aluminum.

2. The generator controller will be removed from its current frame and mounted on one of the existing corner blocks.

3. Two new corner blocks will be added to the front (door side) of the mounting frame.

4. The third detector panel will be attached to one of these corner blocks, which will be hinged so that the assembly acts as a door.

5. One of the corner blocks adjacent to the neutron generator will include a 2.70 cm diameter hole to accommodate a ^{3}He proportional tube to act as a flux monitor.

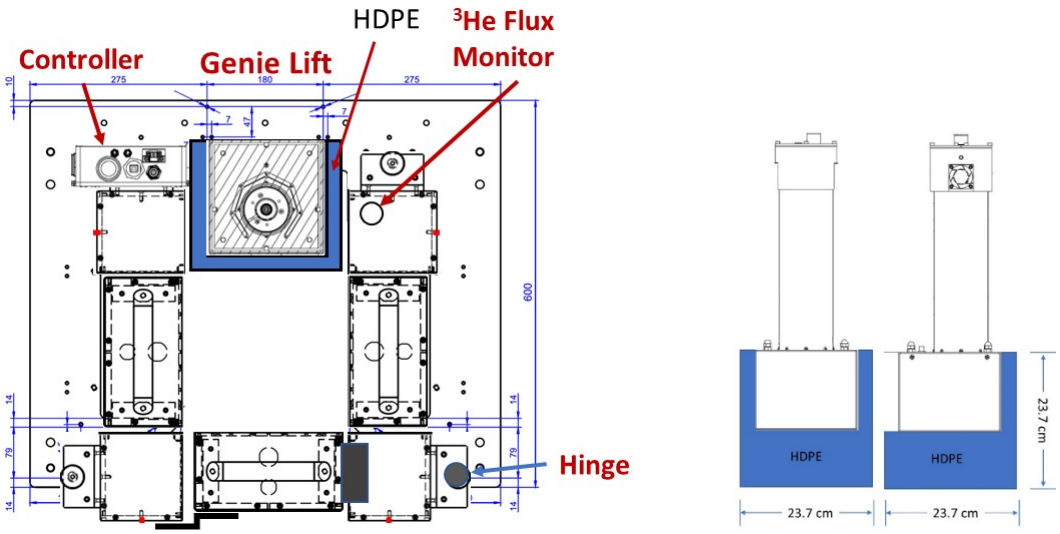

Figure 38. Selected generator mounting approach, the nGen-350 is mounted with the generator tube oriented vertically (left) and the moderating "shoe" generator mounting bracket (right).

6.1 EXPECTED PERFORMANCE OF THE OPTIMIZED NGEN-350/FNCL

An MCNP model has been developed for the FNCL with the flux-tailoring adaptor module for the nGen-350 (Figure 39). The expected performance was evaluated using the descriptions of the simulated fuel assemblies described in Section 4. These are the same as those in the recent neutron rodeo project to examine the performance of alternative neutron detection techniques for the assay of fresh fuel assemblies [11].

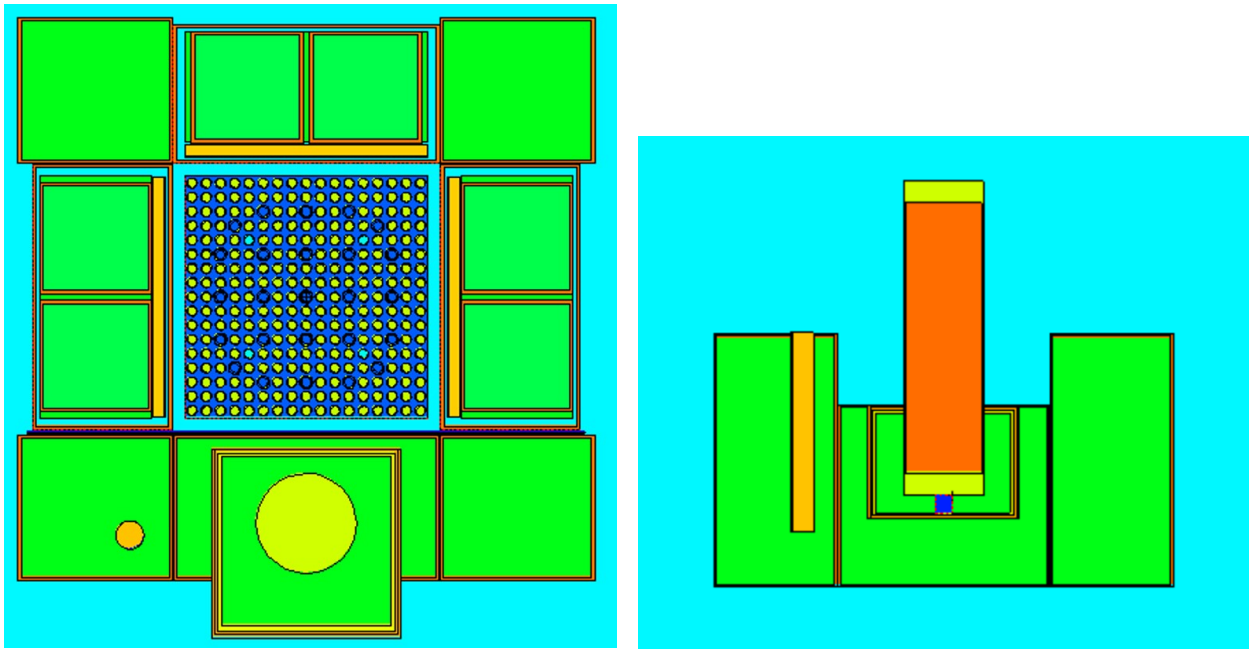

Figure 39. MCNP VISED screenshots of the modified FNCL detector arrangement about a fuel assembly (left) and a vertical cross section through the neutron generator holder.

6.2 SIMULATED CALIBRATION OF THE NGEN-350/FNCL

The simulated calibration rates are based on the assemblies described in Section 4. For each of the assemblies, the doubles rates and errors were estimated assuming a neutron generator yield of 2×10^6 n/s. The simulated calibration curve is shown in Figure 40, the simulated rates and uncertainty estimates are listed in Table 13.

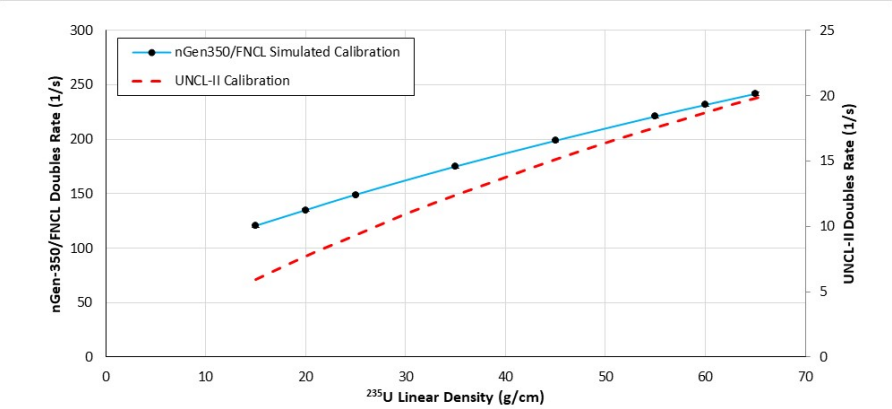

Figure 40. nGen-350/FNCL simulated calibration curve overlain with the measured UNCL-II calibration results [25].

Table 13. Simulated nGen-350/FNCL calibration measurement results for the calibration assemblies‡.

Fuel assembly ID	Declared LD ^{235}U (g/cm)	Singles rate (1/s)	Doubles rate (1/s)	600 sec σ_D (1/s)	1,800 s σ_D (1/s)	Analyzed LD ^{235}U (g/cm)	600 s LD uncert (g/cm)	1,800 s LD uncert (g/cm)	600 s Total uncert (%)†	1,800 s Total uncert (%)†
17x17_cal_15	15.0	11,457.2	120.4	± 0.58	± 0.33	14.94	± 0.19	± 0.11	± 1.6	± 1.2
17x17_cal_20	20.0	11,569.4	134.8	± 0.60	± 0.35	19.88	± 0.21	± 0.12	± 1.5	± 1.2
17x17_cal_25	25.0	11,682.7	148.9	± 0.62	± 0.36	24.96	± 0.23	± 0.13	± 1.4	± 1.1
17x17_cal_35	35.0	11,896.1	174.9	± 0.66	± 0.38	34.95	± 0.26	± 0.15	± 1.3	± 1.1
17x17_cal_45	45.0	12,092.8	198.7	± 0.69	± 0.40	44.87	± 0.30	± 0.17	± 1.2	± 1.1
17x17_cal_55	55.0	12,255.6	221.0	± 0.72	± 0.42	54.93	± 0.34	± 0.19	± 1.2	± 1.1
17x17_cal_60	60.0	12,348.3	231.6	± 0.73	± 0.42	59.96	± 0.35	± 0.20	± 1.2	± 1.1
17x17_cal_65	65.0	12,426.0	241.8	± 0.75	± 0.43	64.90	± 0.37	± 0.21	± 1.1	± 1.1

‡ Uncertainties are the expected measurement performance values.
† Includes a 1% systematic contribution to the uncertainty.

6.3 NGEN-350/FNCL SIMULATED PERFORMANCE FOR VARIOUS INTACT ASSEMBLIES

A series of simulations were performed using the descriptions for the assorted intact fuel assemblies described in Section 4.2. The simulated assay results are provided in

Table 14 and shown in Figure 41 for operation in the thermal and fast assay modes. For consistency with the evaluations in Reference [11] measurement biases are discussed in terms of a somewhat ill-defined "mass defect" (i.e., the difference between the measured and declared linear ^{235}U density). The results are shown before and after application of the heavy metal correction, illustrating the need to apply the correction factors when considering the relative performance of the measurement for a given assembly. As can be seen in Figure 41, the heavy metal correction is quite effective for improving the fast mode measurement performance using the parameters provided by Menlove et al. [26].

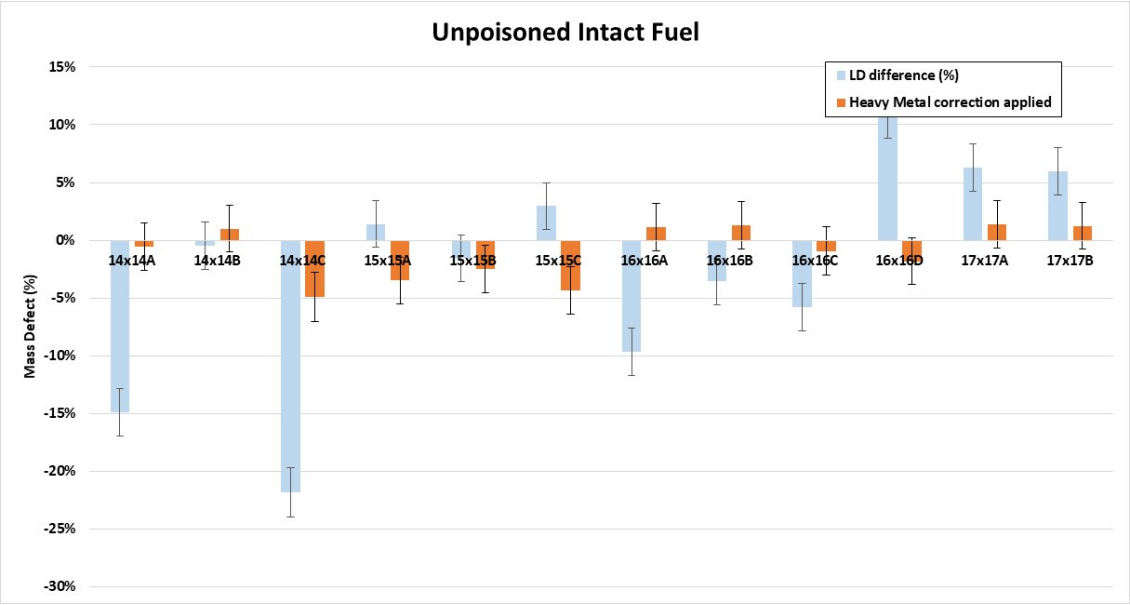

Figure 41. Results of the MCNP simulations for the nGen-350/FNCL for the assorted intact fuel assemblies in the thermal mode. Error bars represent the projected 1 σ uncertainties for an 1,800 s measurement time.

Table 14. Simulated nGen-350/FNCL measurement results for the un-poisoned, intact fuel assemblies‡.

Fuel assembly ID	Declared LD ^{235}U (g/cm)	Singles rate (1/s)	Doubles rate (1/s)	600 s σ_D (1/s)	1,800 s σ_D (1/s)	Analyzed LD ^{235}U (g/cm)	600 s LD uncert. (g/cm)	1,800 s LD uncert. (g/cm)	600 s Total uncert. (%)†	1,800 s Total uncert. (%)†
14x14A	**37.57**	13,019.4	167.4	± 0.67	± 0.39	31.96	± 0.26	± 0.15	± 2.2	± 2.1
14x14B	**37.31**	12,503.0	180.3	± 0.68	± 0.39	37.12	± 0.28	± 0.16	± 2.1	± 2.0
14x14C	**19.78**	12,659.8	121.9	± 0.60	± 0.35	15.46	± 0.20	± 0.12	± 2.4	± 2.1
15x15A	**58.37**	12,764.4	230.0	± 0.74	± 0.43	59.19	± 0.35	± 0.20	± 2.1	± 2.0
15x15B	**61.54**	12,920.2	232.9	± 0.75	± 0.43	60.58	± 0.36	± 0.21	± 2.1	± 2.0
15x15C	**60.91**	12,735.4	237.3	± 0.75	± 0.43	62.72	± 0.36	± 0.21	± 2.1	± 2.0
16x16A	**46.90**	13,063.8	192.8	± 0.70	± 0.41	42.37	± 0.30	± 0.17	± 2.1	± 2.0
16x16B	**50.16**	12,901.8	206.1	± 0.72	± 0.41	48.13	± 0.32	± 0.18	± 2.1	± 2.0
16x16C	**30.95**	12,544.0	160.1	± 0.65	± 0.38	29.15	± 0.25	± 0.14	± 2.2	± 2.1
16x16D	**64.07**	12,454.0	254.0	± 0.76	± 0.44	71.00	± 0.38	± 0.22	± 2.1	± 2.0
17x17A	**41.29**	12,344.6	197.0	± 0.69	± 0.40	44.16	± 0.30	± 0.17	± 2.1	± 2.0
17x17B	**54.82**	12,582.0	226.3	± 0.73	± 0.42	57.43	± 0.35	± 0.20	± 2.1	± 2.0

‡ Uncertainties are the expected measurement performance values.
† Includes a 2% systematic contribution to the uncertainty.

6.4 NGEN-350/FNCL SIMULATED PERFORMANCE FOR BURNABLE POISONS

The performance of the nGen-350/FNCL for assemblies containing burnable poisons is the motivation for pursuing the DD neutron generator as an alternative interrogation source. The difference in neutron energy distribution from the sources and the change in the moderating assembly to accommodate the larger, relative to Am(Li), source change the relative thermal neutron population in the interrogating neutron distribution. The simulated assemblies containing poison rods allow examination of the potential impact. Figure 42 illustrates the impact of the poison rods on the mass assay result. As can be seen, the number of poison rods is more important than the rods' poison loading. The simulated rates and defect levels are presented in Table 15 and Table 16.

We have implemented a provisional poison rod correction based on these simulations.

$$CF = \left[n_{non} + \left(\frac{E_{pois}}{E_{non}} \cdot \frac{k}{wt_{pois}}\right) \cdot n_{pois}\right] \Big/ (n_{non} + n_{pois}),$$

where n_{non} is the number of non-poisoned fuel rods
n_{pois} is the number of poison rods
E_{non} is the ^{235}U enrichment of the non-poison rods
E_{pois} is the ^{235}U enrichment of the poisoned rods

wt_{pois} *is the* gadolinium weight fraction of the poison rods
k is an empirically determined calibration coefficient.

The application of the modified poison rod correction seems to provide excellent agreement between predicted and simulated assay values.

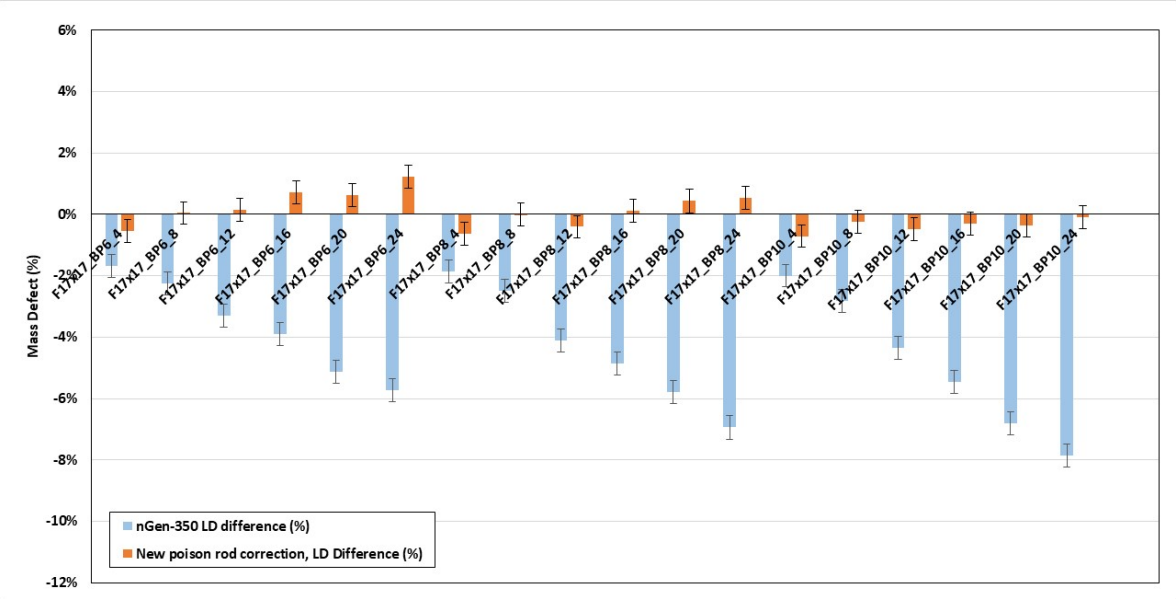

Figure 42. Simulated assay results for the various burnable poison loadings with and without the heavy metal and poison rod correction.

Table 15. Simulated nGen-350/FNCL uncorrected measurement results for the poisoned, intact fuel assemblies‡.

Fuel assembly ID	Declared LD ^{235}U (g/cm)	Singles rate (1/s)	Doubles rate (1/s)	600 s σ_D (1/s)	1,800 s σ_D (1/s)	Analyzed LD ^{235}U (g/cm)	600 s LD uncert (g/cm)	1,800 s LD uncert (g/cm)	600 s Total uncert (%)†	1,800 s Total uncert (%)†
BP6_4	51.50	12,219.4	211.4	± 0.71	± 0.41	50.54	± 0.32	± 0.19	± 0.6	± 0.4
BP6_8	51.20	12,213.6	210.1	± 0.71	± 0.41	49.95	± 0.32	± 0.18	± 0.6	± 0.4
BP6_12	50.90	12,204.4	208.3	± 0.71	± 0.41	49.13	± 0.32	± 0.18	± 0.6	± 0.4
BP6_16	50.60	12,183.2	207.0	± 0.70	± 0.41	48.53	± 0.31	± 0.18	± 0.6	± 0.4
BP6_20	50.30	12,169.8	204.9	± 0.70	± 0.40	47.63	± 0.31	± 0.18	± 0.7	± 0.4
BP6_24	49.90	12,140.2	203.4	± 0.70	± 0.40	46.95	± 0.31	± 0.18	± 0.7	± 0.4
BP8_4	51.50	12,220.8	211.2	± 0.71	± 0.41	50.44	± 0.32	± 0.19	± 0.6	± 0.4
BP8_8	51.20	12,213.8	209.8	± 0.71	± 0.41	49.83	± 0.32	± 0.18	± 0.6	± 0.4
BP8_12	50.90	12,189.6	207.4	± 0.70	± 0.41	48.72	± 0.31	± 0.18	± 0.6	± 0.4
BP8_16	50.50	12,166.6	205.7	± 0.70	± 0.41	47.96	± 0.31	± 0.18	± 0.7	± 0.4
BP8_20	50.20	12,170.8	204.0	± 0.70	± 0.40	47.20	± 0.31	± 0.18	± 0.7	± 0.4
BP8_24	49.90	12,127.8	202.0	± 0.70	± 0.40	46.35	± 0.31	± 0.18	± 0.7	± 0.4
BP10_4	51.50	12,222.2	211.0	± 0.71	± 0.41	50.37	± 0.32	± 0.19	± 0.6	± 0.4
BP10_8	51.20	12,212.2	209.5	± 0.71	± 0.41	49.66	± 0.32	± 0.18	± 0.6	± 0.4
BP10_12	50.80	12,188.2	206.9	± 0.70	± 0.41	48.50	± 0.31	± 0.18	± 0.6	± 0.4
BP10_16	50.50	12,164.4	205.0	± 0.70	± 0.40	47.66	± 0.31	± 0.18	± 0.7	± 0.4
BP10_20	50.20	12,160.6	202.8	± 0.70	± 0.40	46.69	± 0.31	± 0.18	± 0.7	± 0.4
BP10_24	49.80	12,115.8	200.8	± 0.70	± 0.40	45.80	± 0.30	± 0.18	± 0.7	± 0.4

‡ Uncertainties are the expected measurement performance values.
† Includes a 2% systematic contribution to the uncertainty.

Table 16. Simulated defect analysis results for the poisoned, intact fuel assemblies using the compact neutron generator operating at 200,000 n/s.

Fuel assembly ID	Defect without correction			HM and Poison corrections applied		
	LD mass defect (%)	#σ 600 s	#σ 1,800 s	LD mass defect (%)	#σ 600 s	#σ 1,800 s
BP6_4	−1.7	2.6	4.6	−0.5	0.9	1.5
BP6_8	−2.2	3.5	6.1	0.0	0.1	0.1
BP6_12	−3.3	5.1	8.9	0.1	0.2	0.4
BP6_16	−3.9	6.0	10.4	0.7	1.1	1.9
BP6_20	−5.1	7.9	13.6	0.6	1.0	1.7
BP6_24	−5.7	8.7	15.1	1.2	1.9	3.2
BP8_4	−1.9	2.9	5.1	−0.6	1.0	1.7
BP8_8	−2.5	3.9	6.7	0.0	0.0	0.0
BP8_12	−4.1	6.4	11.0	−0.4	0.6	1.1
BP8_16	−4.9	7.5	12.9	0.1	0.2	0.3
BP8_20	−5.8	8.8	15.3	0.4	0.7	1.1
BP8_24	−6.9	10.5	18.2	0.5	0.8	1.4
BP10_4	−2.0	3.1	5.4	−0.7	1.1	1.9
BP10_8	−2.8	4.4	7.6	−0.2	0.4	0.7
BP10_12	−4.4	6.7	11.6	−-0.5	0.8	1.3
BP10_16	−5.5	8.4	14.5	−0.3	0.4	0.8
BP10_20	−6.8	10.3	17.9	−0.4	0.6	1.0
BP10_24	−7.9	11.8	20.5	−0.1	0.2	0.3
Average bias	−4.3			0.0		
Std. deviation	1.9			0.5		

6.5 NGEN-350/FNCL SIMULATED PARTIAL DEFECT ANALYSIS

One of the primary uses of the collar measurement is to identify substitutions of fuel pins with empty channels or pins loaded with DU. This series of simulations examines the performance of the nGen-350/FNCL for increasing numbers of rods substituted with DU. The mass defect relative to the "declared" value is shown in Figure 43. Rates and performance values are provided in Table 17 and Table 18. Although the assembly configuration 17x17-PD_0 is the same as 17x17_Cal_55, the simulations result in noticeable defects where none would normally be expected. This is the result of the MCNP random seed used in these simulations to prevent the injection of unintended biases into the analysis results. Keeping in mind that the effective measurement precision of the simulations is much better than that obtained even in an 1,800 second measurement, it is easy to understand the challenges of identifying substitutions with the UNCL.

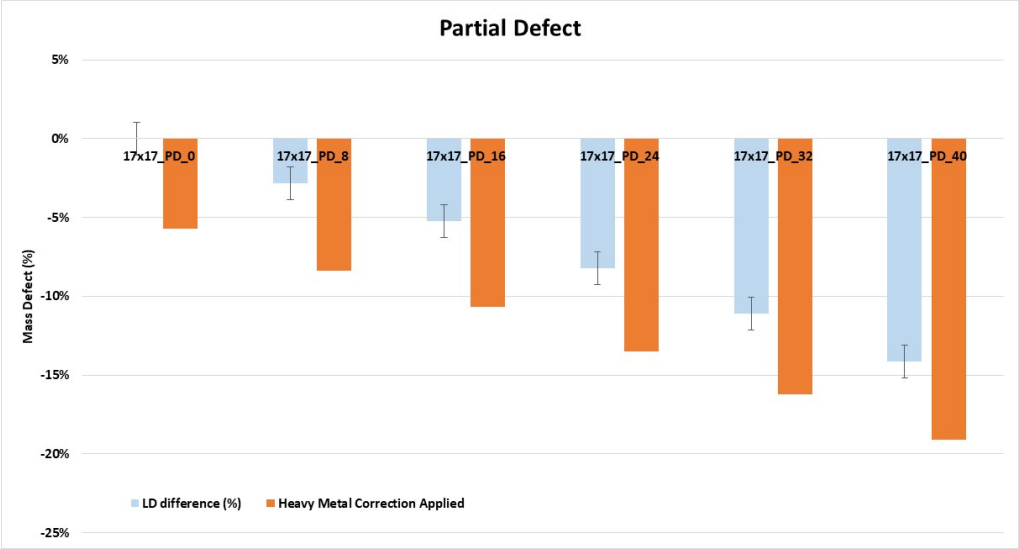

Figure 43. Simulated assay results for the partial defect loadings with and without application of the heavy metal correction.

Table 17. Simulated measurement results for the partial defect assembly configurations.‡

Fuel assembly ID	Declared LD ^{235}U (g/cm)	Singles rate (1/s)	Doubles rate (1/s)	600 s σ_D (1/s)	1,800 s σ_D (1/s)	Analyzed LD ^{235}U (g/cm)	600 s LD uncert (g/cm)	1,800 s LD uncert (g/cm)	600 s Total uncert (%)†	1,800 s Total uncert (%)†
PD_0	54.98	261.3	220.1	± 0.61	± 0.35	54.51	± 0.28	± 0.16	± 1.1	± 1.0
PD_8	54.98	261.0	216.7	± 0.60	± 0.35	52.96	± 0.28	± 0.16	± 1.1	± 1.0
PD_16	54.98	260.4	213.9	± 0.60	± 0.34	51.66	± 0.27	± 0.16	± 1.1	± 1.0
PD_24	54.98	259.9	210.3	± 0.59	± 0.34	50.03	± 0.27	± 0.15	± 1.1	± 1.0
PD_32	54.98	259.4	206.8	± 0.59	± 0.34	48.45	± 0.26	± 0.15	± 1.1	± 1.0
PD_40	54.98	258.7	203.1	± 0.58	± 0.34	46.81	± 0.26	± 0.15	± 1.1	± 1.0

‡ Uncertainties are the expected measurement performance values.
† Includes a 2% systematic contribution to the uncertainty.

Table 18. Simulated defect analysis results for the partial defect assembly configurations†.

Fuel assembly ID	Defect without correction			HM and poison corrections applied		
	LD mass defect (%)	#σ 600 s	#σ 1,800 s	LD mass defect (%)	#σ 600 s	#σ 1,800 s
PD_0	0.0	0.0	0.0	−6	5.1	5.5
PD_8	−2.8	2.5	2.7	−8	7.4	8.0
PD_16	−5.2	4.6	5.0	−11	9.4	10.2
PD_24	−8.2	7.2	7.8	−13	11.9	12.9
PD_32	−11.1	9.8	10.6	−16	14.3	15.5
PD_40	−14.1	12.4	13.5	−19	16.7	18.2

† Cells highlighted in green indicate a reasonable probability of detection of the substitution.

7. DISCUSSION

The FNCL software provided with the system is considered to be a prototype by the vendor. As such, operation of the system and analysis of the data are not expected to be smooth or robust. We have encountered ambiguities in both the data entry and analysis that complicate optimization of the FNCL system. Additionally, the analysis algorithms do not appear to be fully implemented; for example, it is not clear that the cross-talk filters function as intended. These shortcomings impact operation with the DD neutron generator more significantly than when using Am(Li) interrogation sources. Should the FNCL become a common use tool for international safeguards, the software interface will need to be enhanced to simplify acquisition, analysis, and archiving of the data and to allow simpler access to set up and calibration parameters.

To evaluate the measured and simulated measurements of the FNCL it was essential to develop a unified framework for both tasks to ensure that the considerable pulse filtering and processing required, especially for organic scintillators, is identically applied. To this end, a GUI and API tool kit was developed to process the raw pulse waveform list mode data from FNCL measurements and to generate simulated list mode data from MCNP-PoliMi and MPPost. The operating principle of this analysis tool kit is the uniform treatment of simulated and measured data in the application of pulse-processing algorithms and in deriving useful quantities, such as multiplet rates and detector responses, from the resulting pulse streams. The software is divided into two sections: analysis and simulation, that allows the user flexibility in performing the simulation and the analysis of both synthetic and real measurements. This software is described in detail in Appendix A.

A neutron flux-tailoring/adaptor module has been designed to mount the nGen-350 to the FNCL. The interrogating neutron flux from the DD generators must be tailored to reduce the sensitivity to ^{238}U while increasing the sensitivity to ^{235}U. That is, the average neutron interrogating energy must be reduced by the introduction of moderating/reflecting layers about the generator. This tailoring will also serve to reduce the detection efficiency of the interrogating neutrons improving the measurement precision. For the nGen-350/FNCL, this required reorientation of the detector modules on the detector lift such that one of the three detector modules functions as a door to the assay cavity while the neutron generator is placed at the back of the collar assembly. This arrangement places approximately 7.6 cm of cadmium-wrapped HDPE between the neutron generation point and the fuel assembly. The effect is to reduce the relative $^{238}U/^{235}U$ fission ratio by a factor of 6 and enhancing sensitivity to ^{235}U.

8. CONCLUSION

The results of this study indicate that the combination of the FNCL with the nGen-350 DD neutron generator offers significant improvement in measurement precision relative to the Am(Li) source driven ^{3}He-based UNCL and modest improvement compared to the Am(Li) source driven FNCL. The system will be capable of detecting smaller partial defects than either Am(Li)-based approach. However, to accomplish this as a fieldable system, enhancements to the operating software and algorithm base are required. Additionally, as noted in the nGen-350 performance report [20], improvement in the neutron generator stabilization mechanism will be required.

9. REFERENCES

[1] J. Beaumont, T. Lee, H. Mayorov, C. Tintori, F. Rogo, B. Angelucci and M. Corbor, "A Fast-Neutron Coincidence Collar Using Liquid Scintillators for Fresh Fuel Verification," *J. Radioanal Nucl Chem,* vol. 314, p. 803–812, 2017.

[2] R. McElroy, Jr., S. O'Brien and A. Lousteau, "Initial Characterization of a DD Neutron Generator Driven Fast Neutron Coincidence Collar," in *Proceedings of the INMM & ESARDA Joint Virtual Annual Meeting, August 23-26 & August 30-September 1*, 2021.

[3] S. O'Brien, "FNCL Analysis and Simulation. Computer software.," Oak Ridge National Laboratory, 21 April 2022. [Online]. Available: https://github.com/multTMU/FNCL.. [Accessed 21 April 2022].

[4] H. O. Menlove, "Description and Performance Characteristics for the Neutron Coincidence Collar for Verification of Reactor Fuel Assemblies," Report no. LA-9839-MS (ISPO-142), Los Alamos National Laboratory , Los Alamos, NM, 1981.

[5] H. Menlove and M. Krick, "A Portable Neutron Measurement Technique for the Assay of 235U in LWR Fuel Assemblies, LA-UR-81-358," Los Alamos Scientific Laboratory, Los Alamos, NM, 1981.

[6] H. Menlove and A. Keddar, "Field Test and Evaluation of the IAEA Coincidence Collar for the Measurement of BWR Fuel Assemblies, LA-9365-MS," Los Alamos National Laboratory, Los Alamos, NM, 1982.

[7] H. Menlove and A. Keddar, "Implementation of the Active Neutron Coincidence Collr for the Verification of Unirradiated PWR adn PWR Fuel Assemblies," Los Alamos National Laboratory, Los Alamos, NM, 1982.

[8] H. O. Menlove and J. E. Pieper, "Neutron Collar Calibration for LWR Fuel Assemblies," Report no. LA-10827-MS, Los Alamos National Laboratory, Los Alamos, NM, 1987.

[9] H. O. Menlove, J. E. Stewart, S. Z. Qiao, T. R. Wenz and G. P. D. Verrecchia, "Neutron Collar Calibration Evaluation for Assay of LWR Fuel Assemblies Container Burnable Neutron Absorbers," Report no. LA-11965-MS (ISPO 323), Los Alamos National Laboratory, Los Alamos, NM, 1990.

[10] P. Gibbs, R. McElroy, Jr. and B. Ticknor, "Evaluation of Safeguards Measurement Performances against the International Target Values, ORNL/SPR-2021/1956,," Oak Ridge National Laboratory, Oak Ridge, TN, (2021).

[11] A. Belian, A. Dougan, A. Iyengar, D. Chichester, S. Clark, S. Croft, D. Decman, W. Geist, P. Hauladen, H. Jianwei, R. McElroy, H. Menlove, J. Newby, S. Pozzi, M. Prasad, J. Sanders, T. Shin, S. Thompson and J. Verbeke, "Advanced Neutron Detection Technology Rodeo," in *ESARDA 39th Annual Meeting*, Dusseldorf, Germany, 2017.

[12] L. Evans, M. Swinhoe, H. Menlove, P. Schwalbach, P. DeBaere and M. Browne, "A New Fast Neutron Collar for Safeguards Inspection Measurements of Fresh Low Enriched Uranium Fuel Assemblies Containing Burnable Poison Rods," *Nucl. Instrum. Methods Phys. Res. A,* vol. 729, pp. 740-746, 2013.

[13] R. McElroy and S. Cleveland, "The DD Neutron Generator as an Alternative to Am(Li) Isotopic Neutron Source in the Uranium Neutron Coincidence Collar, ORNL/TM-2017/736," Oak Ridge National Laboratory, Oak Ridge, TN, 2017.

[14] H. Menlove, S. Menlove, and C. Rael, "The Development of a New, Neutron, Time Correlated, Interrogation Method for Measurement of 235U Content in LWR Fuel Assemblies," *Nucl. Instrum. Methods Phys. Res. A,* vol. 701, p. 72–79, 2013.

[15] M. Root, W. Geist and H. Menlove, "Fast Neutron Passive Collar Optimization Report, LA-UR-18-24767," Los Alamos National Laboratory, Los Alamos, NM, 2018.

[16] J. Beaumont, T. Lee, M. Mayorov, J. Jeon, A. Bonino, M. Grund, M. Dutra, G. Renha, S. Ahn, K. Kim, J. Park and G. Yang, "Field Testing of a Fast-Neutron Coincidence Collar for Fresh Uranium Fuel Verification," *Nucl. Instrum. Methods Phys. Res. A,* vol. 962, no. 163682, 2020.

[17] Thermo Fisher Scientific, "Thermo Scientific™ MP320 Neutron Generator," [Online]. Available: https://www.thermofisher.com/order/catalog/product/1517021A#/1517021A. [Accessed 2023].

[18] Starfire Industries, LLC, *Starfire Industries®nGen™ 350 Operation Manual Rev. 1,* Champaign, IL, 2021.

[19] R. McElroy, Jr. and S. Cleveland, "The D-D Neutron Generator as an Alternative to Am(Li) Isotopic Neutron Source in the Active Well Coincidence Counter, ORNL/TM-2017/57", Oak Ridge National Laboratory, Oak Ridge, TN, 2017.

[20] R. McElroy, Jr. and A. Laminack, "Performance Evaluation of the Starfire nGen-350 DD Neutron Generator for use with the Fast Neutron Coincidence Collar, ORNL/TM-2023/2946," Oak Ridge National Laboratory, Oak Ridge, TN, 2023.

[21] Starfire Industries, "nGen™-310 FOR PORTABLE CW NEUTRONS," 24 May 2023. [Online]. Available: https://www.starfireindustries.com/uploads/2/2/1/1/22111816/datasheet_ngen-310_rev00-18.pdf.

[22] Radiation Detection Technologies, Inc., "Domino® Neutron Detector Data Sheet," 20 5 2020. [Online]. Available: https://radectech.com/domino-product-page/https://radectech.com/domino-product-page/. [Accessed 25 5 2023].

[23] J. T. Goorley and et.al., "Initial MCNP6 Release Overview - MCNP6 version 1.0, LA-UR-13-22934," Los Alamos National Laboratory, Los Alamos, NM, 2013.

[24] International Atomic Energy Agency, "Evaluated Nuclear Data File (ENDF)," [Online]. Available: https://www-nds.iaea.org/exfor/endf.htm. [Accessed 26 6 2023].

[25] H. O. Menlove, J. E. Stewart, S. Z. Qiao, T. R. Wenz and G. P. D. Verrecchia, "Neutron Collar Calibration Evaluation for Assay of LWR Fuel Assemblies Container Burnable Neutron Absorbers, LA-11965-MS (ISPO 323)," Los Alamos National Laboratory, Los Alamos, NM, 1990.

[26] H. O. Menlove and J. E. Pieper, "Neutron Collar Calibration for LWR Fuel Assemblies, LA-10827-MS," Los Alamos National Laboratory, Los Alamos, NM, 1987.

[27] CaenSys Systems and Spectroscopy Solutions, *VeryFuel, Liquid Scintillator Based, Fast Neutron Detector for Fresh Fuel Verification, product specification sheet, caensys.com,* Viareggio, taly, 2017.

APPENDIX A. FNCL SIMULATION AND ANALYSIS SOFTWARE

APPENDIX A. FNCL SIMULATION AND ANALYSIS SOFTWARE

To evaluate the measured and simulated measurements of the Fast Neutron Collar (FNCL) it was essential to develop a unified framework, for both tasks, to ensure that the considerable pulse filtering and processing required, especially for organic scintillators, is identically applied. To this end, a GUI and API tool kit was developed to process the raw pulse waveform list mode data from FNCL measurements and to likewise generate simulated list mode data from MCNP-PoliMi and MPPost. The operating principle of this analysis tool kit is the uniform treatment of simulated and measured data in the application of pulse-processing algorithms and in deriving useful quantities, such as multiplet rates and detector responses, from the resulting pulse streams. The software is divided into two sections—analysis and simulation (Figure A-1)—that allows the user flexibility in performing the simulation and the analysis of both synthetic and real measurements.

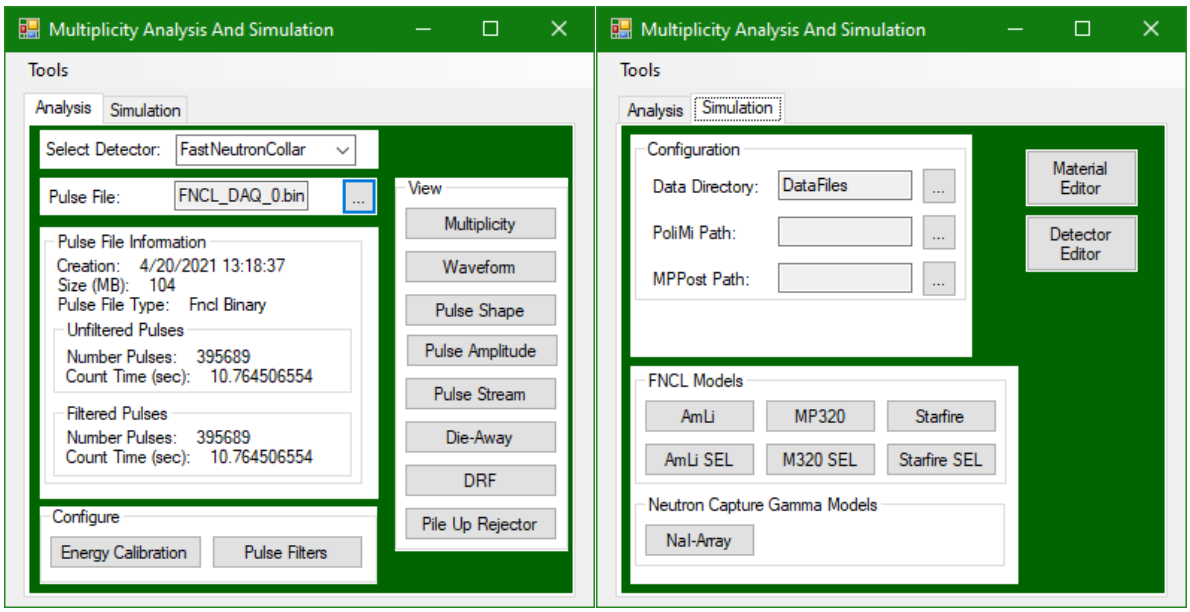

Figure A-1. Multiplicity analysis and simulation GUI.

A1. Analysis

The analysis side is responsible for both the processing and analysis of list mode data. The present work studies the implementation of DD neutron generators in place of Am(Li) neutron sources. This change, though beneficial, necessitates revisiting the default pulse processing occurring on the FNCL data acquisition (DAQ) machine, due to changes in interrogating neutron energy, the introduction of a large Bremsstrahlung x-ray source, and the prospect of pulsed neutron interrogation. For example, pulse discrimination thresholds and cross-talk–eliminating time gates may need adjusting to reduce the impact of the average neutron energy increasing from approximately 0.5 MeV, from Am(Li), to 2.5 MeV, from DD generators.

Fortunately, the FNCL-DAQ writes the unfiltered/unprocessed pulse stream to allow us to explore new pulse-processing settings and methods in simulation. It would be an impossible task to adjust the DAQ settings, perform a normalization, and then repeat the measurement to find more optimal operating parameters. These more ideal DAQ settings can be implemented to provide more fruitful immediate results and to produce improved list mode data to account for unrecoverable losses, such as deadtime and

pile-up, that can then be refined in software again that accounts for hardware settings such as gain and high voltage.

The backbone of the analysis tool kit is the “Pulse Filters” window, in Figure A-2, that generates the pulse stream used by every tool in the GUI. All the pulse filtering and processing is applied here before analysis, such as obtaining the doubles rate. The first option is to filter by particle type, either neutron or photon. For FNCL waveform data, this is coupled to the pulse shape discrimination (PSD) settings and to a simple flag in the synthetic list mode data. Next, pulses from detectors can be excluded, which is beneficial for comparing the response of those near and removed from the neutron generator. The timestamps of each detector can also be shifted forward and backward to account for any timing discrepancies.

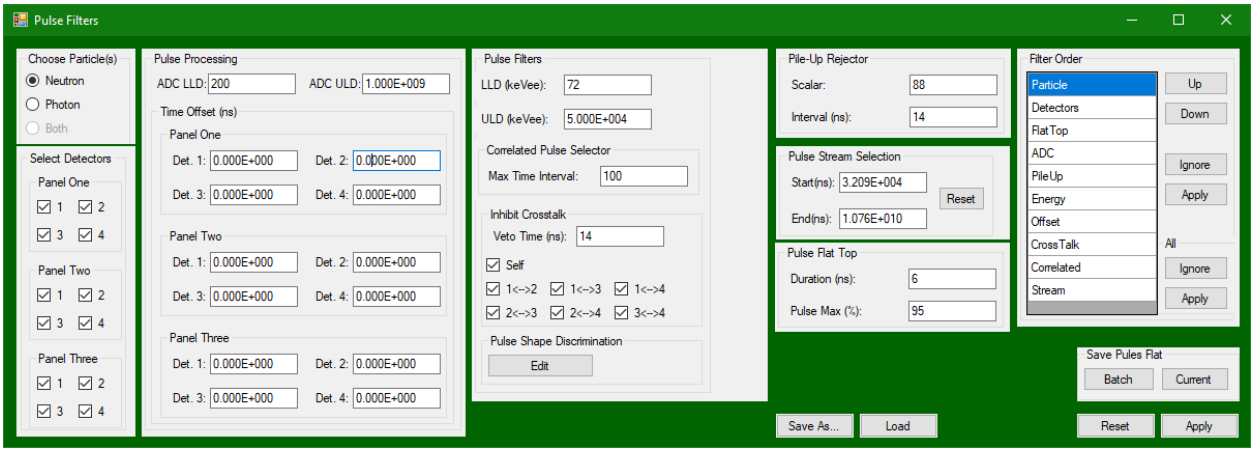

Figure A-2. The pulse filter window is where all pulse processing is set and applied before analysis.

The “Pulse Filters” window can reject pulses by alternating direct current (ADC) value (the baseline subtracted integral of the waveform), or by setting both lower level and upper level discriminators. Additionally, pulses are filterable based on the particle energy with lower and upper thresholds. The pulse height distribution, in both ADC and kiloelectron volt electron equivalent (keVee), of the pulse stream is viewable from the main analysis tab, as shown in Figure A-3.

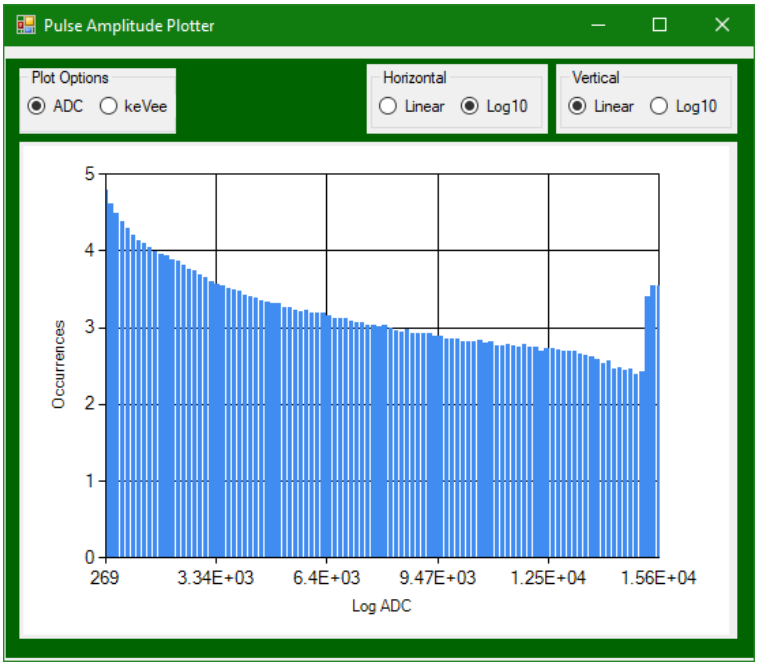

Figure A-3. Pulse amplitude plotter in ADC mode, note the large number of overflow pulses on the far right of the histogram.

Typically, the pulses are filtered with only an ADC lower level discriminator, leaving the ADC upper level discriminator high, and then to make a more "refined" cut on pulse energy, which is difficult to define for organic scintillators. Particle energy filtering requires a defined energy calibration for FNCL waveform data but is a given (though it depends on the MPPost detector settings) in MCNP-PoliMi pulse streams. The energy calibration widget is shown in Figure A-4 and allows the calibration for each detector in the FNCL to be defined using several functional forms for the calibration.

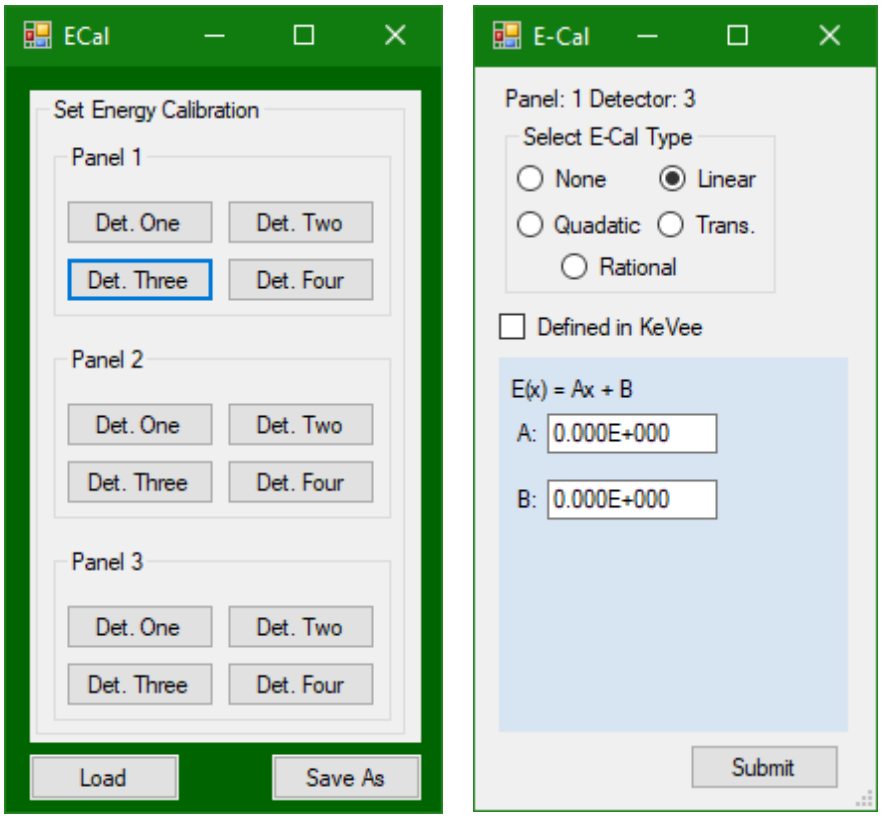

Figure A-4. Energy calibration tool.

Next, are two pulse time filters. First, is the "Correlated Pulse Selector" that eliminates isolated pulses from the stream. For example, if the time interval is 100 ns than a pulse without a neighboring pulse preceding or proceeding it within the time interval is eliminated. Second is the "Pulse Stream Selection" that allows pulses from the given time window to be included and is useful in discarding aberrant data and selecting a representative subset to minimize analysis times. The average number of pulses over time can be observed from the "Pulse Stream" viewer (Figure A-5).

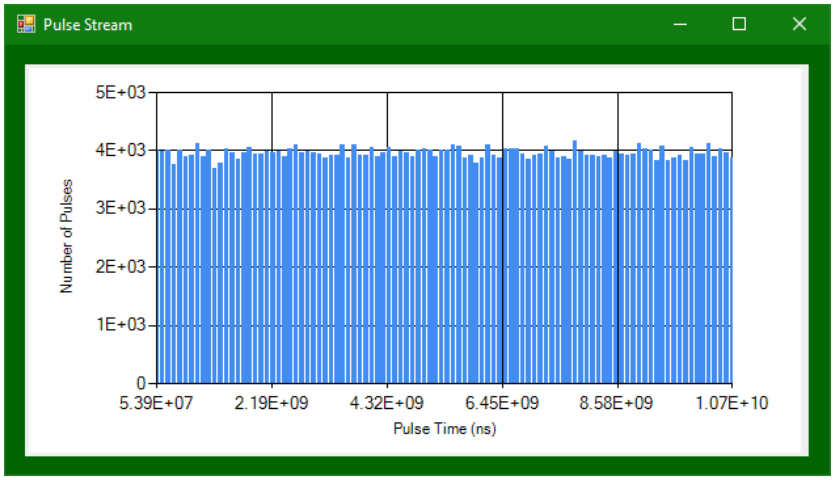

Figure A-5. The Pulse stream viewer can reveal major changes in average count rates.

An exceptionally important filter, which has been explored experimentally, is “Inhibit Crosstalk.” This filter rejects pulses that are suspected of originating from the same particle by rejecting pulses that occur within neighboring detectors in the given time window. This becomes more important as the average energy of the neutron interrogation source increases, where the probability of multiple fast scatters increases. The neighboring detectors are defined using the check boxes, where “Self” refers to pulses within the same detector, and the others “x<->y” refers to pules that occur in detector *x* and *y*, where the order of occurrence in the detector does not matter. In the present implementation, only detectors within a panel can be evaluated for crosstalk.

There are several pulse-shaping filters that are applicable to FNCL waveform pulses. First is “Pulse Shape Discrimination,” which is used to differentiate between neutrons and photons. This “Edit” button launches another window, Figure A-6, to view, modify, and save the pulse shape discrimination settings. The initial PSD curve for each detector is automatically loaded from the FNCL settings file. Each detector PSD curve can be modified by selecting the detector and then adjusting the PSD curve using the “Draw Boundary” using a “Pen” or by modifying/generating a simple text file.

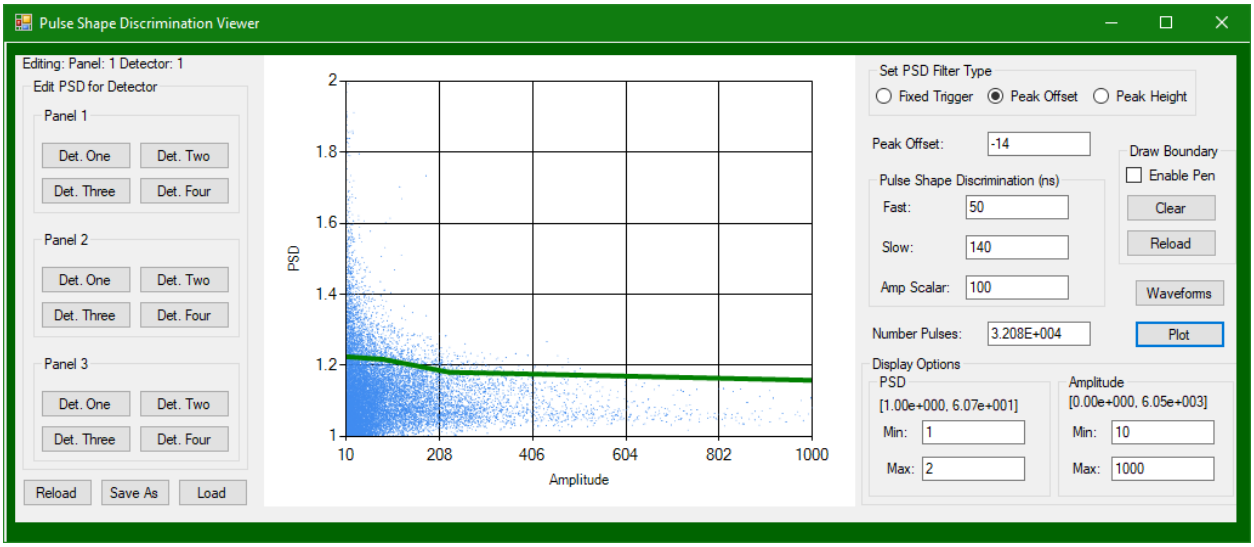

Figure A-6. Pulse shape discrimination editor.

The “PSD Filter Type” and settings can also be set for each detector. There are three trigger options (fixed, peak offset, and peak height) that determine the start of the slow and fast integration times, as well as adjusting the integration intervals. To troubleshoot and evaluate current PSD settings the “Waveforms” button launches an new widget, Figure A-7, that shows the waveform with the trigger and integration intervals, as well as the PSD, amplitude, and particle determination.

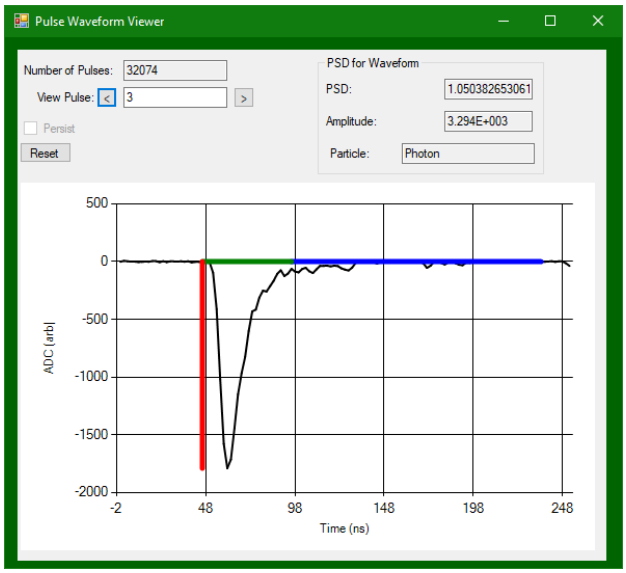

Figure A-7. PSD waveform viewer shows particle determination given PSD editor settings.

Next, is the "Pile-Up Rejector" that attempts to remove pulses that are contaminated by more than one particle detection event. The pile-up rejector uses three windows to integrate over the pulse waveform, as defined in the FNCL DAQ software manual, to determine if more than one pulse exists in the waveform. A pile-rejector viewer is available from the main analysis tab, as shown in Figure A-8, that allows the pile-up settings to be adjusted and to view the pile-up determinations for waveforms. This filter is particularly important to reduce the neutron pulses impacted by the large photon source originating from the neutron generator.

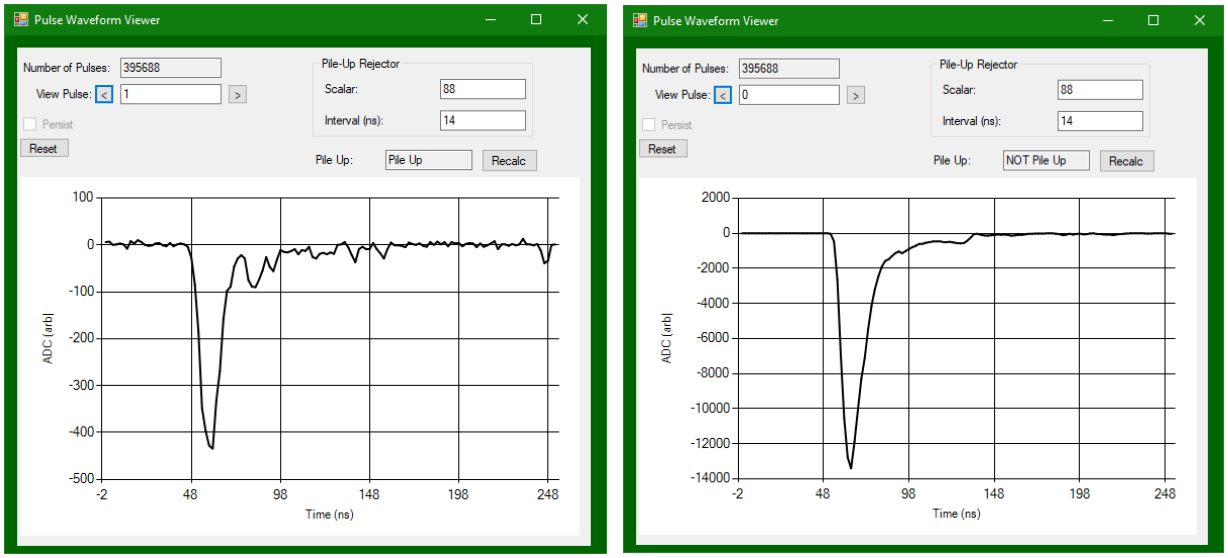

Figure A-8. Pile-up rejector showing a piled-up and non–piled-up pulse given the rejector settings.

Finally, "Pulse Flat Top" attempts to remove pulses with waveforms that overflow the maximum ADC bin, which is not accounted for using the "ADC ULD" (an integral value as defined in the CAEN Software manual). Figure A-9 shows a waveform that would be rejected due to a flat top.

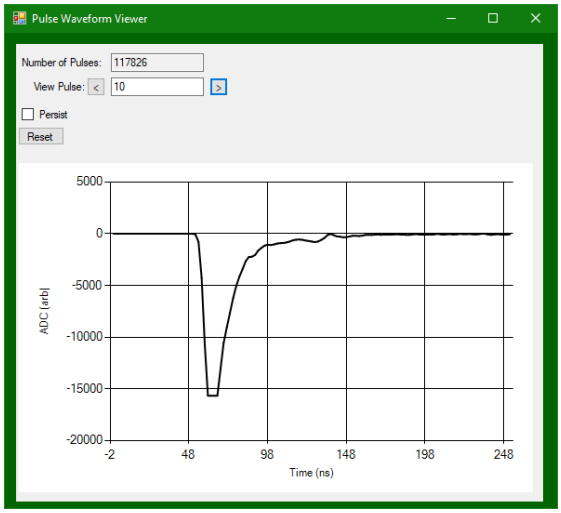

Figure A-9. Example of a pulse waveform rejected for flat top.

There are currently 10 pulse filters available through the GUI. It is often undesirable to apply all of them, and the resulting pulse stream may depend on the order of application of the filters. The "Filter Order" tool allows the order of pulse filter application to be set and whether to apply a filter. The current pulse configuration is then applied to the raw pulse stream, either from a FNCL waveform file or MCNP-PoliMi simulation files. The resulting processed pulses are then used for all subsequent analysis. The filter configuration can be saved for later, and previously saved filter settings can be applied.

The resulting filtered/processed pulses can be saved to a simple timestamp list file using the "Save Pulses Flat" buttons. In the special case of the FNCL waveform pulses, which are saved in 100 MB batches (often hundreds of files per measurement), the pulses from the entire measurement, both active and passive, can be saved/compressed as the simple file using the widget in Figure A-10. The filters can be applied, and the user can batch the files either by count time or by the maximum compressed file size.

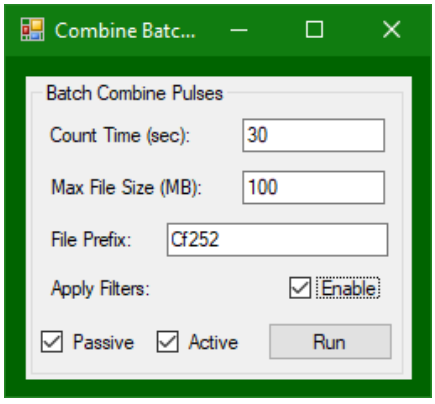

Figure A-10. Batch save of FNCL waveform pulses to flat files.

With a processed/filtered pulse stream the "View" panel lets users analyze the current pulse stream. First is the "Multiplicity" window, shown in Figure A-11. That calculates the singles, doubles, and triples rates (where the uncertainties are yet to be implemented) for several gate types. The FNCL by default uses a "Triggered" gate, where each pulse initiates its own gate, with a 60 ns gate width. Using this window, different gate widths can be explored as well as different gate types, such as the shift register.

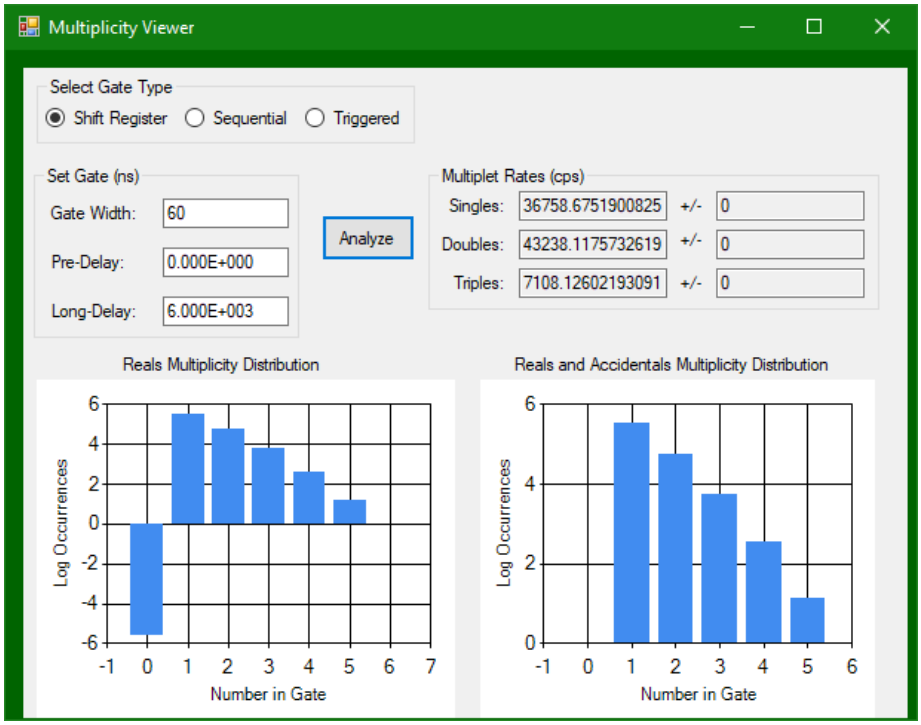

Figure A-11. Multiplicity counting rates window.

The die-away time is a useful metric, determined from the interval distribution, to estimate the average lifetime of a neutron in the measured item and detector, and this parameter is needed to assay fissile material. The "Die-Away Time" window is shown in Figure A-12, where we note the dominate peak at low time intervals due to the counting of fast neutrons. The die-away time is not as simply applicable to fast organic scintillators, but the capability is directly applicable to the ^{3}He flux monitor for the Mp320 neutron generator.

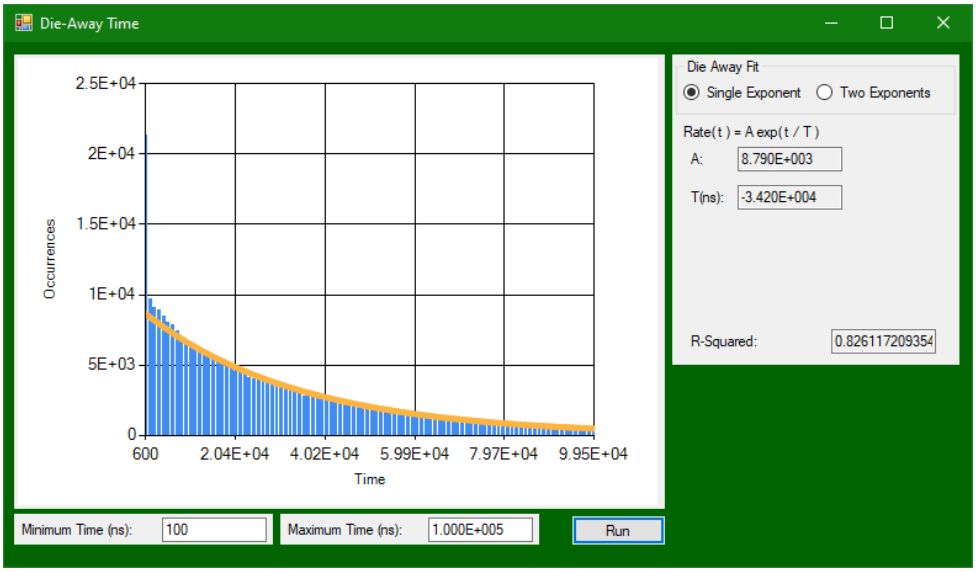

Figure A-12. Particle die-away time fit with a single exponential function on the interval distribution.

A.2 Simulation

The second tab in the GUI, Figure A-13, is dedicated to simulating list mode data of the FNCL using MCNP-PoliMi to generate particle histories and MPPost to simulate the detector response function. The simulation capability requires the installation of MCNP-PoliMi and MPPost, only requiring that the absolute path to the executables be defined, and a "Data Directory" that stores material definitions and configuration files. Several FNCL models exist as a foundation for the addition of source terms for the generation of synthetic list mode data. These foundational models dictate the interrogation source model and those postpended with "SEL" add models of the measurement room, such as the source stand orconcrete floor, and allow for placement of sources in terms of stacked foam pucks.

First the Am(Li) source holders window, as shown in Figure A-13, is used to show the general capabilites of the simulation modeling GUI. The "MCNP-PoliMi" section requires the specification of the "Top Directory" and "Directory" where MCNP simulations will be saved. The number of source histories to simulate is specified by "NPS" and the "Activity(Bqs)" specifies the source strength (which can be modified without resimulating). Next, the particles to be tracked is set to either neutron, photon, or both. Neutron-only simulations are favored because of the speed of calculation, because lead shields line the FNCL cavity, and because particle filtering is perfect in simulation space. Until DRiFT is implemented to simulate pulse waveforms to account for imperfect PSD, perhaps an approximate figure of merit could be developed as a placeholder.

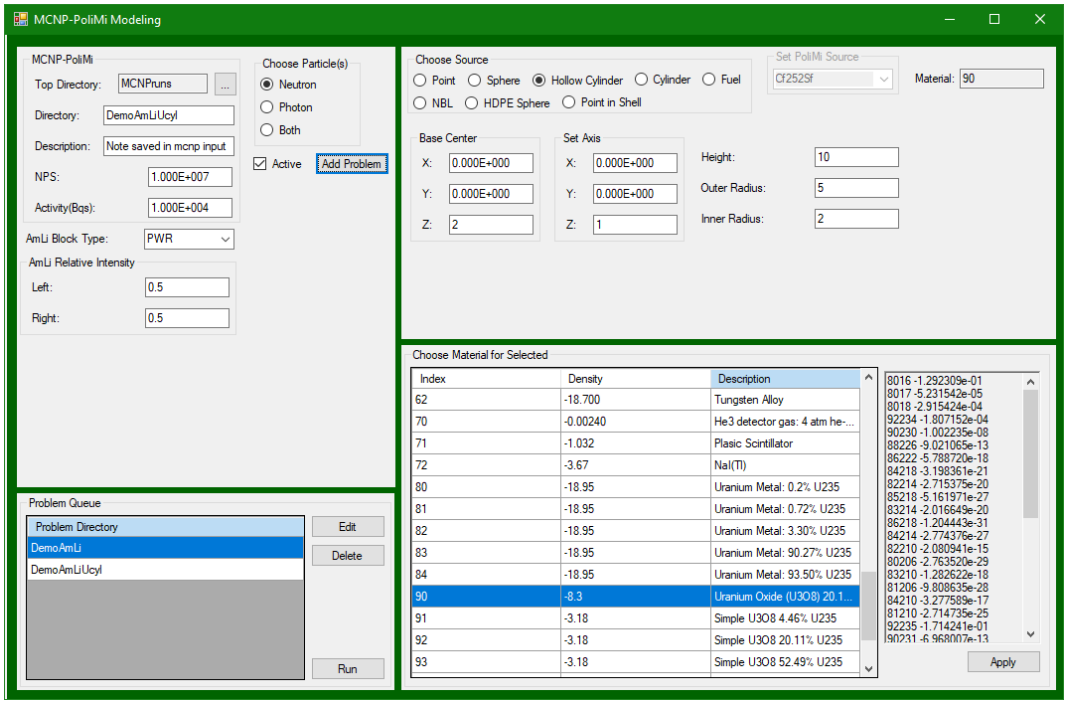

Figure A-13. FNCL model generation for Am(Li) source holder models.

A standard FNCL measurement requires a passive and active measurement. This is facilitated by the "Active" checkbox that sets the source term to that specified by the interrogation source. As MCNP-PoliMi can only run one source at a time, the simulation of an active interrogation measurement of an item, with an appreciable source intensity, requires an "Active" simulation and a run for each additional independent source term present in the item.

The synthetic pulse streams from many simulations can be combined into a single pulse stream using the "Combine PoliMi" tool shown in Figure A-14. Synthetic pulse files are added by specifying the source activity and number of histories simulated. The maximum dwell time (the wall time duration of a measurement) is limited by prohibiting the reuse of any source history. The final pulse stream is generated by randomly sampling histories, then randomly selecting a history start time based on the activity of each pulse stream and injecting that history into the final pulse stream. This synthetic pulse stream is subjectable to all the applicable (i.e., those that do not require a waveform) processing/filtering, and analysis).

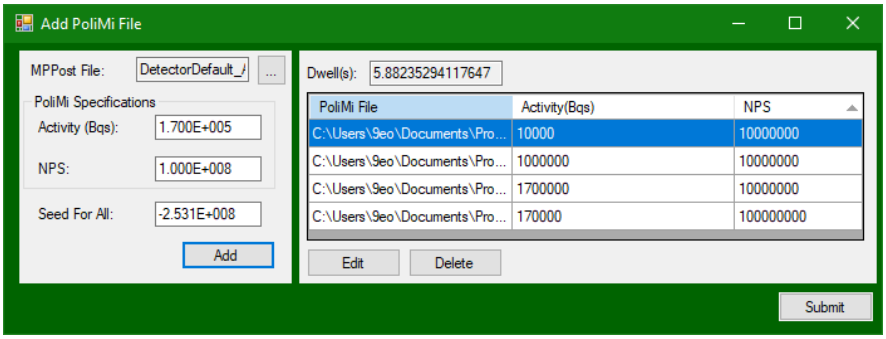

Figure A-14. Tool that combines multiple particle history files into a single pulse stream.

There are several source terms that are definable in the GUI, where the user can specify the material, using a material manager, and apply 1 of 20 MCNP-PoliMi sources. The source specification allows for great flexibility in defining the size and orientation of sources. For example, as shown in Figure A-15, the NBL can model can vary both the fill height, axis (whether the can is upright or not), and where it is positioned inside the FNCL-cavity. The material, such as the enrichment of the uranium oxide or any other material, and source term can both be varied as well.

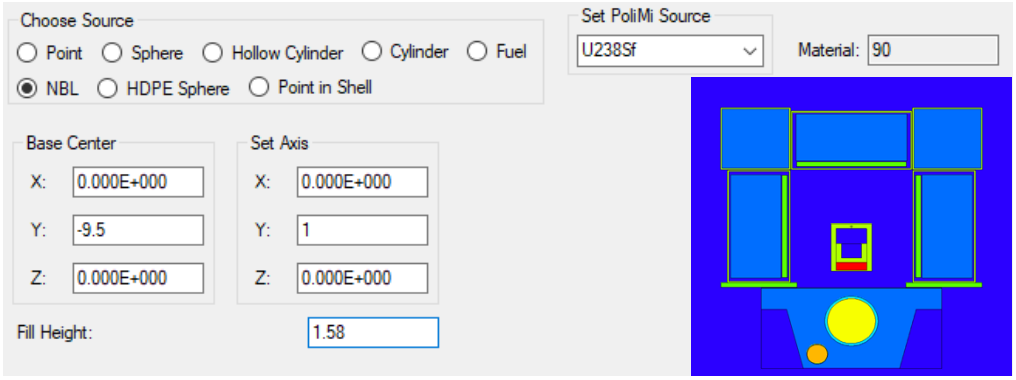

Figure A-15. NBL can on side inside FNCL-cavity with MP320 neutron generator with side shielding. Note, the MCNP drawing is not present in the GUI.

The other source models, which can be expanded upon, and source terms, which can be extended beyond those defined in MCNP-PoliMi, are similarly defined in the GUI. Fuel assemblies are specified by both a fuel file, as shown in Figure A-16, a source term (which currently is uniformly applied throughout fuel pins without regard for varying enrichments), and the position of the FNCL relative to the center of the assembly.

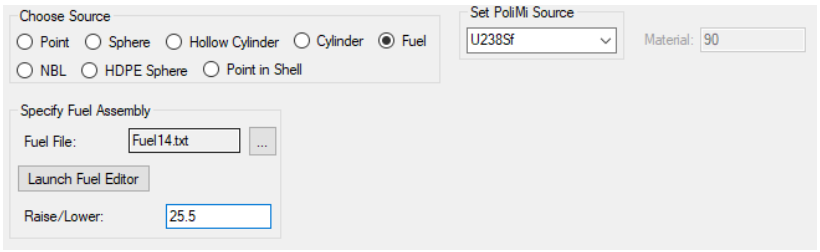

Figure A-16. Fuel assembly specification with option to launch an editor to modify the fuel assembly.

The specification of the fuel file can be made by hand, by another tool (e.g., Excel), or by the fuel editor in Figure A-17. The fuel editor enables us to quickly modify the number and layout of fuel pins by setting the number of rows and columns. The number and location of cooling channels are specified by checkboxes. The material can be set for multiple pins at once by selecting them (green denotes selected) and applying the material selected in the material manager. Additionally, the particulars of the fuel assembly such as length, the dimension of the pins, and pitch are editable in a pop-out window.

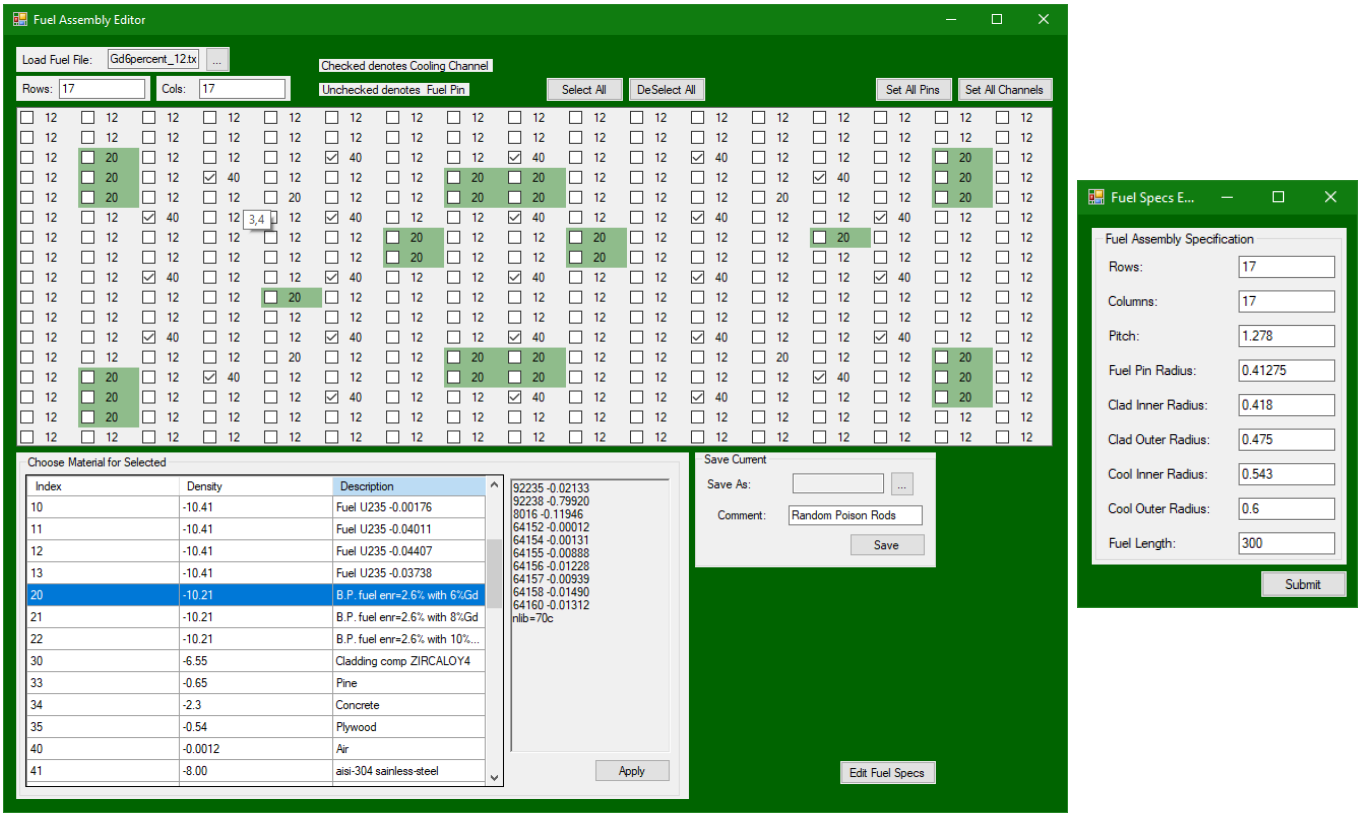

Figure A-17. The fuel assembly editor can vary number of pins, materials, and locations of cooling channels. Specifications can be saved, and template files loaded for modification. The details of the assembly and pins can be set in the "Edit Fuel Specs" tool.

With sources specified, the interrogation source needs to be specified. For the Am(Li) sources, there are three interrogation source holders available: the pressurized water reactor (PWR), boiling water reactor (BWR), and water–water energy reactor (VVER, under development). The type of source holder is specified by a drop-down menu. The relative intensity of the Am(Li) sources can be specified to enable the active simulation for imbalanced sources, including those where a single source is desired, in a single run.

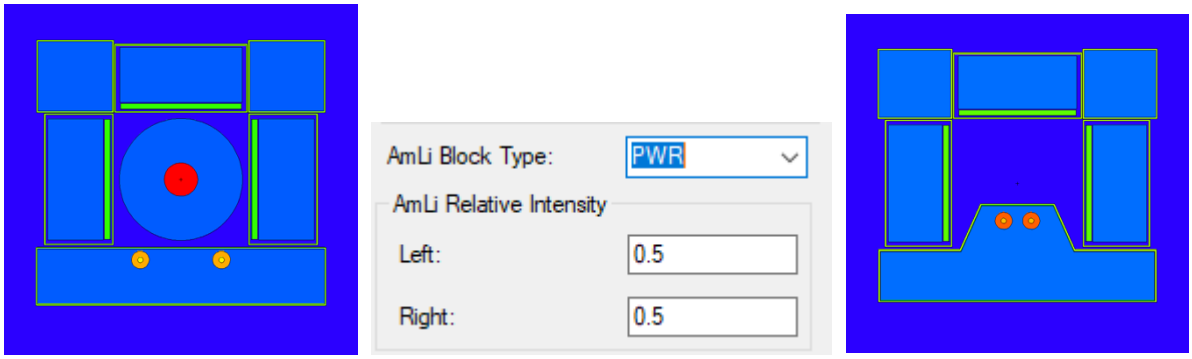

Figure A-18. Am(Li) source holder are specified by a the Am(Li) Block Type drop-down. Left is the, PWR and right is the BWR source holder. The VVER is under development.

The specification for the neutron generator is more involved than the Am(Li) sources because of the issues with moderating the higher energy DD-neutrons (which the FNCL is more sensitive too), and the large Bremsstrahlung source that can penetrate the unshielded sides of the FNCL. The MP320 DD-neutron generator is modeled in a base polyethylene (PE) block with a ^{3}He tube inserted as a neutron flux monitor. The MP320 could require additional neutron moderator and photon shielding. The MP320 specification component, pulled from the general model window, is shown in Figure A-19 between two MP320 models, as well as with and without modifications to the base model. The tool allows layers of cadmium and lead of varying thicknesses to be specified across the face of the MP320 PE block, as well as to increase the thickness of PE In front of the neutron generator. Finally, lead panels of varying size can be inserted between the left (2) and right (1) detector panels and the neutron generator.

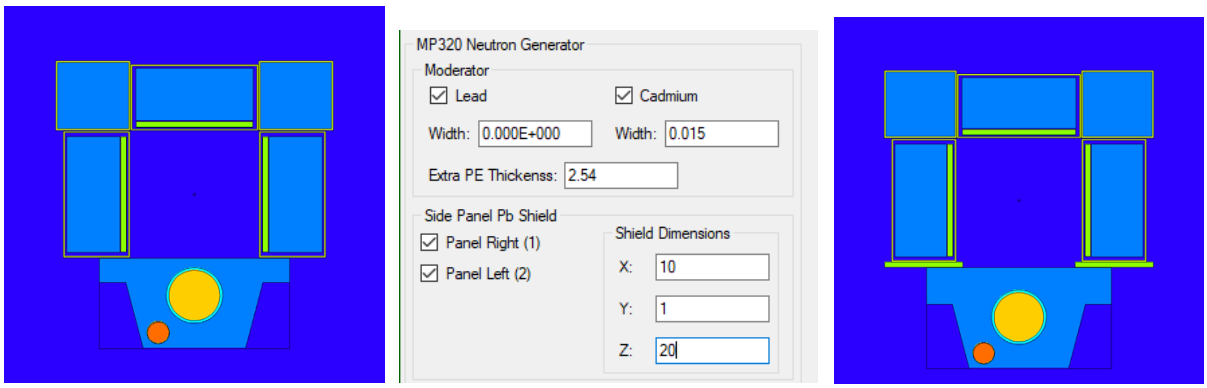

Figure A-19. MP320 neutron generator specification GUI, where additional neutron moderator and lead photon shielding can be added. The left MP320 is the base case, and the right model has side panel shielding and an additional PE moderator. The orange circle is the ^{3}He neutron detector.

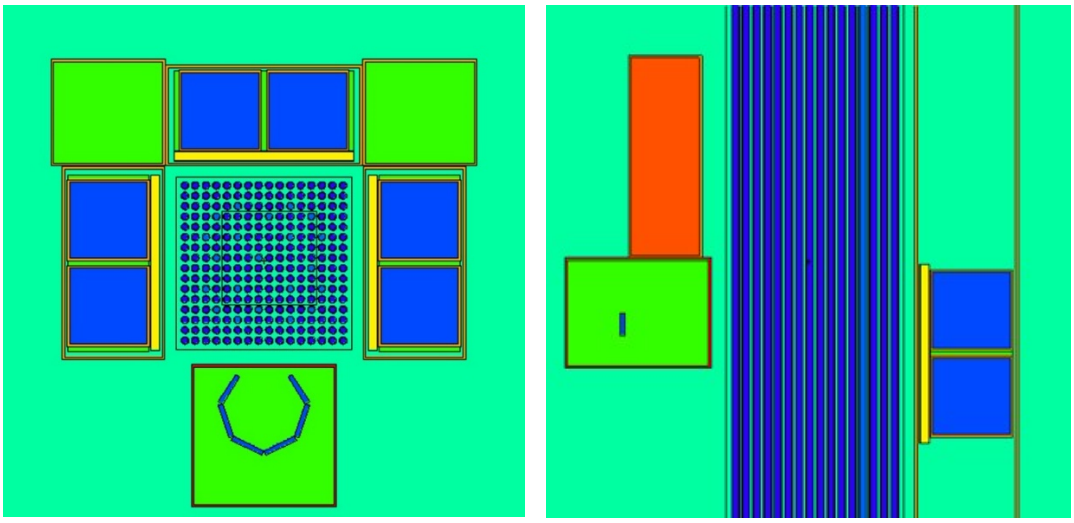

Figure A-20. nGen350 neutron generator with 16 × 16 fuel assembly, two perspectives.

A.3 Measurement and Simulation

A DD-neutron generator has been proposed as a replacement for the Am(Li) neutron source. Neutron generators offer the advantages of commercial availability, tunable source intensity, and pulsed mode operation and they do not present a radiation hazard when deactivated. However, given the higher energy of DD-neutrons over Am(Li) neutrons, 2.5 and 0.5 MeV, respectively, the liquid plastic scintillator in the FNCL is sensitive to the interrogation neutrons, and the higher energy neutrons are more likely to induce undesirable ^{238}U fissions. Through simulation and measurements we aim to compare the capabilities of the Am(Li) and DD neutron sources and to explore modifications to the FNCL to mitigate the drawbacks of using a neutron generator.

A.4 Measurements

A single FNCL measurement consists of a passive and active component. The results of the measurement, as presented in the DAQ-GUI, are the following count rates with their associated uncertainties:

- Filtered gammas: Pulses identified as gammas
- Non–pile-up events: Pulses identified as neutrons that pass pile-up rejection
- Filtered neutrons: Pulses identified as neutrons
- Doubles: Doubles rate of neutron events

To extract more information from the FNCL, including triples rates, detector specific behaviors, and to explore the impact of pulse filters without performing a new normalization and remeasuring, requires reprocessing the digitized waveform binary files generated during the measurement. To accurately extract more information from the FNCL pulse stream requires implementation of the existing filters, as detailed above in Sections A.2 and A.3.

The impact of several filters on the measurements of a ^{252}Cf source in the center of the FNCL cavity and the MP320 with and without an extra inch of PE is shown in Table A1. The fraction of pulses passing through the filters is generally similar for californium and the MP320 cases, where more cross talk is likely to occur for californium given an actual “reals” rate, except for the large reductions due to pile-up rejection. The increase in pile-up rejected pulses for the MP320 could be due to gammas generated in the

PE that enter the side of FNCL panels that are not well gamma shielded as compared to those facing the cavity.

Table 1A. Percent of filtered pulses remaining.

	Cf252	MP320	MP320-PE
Flat Top	97.24	97.54	97.67
ADC	99.92	99.96	99.96
Cross Talk	98.91	99.30	99.35
Pile-Up	47.97	28.85	25.46

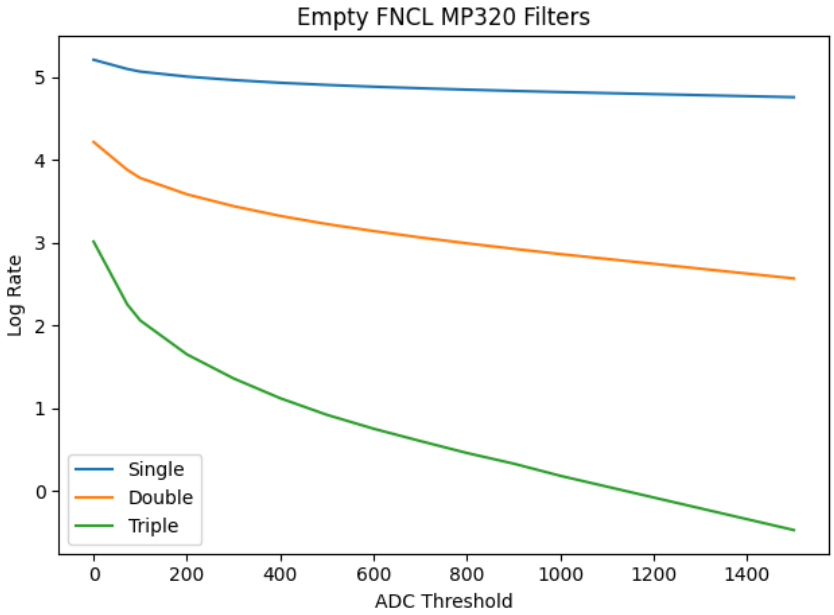

Figure A-21. Impact of raising ADC low level discrimination threshold on multiplet rates.

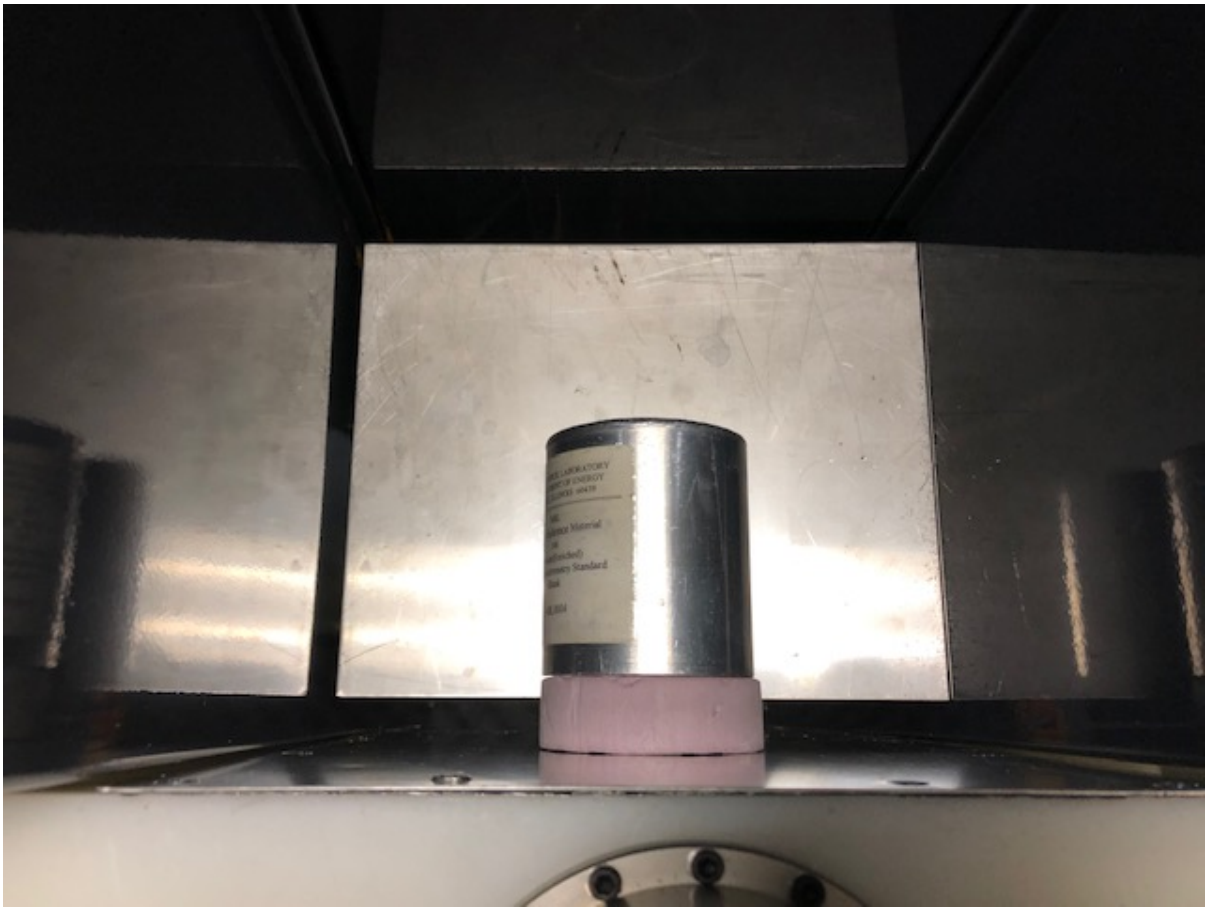

Figure A-22. Position of NBL cans to maximize interrogation neutron interactions given the small volume of material for all reported measurements.

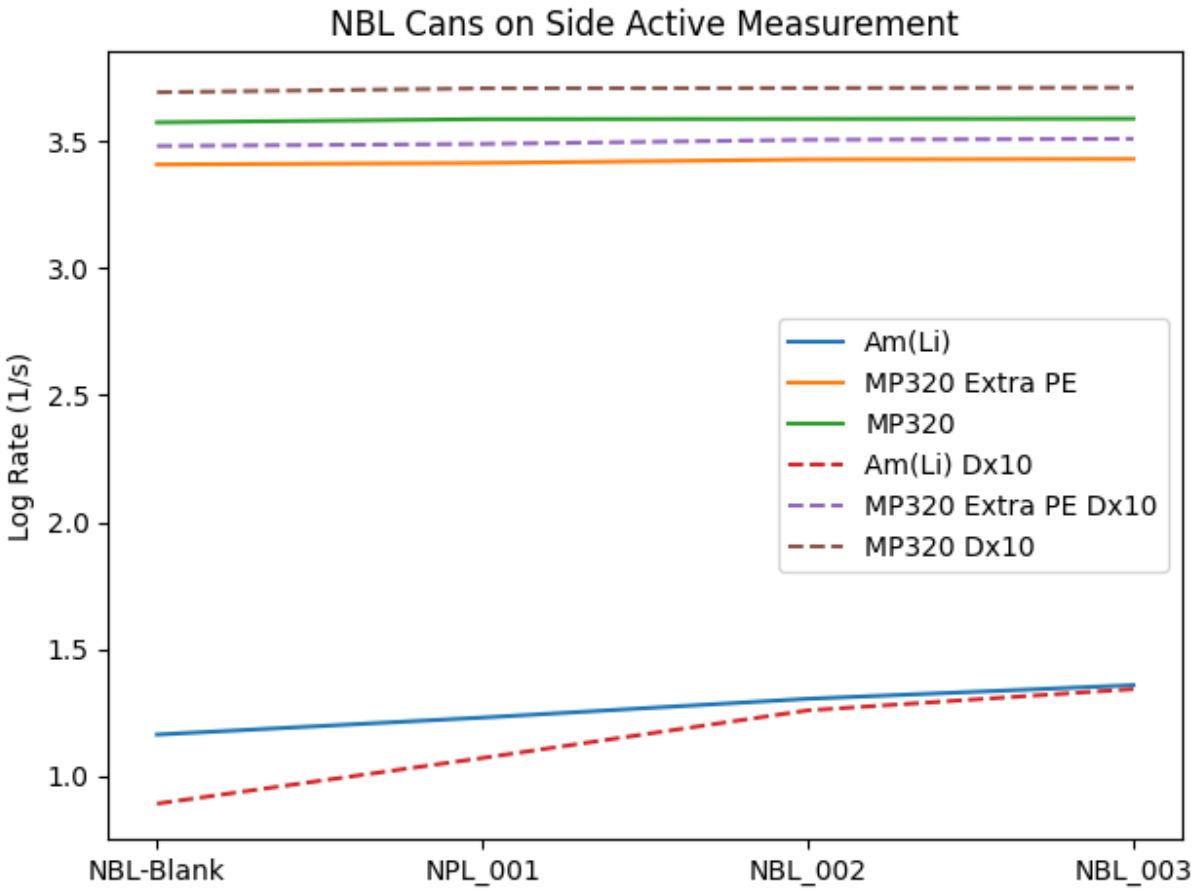

Figure A-23. Singles and doubles rates reported by the FNCL DAQ for the PWR Am(Li) interrogations sources and for the Mp320, with and without extra PE.

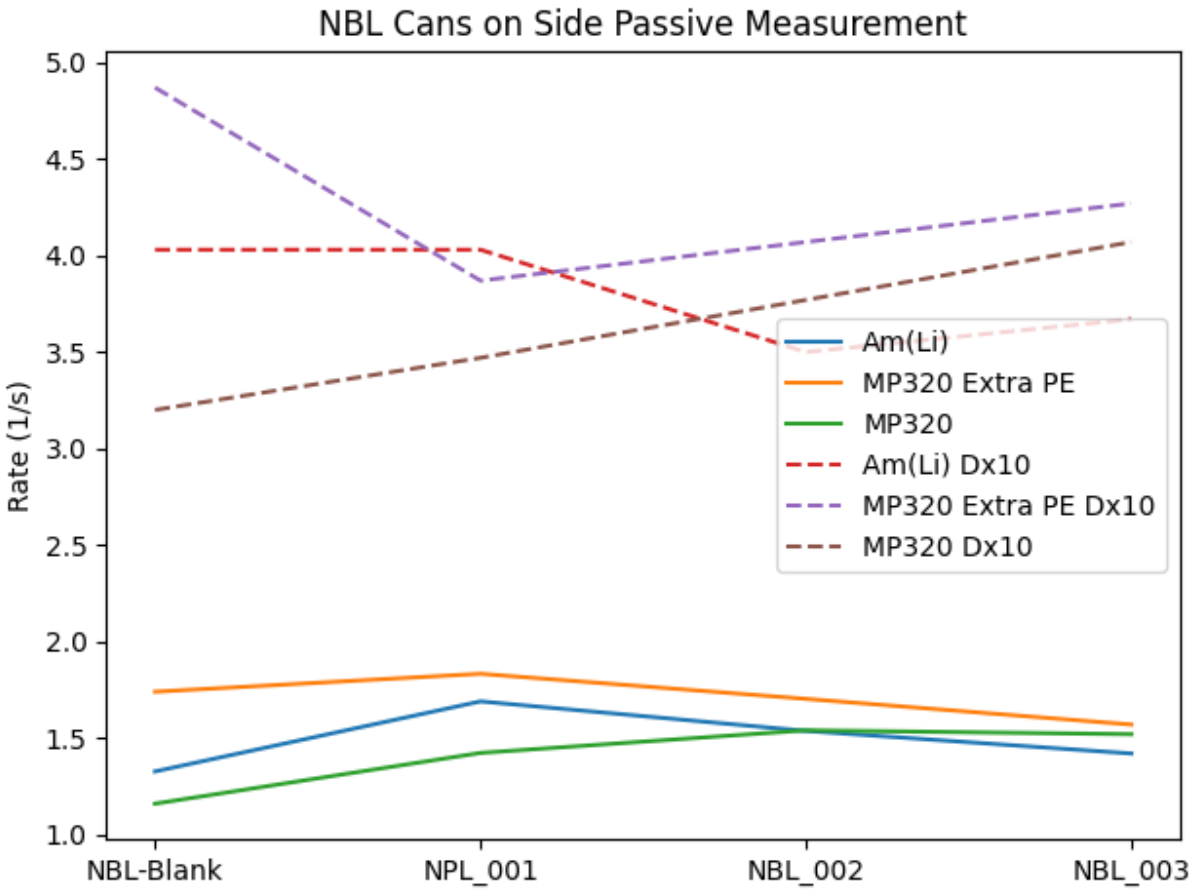

Figure A-24.Singles and doubles rates for passive measurements reported by the FNCL DAQ for the PWR Am(Li) source holder and for the Mp320, with and without extra PE.

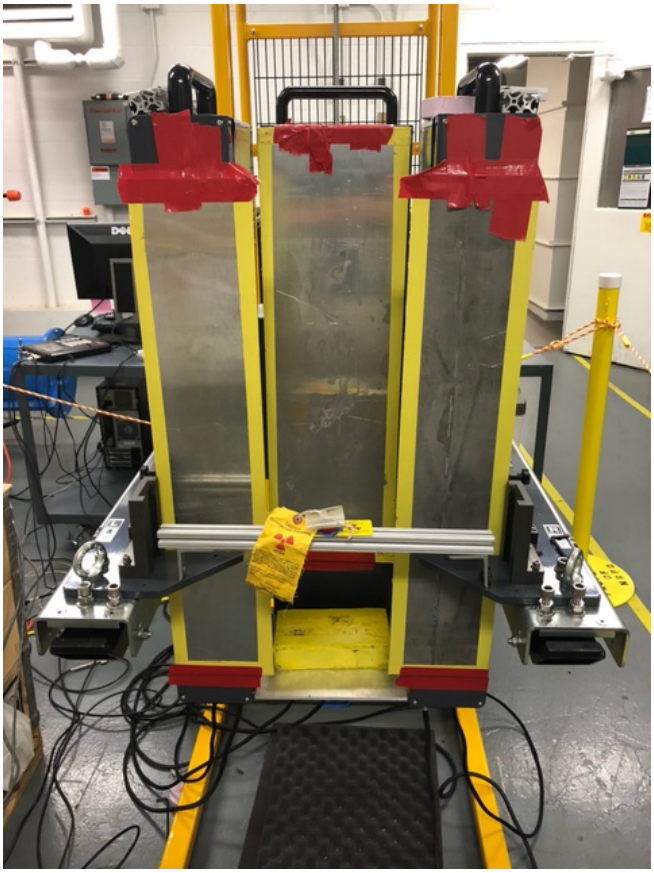

Figure A-25. Californium-252 and cesium-137 sources with cadmium sheet shielding.

Table A2. Relative difference (%) in count rate relative to no extra shielding.

Cd Shields	Gamma	S	D
Panel 1,2,3	3.73	5.63	5.30
Panels 1,2	2.50	4.08	3.05
Panel 2	2.48	3.49	2.65

Table A3. Relative difference (%) in count rates with active MP320 to half-inch lead shield.

0.5 in. Lead	Gamma	S	D
Panel 1,2	–9.57E+00	–3.25E+01	–2.61E+01
Panel 3	–9.37E+00	–3.23E+01	–7.49E+00
Panel 1,2,3	–1.14E-01	4.44E-01	1.31E+00

Poisson Rods

The FNCL should be able to distinguish, to some threshold, between a fuel assembly with and without poison rods. A fuel assembly, 17 × 17, was simulated across several enrichments, with varying number and concentration of gadolinium poison rods. This capability was explored between the Am(Li) sources and the MP320 neutron generator. The positioning of cooling channels and gadolinium rods, 20 for this initial case, is shown using the fuel editor tool in Figure A-26.

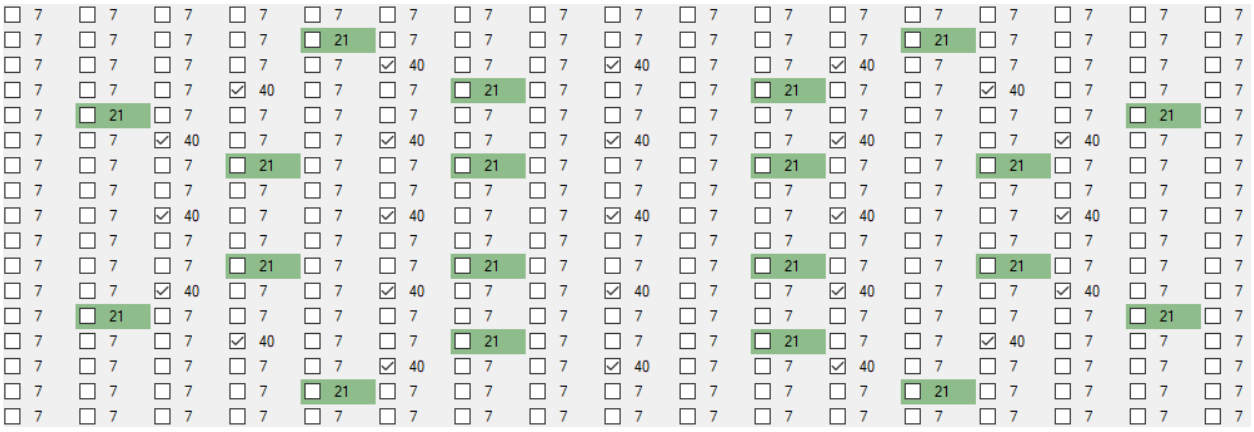

Figure A-26. A 17 × 17 fuel assembly with 20 gadolinium poison rod positions marked in green, and the cooling channels are checked.

To compare the effectiveness of identifying the presence of gadolinium rods the relative difference between poison rods and lack of poison rods is compared across several fuel enrichments for the singles, doubles, and triples rates of the filtered MCNP-PoliMi pulse stream. First, consider the sensitivity to poison rods using Am(Li) interrogation neutrons in Figure A-27.

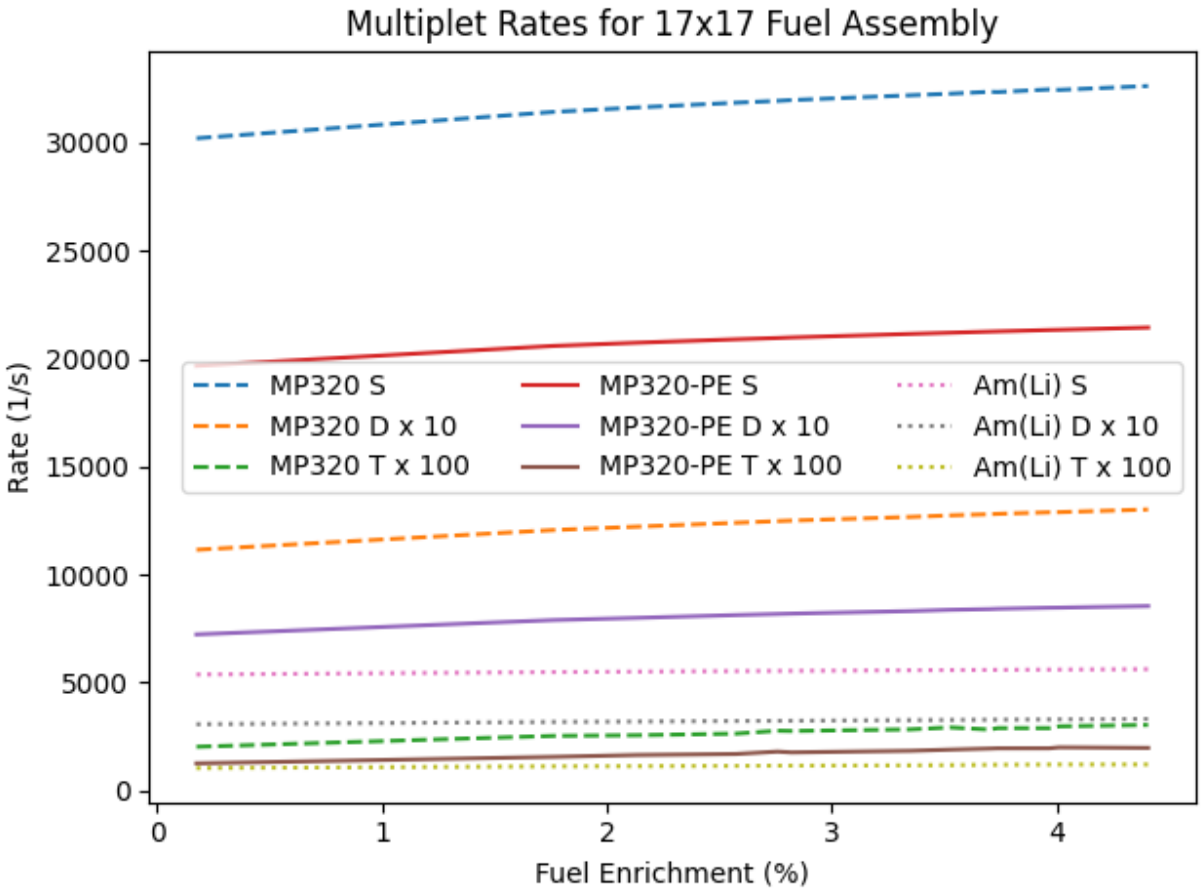

Figure A-27. Simulated rates across fuel enrichments for the several interrogation sources. The Mp320 without extra PE has the highest rates.

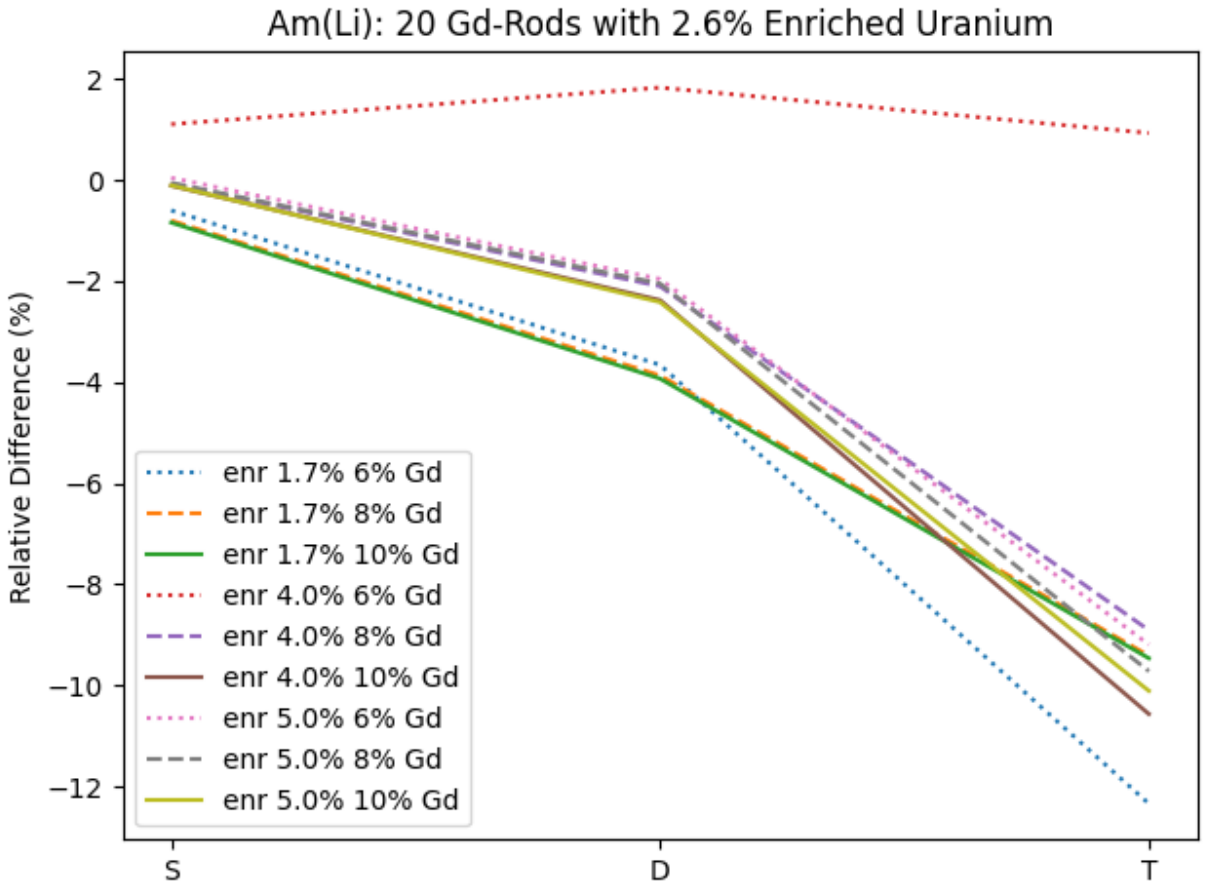

Figure A-28. Relative difference between the simulated singles, doubles, and triples rates between fuel assemblies with gadolinium poison rods and a fuel assembly without gadolinium poison rods that preserves the total mass of ^{235}U using the PWR Am(Li) source holder.

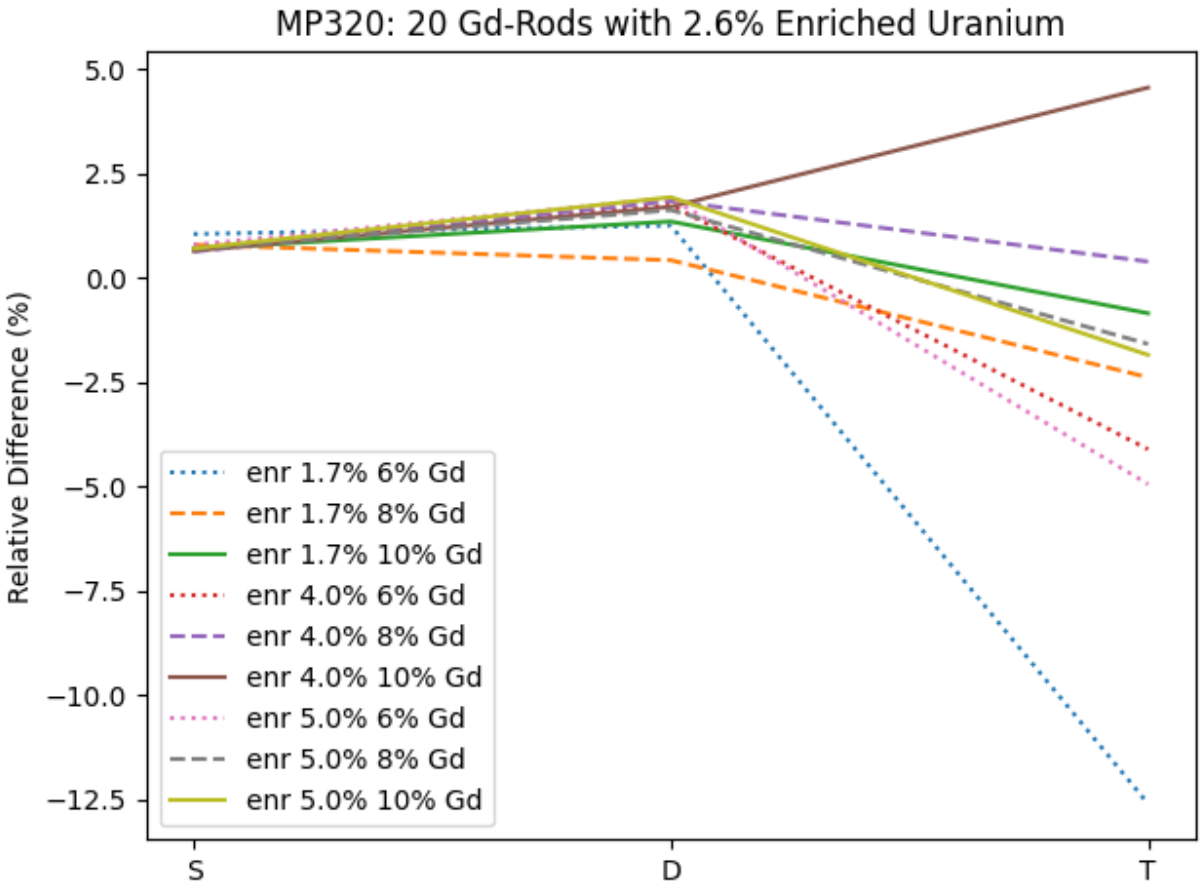

Figure A-29. Relative difference between the simulated singles, doubles, and triples rates between fuel assemblies with gadolinium poison rods and a fuel assembly without gadolinium poison rods that preserves the total mass of ^{235}U using the MP320 neutron generator.

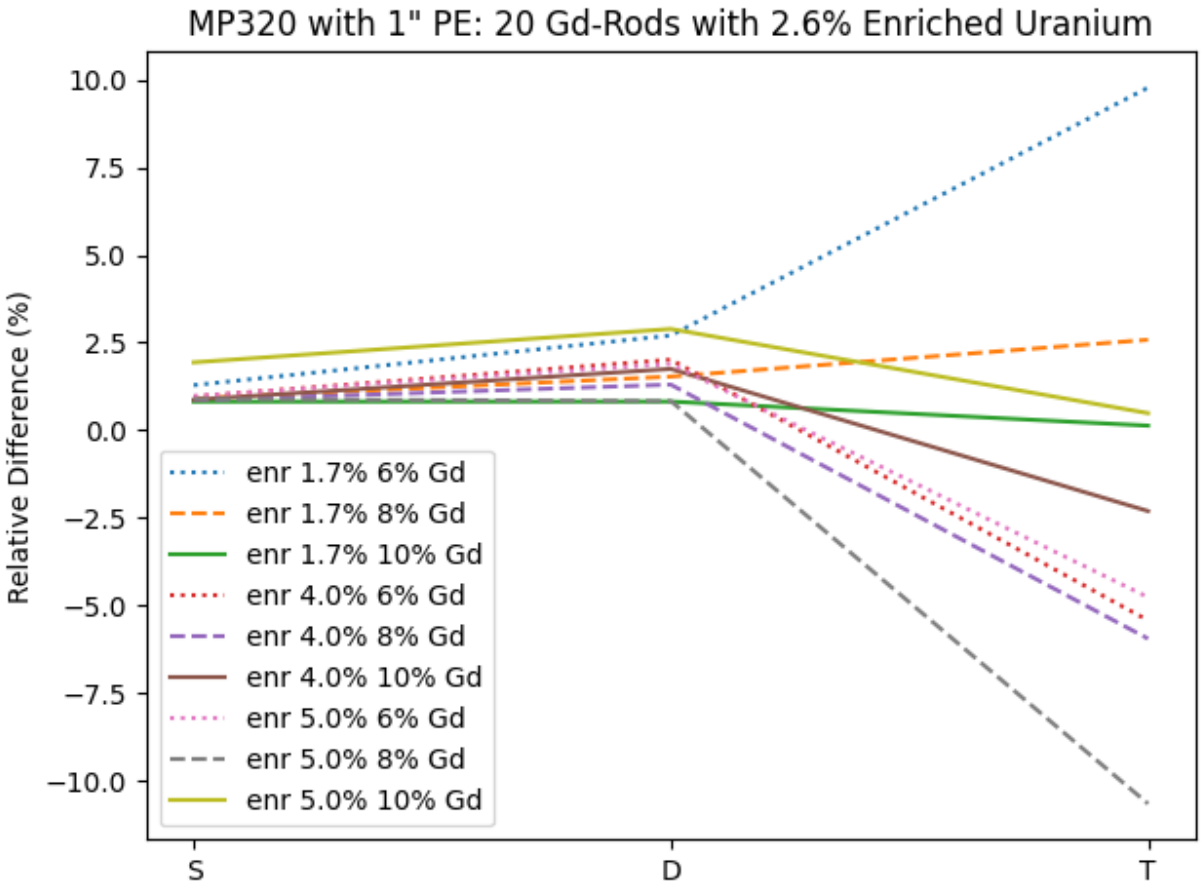

Figure A-30. Relative difference between the simulated singles, doubles, and triples rates between fuel assemblies with gadolinium poison rods and a fuel assembly without gadolinium poison rods that preserves the total mass of ^{235}U using the MP320 neutron generator with extra PE.

Table A4. Detector response to 100 sec simulated ^{252}Cf source emitting 3.757×10^5 n/s of FNCL with MP320 (no extra shielding nor moderator).

	DRF(%)	Rel. Singles(%)	Rel. Doubles (%)	Rel. Triples (%)
Center Low	8.10	64.24	44.95	33.56
Center Middle	8.63	68.41	50.71	40.56
Center High	8.10	64.22	44.77	33.20
Panel-1 Low	10.11	80.15	65.77	54.86
Panel-1 MIddle	10.88	86.25	76.12	68.77
Panel-1 High	10.11	80.14	65.74	54.83
Panel-3 Low	11.70	92.78	85.92	79.94
Panel-3 Middle	12.61	100.00	100.00	100.00
Panel-3 High	11.70	92.79	85.66	78.92

Table A5. Ratio with maximum value of a simulated and a measured ^{252}Cf source

	S (%)	Meas. S (%)	D (%)	Meas. D (%)
Center Low	64.24	67.84	44.95	62.02
Center Middle	68.41	65.81	50.71	64.05
Center High	64.22	54.35	44.77	52.47
Panel-1 Low	80.15	78.29	65.77	73.39
Panel-1 Middle	86.25	72.77	76.12	65.98
Panel-1 High	80.14	55.82	65.74	49.39
Panel-3 Low	92.78	96.07	85.92	93.28
Panel-3 Middle	100.00	100.00	100.00	100.00
Panel-3 High	92.79	83.48	85.66	84.60

NGEN-350

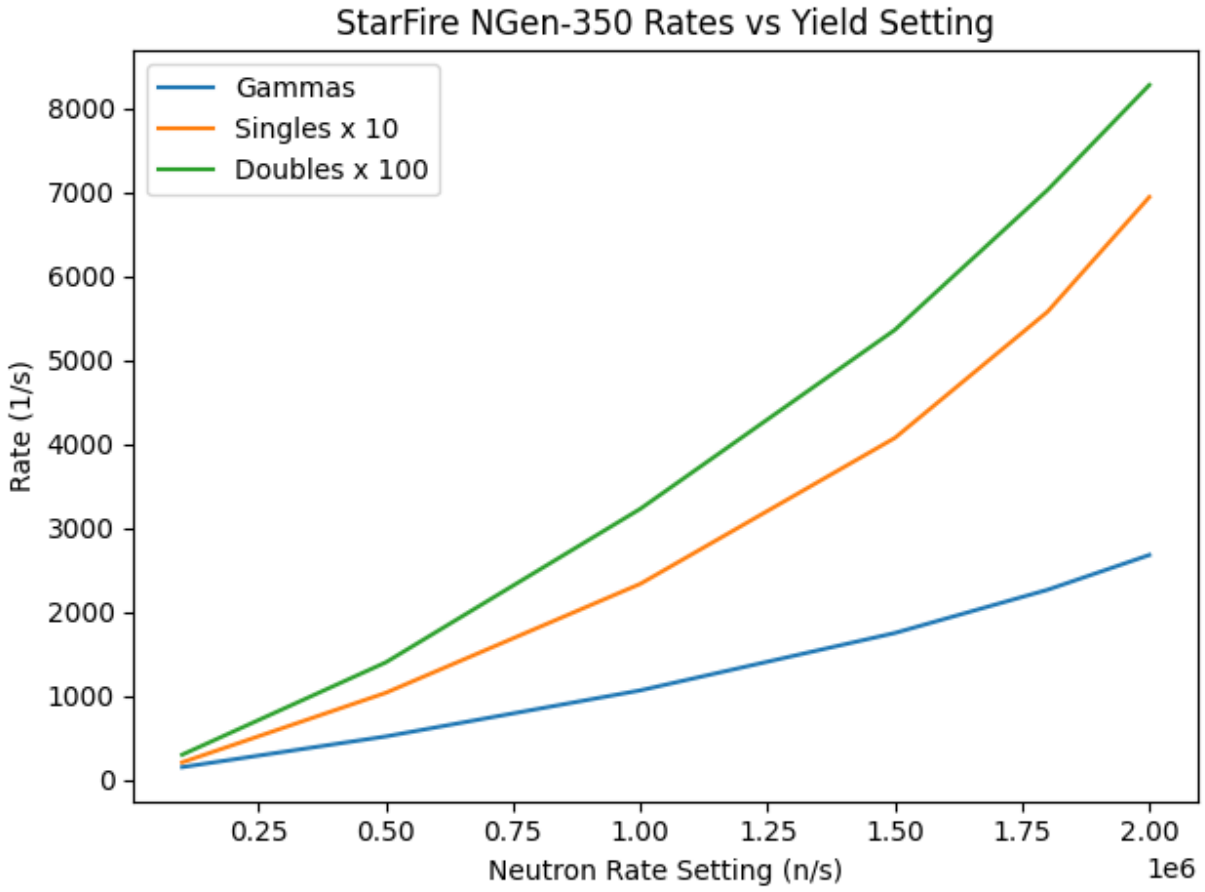

Figure A-31. Resulting count rates, reported by the FNCL-DAQ, over a range of "auto" neutron yield settings.

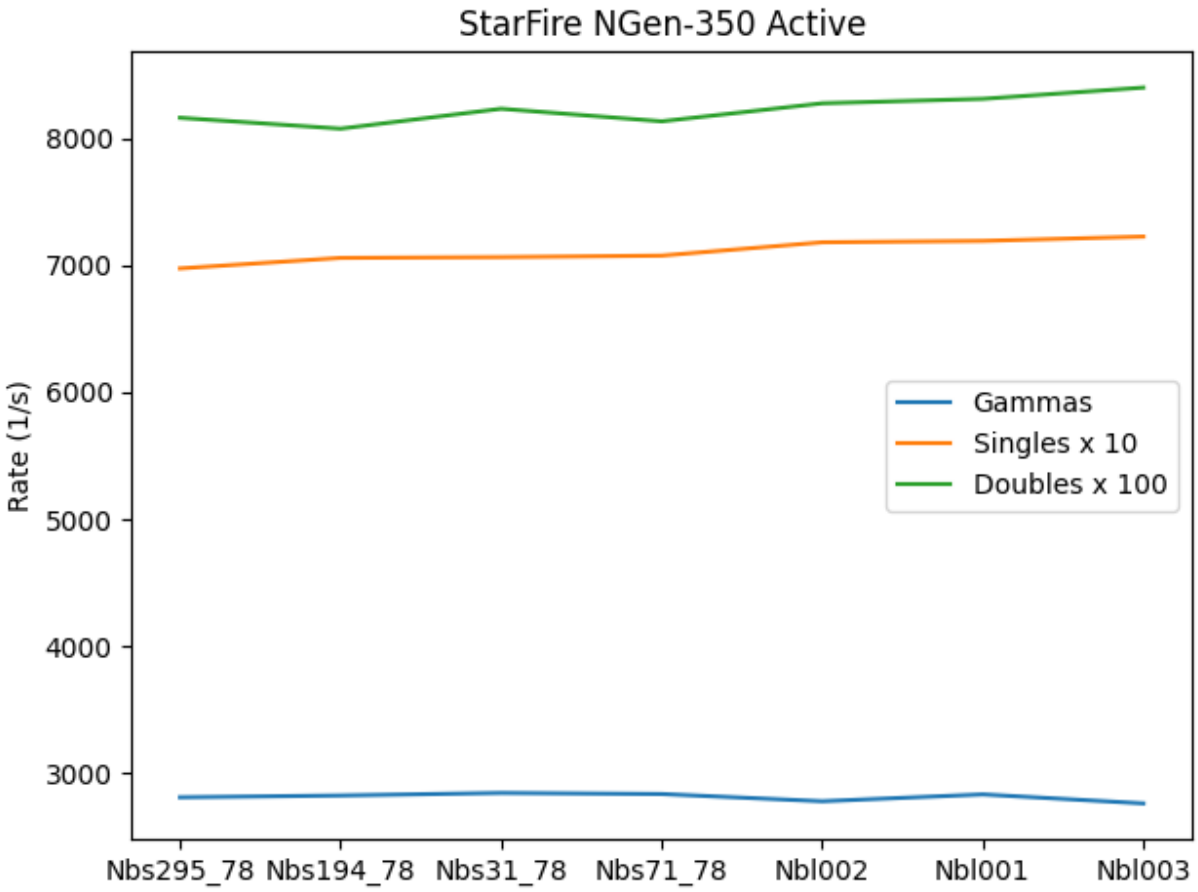

Figure A-32. Rates reported by the FNCL-DAQ for several U-standards.